

AMERICAN UNIVERSITY OF BEIRUT

MODIFIED STOCHASTIC GEOMETRY MODELS FOR THE
ANALYSIS OF DENSE NETWORKS IN 5G

by
HUSSEIN ALI AMMAR

A thesis
submitted in partial fulfillment of the requirements
for the degree of Master of Engineering
to the Department of Electrical and Computer Engineering
of the Faculty of Engineering and Architecture
at the American University of Beirut

Beirut, Lebanon
September 2017

AMERICAN UNIVERSITY OF BEIRUT

MODIFIED STOCHASTIC GEOMETRY MODELS FOR THE
ANALYSIS OF DENSE NETWORKS IN 5G

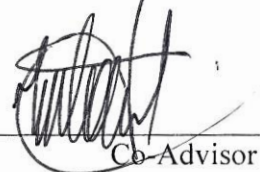
by
HUSSEIN ALI AMMAR

Approved by:

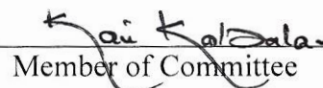
Dr. Youssef Nasser, senior lecturer
Electrical and Computer Engineering


Advisor


Dr. Hassan Artail, professor
Electrical and Computer Engineering


Co-Advisor

Dr. Karim Kabalan, professor
Electrical and Computer Engineering


Member of Committee

Dr. Ibrahim Abo Faycal, associate professor
Electrical and Computer Engineering


Member of Committee

Date of thesis defense: September 5, 2017

AMERICAN UNIVERSITY OF BEIRUT

THESIS, DISSERTATION, PROJECT RELEASE FORM

Student Name:

Ammar
Last

Hussein
First

Ali
Middle

Master's Thesis

Master's Project

Doctoral Dissertation

I authorize the American University of Beirut to: (a) reproduce hard or electronic copies of my thesis, dissertation, or project; (b) include such copies in the archives and digital repositories of the University; and (c) make freely available such copies to third parties for research or educational purposes.

I authorize the American University of Beirut, to: (a) reproduce hard or electronic copies of it; (b) include such copies in the archives and digital repositories of the University; and (c) make freely available such copies to third parties for research or educational purposes after:

One year from the date of submission of my thesis, dissertation, or project.

Two ---- years from the date of submission of my thesis, dissertation, or project.

Three ---- years from the date of submission of my thesis, dissertation, or project.

Mr. A.A.
Signature

September 11, 2017
Date

ACKNOWLEDGMENTS

I would like to start this report by wishing all the success for this inspiring place, the American University of Beirut (AUB), that gave me the chance to delve deeper in my major and continue an important stage in my life to build a professional career. I want also to present a very special gratitude for my advisor, kind professors, students, and faculty staff that I met inside this university, for every single help, knowledge and valuable guidance they gave me during my study.

Equally important, I would like to thank my graduate assistantship supervisors who gave me a great valuable professional experience, which I have gained from preparing, instructing and guiding students during my assigned labs duties in each semester.

Moreover, I would like to thank my parents for supporting me spiritually throughout writing this thesis and my life in general.

And finally, last but by no means least, I present my deep appreciation for the establishers and organizers of the successful graduate assistantship program at AUB. And I will not forget how this program contributed to my intellectual growth and degree goals.

With all my respect. Hussein Ammar

“The future belongs to those who believe in the beauty of their dreams”, Eleanor
Roosevelt

AN ABSTRACT OF THE THESIS OF

Hussein Ali Ammar for Master of Engineering
Major: Communications Area

Title: Modified Stochastic Geometry Models for the Analysis of Dense Networks in 5G.

In-Band Full-Duplex (IBFD) has emerged as a technology to increase throughput and spectral efficiency for the users. It is a key potential technology expected to be a part of the future enhancements on the next generation cellular networks. Nodes operating at IBFD can transmit and receive simultaneously at the same time/frequency resource blocks, without the need to orthogonalize the Uplink/Downlink (UL/DL) frequency bands. Transceivers of such users implement Self-Interference Cancellation (SIC) techniques, and are able to route incoming and outgoing signals while transmitting at the same network resources, thus potentially doubling the capacity of the wireless channel.

Stochastic geometry, a field focusing on the study of random spatial patterns, provides an elegant way of analyzing the performance of wireless networks and its technologies. In view of that, we develop approaches using this tool to derive network performance metrics. We use stochastic geometry to study the performance of a possible deployment scheme of IBFD in cellular networks. Mainly, we make use of the mathematical tools used in stochastic geometry to tackle two topics. At first, we study the Base Stations (BSs) locations in real cellular networks. We use data for the Evolved NodeB (eNB) locations from real deployed LTE networks in specific urban areas. We start our analysis by obtaining the spatial density distribution of these eNBs. Then, we try to fit this distribution with some candidate distributions, in which we determine the distribution that best fits with the actual density and gives the lowest Root Mean Square Error (RMSE). The aim from this procedure is to use this fitted density distribution in a framework that derives general performance metrics for the whole studied network. Henceforth, these metrics give a general idea about how the spatial density distribution can affect the network in general. Among these metrics, we show that the exact closed form expressions for the interference power PDF can be obtained for some cases.

Then, we study the performance of the users operating at IBFD in a general cellular network model. We assume that this network uses Fractional Frequency Reuse (FFR) and some sort of shared channel resources or imperfect orthogonal channel resources i.e. non-orthogonal transmissions between the users such as Non-Orthogonal Multiple Access (NOMA). The first technology is already in LTE networks while the second is one of the potential candidates. Markedly, the use of shared network resources

is aligned with the vision for future networks. With this intention, we analyze the performance of the network using two different approaches based on the Poisson Point Process (PPP) and the inner-city model, and we show the effect of using such network configuration. Also, we show the decrease in the Signal to Interference plus Noise Ratio (SINR) experienced by the users operating at IBFD, and how FFR can mitigate this decrease for the cell edge users that experience weaker signal than the cell core users. Given these points, we compare the performance of IBFD users to that of half duplex users, and we show how much throughput is gained in the IBFD case.

CONTENTS

ACKNOWLEDGEMENTS.....	V
ABSTRACT.....	VI
LIST OF ILLUSTRATIONS.....	XI
LIST OF TABLES.....	XIV

Chapter

I. INTRODUCTION.....	15
A. Point Processes.....	17
B. Mathematical Preliminaries.....	20
1. SINR in downlink.....	20
2. Probability of Coverage	22
3. Mean achievable Rate	25
C. Literature	26
II. DENSITY DISTRIBUTION OF BASE STATIONS	30
A. Density Distribution	30
1. Area 1	31
2. Area 2	33
3. Area 3	34
B. Analysis: Coverage and Rate	36
1. Network Model	36
2. Signal to Interference plus Noise Ratio.....	37
C. Network Coverage.....	40
D. Mean Achievable Rate	41
E. Numerical Results	42
F. Conclusion.....	47

III. PROBABILITY DENSITY FUNCTION OF THE INTERFERENCE POWER IN PPP NETWORKS	48
A. Mathematical Background	50
B. Interference Power PDF Analysis	53
1. The PDF of the Interference Power in Homogeneous PPP.....	55
2. The PDF of the Interference Power in a Cox Process.....	57
C. Approximating interference PDF using GEV	58
D. Conclusion.....	61
IV. IN-BAND FULL-DUPLEX (IBFD) SHARED CHANNEL ACCESS	62
A. Introduction:	62
B. In-Band Full-Duplex:	63
C. Fractional Frequency Reuse:	64
D. Related Work:	66
E. General Network Model:.....	67
F. Coverage of Users Operating at IBFD:	71
1. Cell-Edge Users:	71
2. Cell-Core Users:	73
1. Approach I:.....	75
2. Approach II:	80
3. A Use Case for the General Model:	87
G. Mean Achievable Rate:	88
H. Simulation Results:	89
I. Conclusion:.....	96
CONCLUSION	97

Appendix

II.A.....	98
II.B.....	99
IV.A.....	100
IV.B.....	101
IV.C.....	101
IV.D.....	102
IV.E.....	103
IV.F.....	104
IV.G.....	104
IV.H.....	110
BIBLIOGRAPHY.....	112

ILLUSTRATIONS

Figure	Page
2.1: BS towers across area 1.	31
2.2: BS density distribution in area 1 for 2x2 km² randomly chosen regions.....	32
2.3: BS towers across area 2.	33
2.4: BS density distribution in area 2 for 2x2 km² randomly chosen regions.....	33
2.5: BS towers across area 3.	34
2.6: BS density distribution in area 3 for 2x2 km² randomly chosen regions.....	35
2.7: Probability of coverage when the density follows Levy distribution, and the interference experiences Rayleigh fading.....	44
2.8: Probability of coverage when density follows Weibull distribution (shape $n=1$), and the interference experiences Rayleigh fading. Normal plot ($m = 0.5$), dashed ($m = 20$).....	44
2.9: Probability of coverage when the density follows Generalized Pareto distribution, and the interference experiences Rayleigh fading. Normal plot ($\gamma = 1, k = 0.54$), dashed ($\gamma = 1.2, k = 2$).....	45
2.10: Mean data rate when $\eta = 3$ the density follows Levy distribution, and the interference experiences Rayleigh fading.....	46
2.11: Mean data rate when $\eta = 4$, the density follows Levy distribution, and the interference experiences Rayleigh fading.....	46
2.12: Mean data rate when $\eta = 3$, the density follows Weibull distribution (shape $b=1$), and the interference experiences Rayleigh fading.....	46

2.13:	Mean data rate when $\eta = 4$, the density follows Weibull distribution (shape $b=1$), and the interference experiences Rayleigh fading.....	47
3.1:	Interference power PDF (conditioned and decondition on T).....	56
3.2:	PDF when density follows Levy distribution.	58
3.3:	Fitting interference power distribution in a PPP network with GEV distribution	60
4.1:	Left: St-FFR. Right: So-FFR. Possible interference experienced by a typical user operating at IBFD.....	65
4.2:	Network Model for $\lambda_{BS} = 0.5 \text{ BSkm}^2, \lambda_U = 200 \text{ userskm}^2, d_F =$ 0.3 km, Tedge = -1 dB	69
4.3:	Schema showing different possible types of interference sources from the users operating at IBFD	71
4.4:	Upper bound for LT of interference. For case 1, we consider one disk $\mathbf{b}(\mathbf{r}_0, \mathbf{d}_F)$, and for case 2 we consider two disks $\mathbf{b}(\mathbf{r}_0, \mathbf{d}_F)$ and $\mathbf{b}(\mathbf{r}_1, \mathbf{d}_F)$	80
4.5:	Lower and upper bounds for the LT of $\mathbf{L} \mathbf{U} \mathbf{e}$, IBFD's plus noise. The more disks we take the tighter the upper bound becomes.....	85
4.6:	Resources allocation example in cell 1; same scheme is used in each Nth neighbor cell according to the FFR.....	87
4.7:	Coverage probability using approach 1 for $\mathbf{U} \mathbf{e}$ operating at IBFD at different \mathbf{d}_F , and for half-duplex $\mathbf{U} \mathbf{e}$	91
4.8:	Coverage probability using approach 1 for $\mathbf{U} \mathbf{c}$ operating at IBFD at different \mathbf{d}_F , and for half-duplex $\mathbf{U} \mathbf{c}$	91
4.9:	Coverage probability using approach 1 comparison between $\mathbf{U} \mathbf{e}$ and $\mathbf{U} \mathbf{c}$ at different λ_{BS}	92

4.10:	Coverage probability using approach 1 for Ue with respect to different N	92
4.11:	Mean achievable rate for Ue and Uc operating at IBFD compared to the half-duplex case without any shared resources.	93
4.12:	Mean achievable rate for Ue and Uc operating at IBFD with dF = 0.5 km compared to the half-duplex case without any shared resources.	94
4.13:	Probability of coverage for a typical edge user at distance r = 0.17 km > a1 using Approach 1 and 2.	95
4.14:	Probability of coverage for a typical core user at distance r = 0.14 km < a1 using Approach 1 and 2.	95
4.15:	Probability of coverage for a typical edge user at distance r = 0.3 km > a1, λBS = 0.5BSkm², λU = 50userskm², dF = 0.4km using Approaches.	95
4.16:	Probability of coverage for a typical core user at distance r = 0.23 km < a1, λBS = 0.5BSkm², λU = 50userskm², dF = 0.4 km using Approaches.	96
4.17:	Approximating the region separating the core-edge users as circular for the network configuration dF = 0.3 km and Tedge = -1 dB	107

TABLES

Table		Page
1.1:	Used path loss exponents for different environments [3].	22
2.1:	RMSE results for different distributions for area 1.	32
2.2:	RMSE results for different distributions for area 2.	34
2.3:	RMSE results for different distributions for area 3.	35
2.4:	Probability of coverage for the different considered density distributions.	41
2.5:	Mean achievable rate for the different considered density distributions.	42
2.6:	Common simulation parameters; unless specified.	43
3.1:	Inverse Laplace for scaled KWW for mostly needed β indexes.	53
3. 2:	Simulation Parameters	55
4.1:	Notations used.	70
4.2:	Upper and lower bounds of the LT of the different interference, Approach 2.	84
4.3:	Upper and lower bounds of the joint LT of IUc , IBFD , IUIBFD , Approach 2.	86
4.4:	Use case channel resources allocation.	87
4.5:	Simulation Parameters.	90

CHAPTER I

INTRODUCTION

Stochastic geometry [1] is a necessary tool to analyze random spatial patterns in the plane \mathbb{R}^2 or higher. It has recently emerged as a powerful tool to study the performance of wireless networks, which created an interesting field of study named Stochastic Geometry for Wireless Networks. This field is very useful in wireless communication, especially in characterizing the interference statistics. It allows to study the average behavior of a network whose nodes are placed according to some probability distribution.

In a wireless network, data transmission through the wireless channel is defined through some input parameters including, transmit (Tx) power, frequency, bandwidth, modulation, channel coding scheme and protocols to schedule transmission... In transmission, the signal undergoes attenuation due to the propagation in the wireless medium with an inverse power law that is mainly dependent on the distance traveled in the medium. A general path loss model is the singular path loss model $r^{-\eta}$, where r is the distance traveled by the signal and η is the path loss exponent that is related to the type of the medium that the signal is traveling through (desert, urban area, ...). The distance between the transmitter and the receiver depends on how the network is deployed; it is affected by the size of the cells and the density of the Base Stations (BS) deployed. Also, the signal experiences interference from other transmitters in the network, this interference depends on the resource allocation scheme used to separate the transmitters from each other and how much common channel resources are used between them. It mainly depends on the deployment plan of the transmitters in the network. Again, the geometry of the network is greatly affecting its performance. Hence, the tools introduced by stochastic geometry to study the performance of the network, and the effectiveness of deployment patterns and transmission schemes in enhancing the performance are very

important. Therein, the Signal to Interference Plus Noise Ratio (SINR) is widely used as a performance metric. A user receiving signal with SINR above a specific threshold T called *SINR* threshold, will be assumed in the coverage area. In the whole analysis of stochastic geometry, it is not common to consider the receiver operations (error correction, equalization, etc).

The analysis of the performance of a network of specific configurations requires a network model that determines the geometry of the network. Since each network has a different geometry, choosing a network model may be hard. In fact, the transmitters in a network are very random which makes modeling the exact locations an impossible task. Even if we tried to capture the exact locations of the transmitters, we would get a network model that can't be applied on a general network type or configuration. Additionally, the model will not be able to derive performance metrics for the network due to the resulted complexity of the model. For that, some convenient network models are used to model the transmitters and the receivers. Some models may be more convenient for some network types (example: ad-hoc networks), or for some specific types of areas (example: urban areas). Instantly, probabilistic models called point processes are used to model the network nodes (transmitters and receivers) locations and to capture their properties. The probabilistic models can account for the randomness of the available network nodes while preserving many important characteristics that ensure that the model is still reliable. Such characteristics include but are not limited to MAC layer behavior, nodes density, some conditions on the positions of the network nodes. Important network models are homogeneous PPP, PHP, Poisson Cluster Processes (PCP) which includes two important processes, which are Matérn Cluster Process (MCP) and Thomas Cluster Process (TCP)... Each model can be convenient for a specific scenario for the network. But in general, PPP is the most famous one due to its high tractability, and it is a widely-used and accepted network model. PPP model defines an intensity λ , which is the number of nodes in a certain

area A . Furthermore, PPP models the network nodes' locations randomly and provides an easy and flexible statistical model. PPP is commonly used as a mathematical model across numerous disciplines due to its highly tractable and well-studied nature. PPP is also used for extended analyses, including the impact of power control, spread-spectrum, interference cancellation techniques, and the derivation of interference correlation coefficients.

A. Point Processes

A point process Φ is a collection of mathematical points randomly located on some underlying mathematical space such as the real line, the Cartesian plane, or more abstract spaces. We use point processes in wireless networks to model the nodes (transmitters, receivers, relays...) locations, and then we use tools from wireless communication and information theory to study the performance of this network, specific communication schemes, or solve some problems related to the network performance.

In this section, we briefly present simple definitions [2] for some of the point processes used in wireless communication.

Definition 1.1: (Homogeneous Poisson Point Process PPP) A homogeneous PPP is a point process that has an intensity λ in general dimensions \mathbb{R}^d such that:

- For every compact set B , $N(B)$ has a Poisson distribution with mean $\lambda|B|$, where $| \cdot |$ denotes the Lebesgue measure (standard way of assigning a measure to subsets of n -dimensional Euclidean space) or simply the area/volume of B .
- If B_1, B_2, \dots, B_m are disjoint bounded sets, then $N(B_1), N(B_2), \dots, N(B_m)$ are independent random variables.

Here, the intensity λ is the expected number of points of the process per unit area or volume.

The probability of having k nodes in the compact set B is:

$$P[N(B) = k] = \frac{(\lambda|B|)^k}{k!} e^{-\lambda|B|} \quad (1.1)$$

Surely, we are interested in the study of point processes on the 2D plane, so with circular sets we get $|B| = \pi r^2$.

Definition 1.2: (Cluster Processes) A cluster process is composed of two processes, a parent point process and a daughter point processes, one per parent with translating the daughter processes to the position of their parents. The cluster is then the union of all the daughter points. Denote $\Phi_p = \{x_1, x_2, \dots\}$ as the parent process and let $n \in \mathbb{N}$ be the number of these points, and Φ_i be the family of finite daughter processes. The cluster process is the union of the translated clusters N_{x_i} :

$$\Phi_c = \bigcup_{i \in n} N_{x_i} = \bigcup_{i \in n} \Phi_i + x_i \quad (1.2)$$

There are many types of point processes depending on the properties and the way these processes are generated, i.e. stationary, independent, homogenous clustering ... If the parent process is a lattice, the process is called Lattice Cluster Process, and similarly if the parent process is Poisson the process is called Poisson Cluster Process (PCP). We will mention two important processes that are subtypes of PCP and belongs to the class of Nyman-Scott process. A point process belongs to this class when the parent process is PPP and the daughter points are independent and identically distributed (iid). These two processes are the following:

- 1- Matérn Cluster Process (MCP): a point process where the daughter points are independently and uniformly scattered on the ball of radius a centered at each parent point with mean number of points of \bar{c} . Since all the formed clusters are identically distributed, we can talk about a representative cluster N_0 with the same distribution as that of the clusters of the process. The daughter points of this N_0 are scattered independently with an identical spatial distribution around the origin:

$$F_c(A) = \int_A f_c(x) dx, \quad A \subset \mathbb{R}^2 \quad (1.3)$$

where

$$f_c(x) = \begin{cases} \frac{1}{\pi a^2}, & \|x\| \leq a \\ 0, & \text{otherwise} \end{cases} \quad (1.4)$$

$\| \cdot \|$ is the Euclidean distance.

2- Thomas Cluster Process: is generated like MCP, but with daughter points scattered using a symmetric normal distribution with variance σ^2 around the parent point. So:

$$f_c(x) = \frac{1}{2\pi\sigma^2} e^{-\frac{\|x\|^2}{2\sigma^2}} \quad (1.5)$$

Definition 1.3: (Hard Core Point Process HCPP) are point processes where points are forbidden to be closer than a certain distance. One way to achieve such a minimum distance is to start with a point process that has no restrictions and then remove points that violate the condition. Some types of HCPP are the Matérn Type I and Type II which differs in how the point process is constructed and produce different models.

Definition 1.4: (Poisson Hole Process PHP) is a type of point processes that is very useful to study some network types like cognitive radios in which some network nodes are considered primary users and other as secondary. The secondary users can transmit if they are at least at distance a from the primary users and therefore does not cause interference. This point process is created from two independent homogeneous PPP Φ_1 and Φ_2 with intensities λ_1 and λ_2 respectively. We define the germ-grain model \mathcal{E}_a :

$$\mathcal{E}_a = \triangleq \cup \{x \in \Phi_1 : b(x, a)\} \quad (1.6)$$

It consists of the circles $b(x_i, a)$ centered at each point of Φ_1 and having radius a . Now we define the PHP as:

$$\Phi_{PHP} = \{x \in \Phi_2 : x \notin \mathcal{E}_a\} = \Phi_2 \setminus \mathcal{E}_a \quad (1.7)$$

So, every point from Φ_1 is curving out a circle of radius a from Φ_2 . This means the points of Φ_2 inside these holes do not exist in the resulted PHP. Such a model will produce an intensity formulation:

$$\lambda_{PHP} = \lambda_2 e^{-\lambda_1 \pi r^2} \quad (1.8)$$

In addition to the defined point processes, there are other point processes. The use of a specific process depends on the network configuration, and the amount of tractability the model can produce for the network performance metrics that will be introduced next.

B. Mathematical Preliminaries

Stochastic geometry allows to study the average behavior over many spatial realizations of a network whose nodes are placed according to some probability distribution. It is a strong mathematical tool that provides spatial averages, i.e. averages taken over large number of nodes at different locations or over many network realizations. The aim of using stochastic geometry in wireless networks is to analyze the network performance and to give statistical results for it.

1. SINR in downlink

The SINR is the main quantity of interest that determines the reliability and the maximum throughput that could be achieved in a communication system. Higher SINR means that the signal is stronger in relation to the noise and interference levels, which allows better performance, higher data rates and fewer retransmissions. SINR is influenced mainly by the locations of the nodes and the path loss law being used.

To study the average SINR, we model the BSs according to a specific point process that can mostly represent the network geometry. We use PPP with intensity λ to represent the BSs

locations. And without loss in generality, the analysis is conducted for a test receiver (we will call it a typical user) located at the origin. We note that according to Slivnyak's theorem [1], any location in the space has an identical statistical behavior to the origin.

The SINR of a typical user at a random distance r from its associated BS can be expressed as:

$$SINR = \frac{S}{P_n + I_r} = \frac{P_t L_p h r^{-\eta}}{P_n + P_t L_p \sum_{i \in \Phi / BS_0} g_i R_i^{-\eta}} \quad (1.9)$$

where S , P_n and I_r are the received signal, noise and interference powers respectively. P_t is the transmit power, r is the distance separating the user to its serving BS denoted by BS_0 , and η is the path loss exponent. L_p is a constant that can account for transmitter and receiver characteristics and transmission frequency, a simple formula for it can be:

$$L_p = G_t G_r \left(\frac{\text{wavelength}}{4\pi} \right)^2 \quad (1.10)$$

Other expressions from Ray tracing path loss models can be used to characterize a specific technology or specific environments. The cumulative effect of shadowing and fading in signal power domain is denoted by h and it is assumed independent and non-distorting. When the fading experienced by the signal is Rayleigh fading, the power of the fading has exponential distribution with mean $1/\mu$, which is denoted as $h \sim \exp(\mu)$. Moreover, the noise power P_n is assumed additive with constant value. Besides, the interference is written as $I_r = P_t L_p \sum_{i \in \Phi / b_0} g_i R_i^{-\eta}$ in which contains unbounded path-loss model like the received signal power. g_i is the fading value for the interference, and it follows a general distribution that can include fading, shadowing, and any other desired effects.

In the next table, we present typical used path loss exponents for some environments:

Environment Type	Path Loss Exponent η
Free space	2
Urban area cellular radio	2.7 to 3.5
Shadowed urban cellular radio	3 to 5
In building line-of-sight	1.6 to 1.8
Obstructed in building	4 to 6
Obstructed in factories	2 to 3

Table 1.1: Used path loss exponents for different environments [3].

The distances r and R_i in the SINR formula depend on the location of the nodes in the network, and thus on the point process used to model them. A first step in performance analysis is to derive the probability density function (PDF) of the distance r . If we assume that the typical user is connected to the nearest BS. This means that there is no BS nearest than the serving BS to user, which means $r < R_i$ for all $i \in \Phi_{BS \setminus b_0}$.

In the case where the transmitters locations are modeled using PPP, the pdf of r can be expressed using the null probability of a 2-D Poisson process in an area A .

$$P[r > R] = P[\text{No BS closer than } R] = e^{-\lambda\pi R^2} \quad (1.11)$$

The Cumulative Distribution Function (CDF) is given by:

$$P[r \leq R] = F_r[R] = 1 - CCDF \quad (1.12)$$

So, the Probability Density Function (PDF) will be: $f_r(r) = \frac{df_r(r)}{dr}$ resulting in:

$$f_r(r) = 2\pi\lambda r e^{-\lambda\pi r^2} \quad (1.13)$$

2. Probability of Coverage

The probability of coverage for a typical user located in the network is defined as the probability of the user receiving SINR greater than a threshold value T . The threshold value determines the starting value at which the received signal is considered useful so that the user

can decode and use it. If the received signal is below the threshold, it is considered not useful and the sent data will be unreadable. The threshold depends on the type of services delivered in the system, the ability of the receiver to extract the signal (Forward Error Correction (FEC) being used) and the needed system performance.

The probability of coverage is defined as:

$$\begin{aligned}
p_c(T, \eta, \dots) &= \mathbb{E}_r[\mathbb{P}[SINR > T|r]] = \int_{r>0} \mathbb{P}[SINR > T|r] f_r(r) dr \\
&= \int_{r>0} \mathbb{P}\left[\frac{P_t L_p h r^{-\eta}}{P_n + P_t L_p \sum_{i \in \Phi/b_0} g_i R_i^{-\eta}} > T|r\right] f_r(r) dr \\
p_c(T, \eta, \dots) &= \int_{r>0} \mathbb{P}\left[h > \frac{T}{P_t L_p} r^\eta (P_n + P_t L_p I_r)\right] f_r(r) dr
\end{aligned} \tag{1.14}$$

If the useful signal experiences Rayleigh fading, therefore the power of the fading h has exponential distribution with mean $1/\mu$. So:

$$\begin{aligned}
\mathbb{P}\left[h > \frac{T}{P_t L_p} r^\eta (P_n + P_t L_p I_r)\right] &= \mathbb{E}_{I_r}\left[\mathbb{P}\left[h > \frac{T}{P_t L_p} r^\eta (P_n + P_t L_p I_r)\right|r, I_r\right] \\
&= \mathbb{E}_{I_r}\left[\exp\left(-\mu \frac{T}{P_t L_p} r^\eta (P_n + P_t L_p I_r)\right)\right] \\
\mathbb{P}\left[h > \frac{T}{P_t L_p} r^\eta (P_n + P_t L_p I_r)\right] &= e^{-\mu \frac{T}{P_t L_p} r^\eta P_n} L_{I_r}(\mu T r^\eta)
\end{aligned} \tag{1.15}$$

The Laplace Transform (LT) for the interference appears naturally into the formula for the probability of coverage. So, even if we can't know or write a formula for the distribution of interference experienced in a network, we can still evaluate the LT and get the results for the

probability of coverage. Now, the LT of the interference I_r should be evaluated. It is evaluated at $s = \mu T r^\eta$ conditioned on the distance to the nearest BS from the origin. It is equal to:

$$\begin{aligned} L_{I_r}(s) &= \mathbb{E}_{I_r}[e^{-sI_r}] = \mathbb{E}_{\Phi, g, i} \left[\exp \left(-s \sum_{i \in \Phi \setminus \{b_0\}} g_i R_i^{-\eta} \right) \right] \\ &= \mathbb{E}_{\Phi, \{g_i\}} \left[\prod_{i \in \Phi \setminus \{b_0\}} \exp(-s g_i R_i^{-\eta}) \right] = \mathbb{E}_{\Phi} \left[\prod_{i \in \Phi \setminus \{b_0\}} \mathbb{E}_g[\exp(-s g R_i^{-\eta})] \right] \end{aligned}$$

where, as stated before, g is the fading power for the interfered signal and it has arbitrary but identical distribution for all I , and $R_i^{-\eta}$ is the path loss model. The last term follows from the independence of the fading. We note that the 2 variables R and g are independent.

In the normal case, when homogenous PPP is used we can write the formula as:

$$\begin{aligned} L_{I_r}(s) &= \mathbb{E}_{\Phi} \left[\prod_{i \in \Phi \setminus \{b_0\}} \mathbb{E}_g[\exp(-s g R_i^{-\eta})] \right] = \mathbb{E}_{\Phi} \left[\prod_{i \in \Phi \setminus \{b_0\}} \mathbb{E}_g[\exp(-s g R_i^{-\eta})] \right] \\ L_{I_r}(s) &= \exp \left(-2\pi\lambda_i \int_r^\infty (1 - \mathbb{E}_g[\exp(-s g x^{-\eta})]) x dx \right) \end{aligned} \quad (1.16)$$

Where this step follows from the probability generating functional (PGFL) of the PPP of intensity λ . The formula is $\mathbb{E}_{\Phi}[\prod_{x \in \Phi} f(x)] = \exp(-\lambda \int_{\mathbb{R}^2} (1 - f(x)) dx)$

After that we substitute $s = \mu T r^\eta$, and we use

$$\mathbb{E}_g[\exp(-\mu T r^\eta g x^{-\eta})] = \int_{g>0} \exp(-\mu T r^\eta g x^{-\eta}) f(g) dg \quad (1.17)$$

where $f(g)$ is the pdf for the fading g , and it depends on the type of fading experienced by the interfering signal. Important to realize, x and g are independent. After evaluating the Laplace transform, the resulted expression will be in terms of μ , T , r , η , g , and other parameters related

to the distribution of λ . And after the substitution of the LT in equation (1.15), the probability of coverage is obtained.

3. Mean achievable Rate

The average achievable rate is another important metric related to the system performance. It is indeed related to the density and the location of the transmitters. We derive the formula for the rate for the network users such that they achieve the Shannon bound for their instantaneous SINR. Thus, we study the mean achievable rate for a typical user, which is an outage-based metric that is used in stochastic geometry. The unit of measure is in nats/Hz because we are using \ln in the formula, and we have $1 \text{ bit} = \ln(2) \sim 0.69315 \text{ nats}$. The presented results and formulas are for the Rayleigh fading i.e. exponential distribution for the fading power.

The mean achievable rate for a typical user is:

$$\tau = \mathbb{E}[\ln(1 + SINR)] \quad (1.18)$$

In a PPP network, the ergodic rate for a typical user depends on the spatial PPP and the fading distribution.

$$\begin{aligned} \tau = \mathbb{E}[\ln(1 + SINR)] &= \int_{r>0} \mathbb{E} \left[\ln \left(1 + \frac{P_t L_p h r^{-\eta}}{P_n + I_t} \right) \right] f_r(r) dr \\ &= \int_{r>0} f_r(r) \int_{t>0} \mathbb{P} \left[\ln \left(1 + \frac{P_t L_p h r^{-\eta}}{P_n + P_t L_p I_r} \right) > t \right] dt dr \\ &= \int_{r>0} f_r(r) \int_{t>0} \mathbb{P} \left[\frac{P_t L_p h r^{-\eta}}{P_n + P_t L_p I_r} > e^t - 1 \right] dt dr \end{aligned}$$

$$= \int_{r>0} f_r(r) \int_{t>0} \mathbb{P} \left[h > \frac{r^\eta}{P_t L_p} (P_n + P_t L_p I_r)(e^t - 1) \right] dt dr \quad (1.19)$$

Using the fact that $h \sim \exp(\mu)$, i.e. signal experiences Rayleigh fading.

$$\begin{aligned} \tau &= \int_{r>0} f_r(r) \int_{t>0} \mathbb{E} \left[\exp \left(-\mu \frac{r^\eta}{P_t L_p} (P_n + P_t L_p I_r)(e^t - 1) \right) \right] dt dr \\ &= \int_{r>0} f_r(r) \int_{t>0} e^{-\mu r^\eta \sigma^2 (e^t - 1)} L_{I_r}(\mu r^\eta (e^t - 1)) dt dr \end{aligned} \quad (1.20)$$

C. Literature

In this section, we present a general literature about stochastic geometry for wireless networks. In the literature, the transmitters' locations have been modeled using different mathematical models. The standard assumption is that the transmitters, BSs or access nodes, are represented by idealized points in some space, usually in a plane \mathbb{R}^2 , in which they form a stochastic or random structure known as a spatial point process. At first, a two-dimensional hexagonal grid model was used. The grid model at first glance consists an ideal and logical model for BSs distribution, but in fact this is far from the real scenarios. In grid model, the area is sectorized into grids and each transmitter is located at the center or on one side of the grid. Unfortunately, SINR formulas resulted from such models are hard to estimate and depend on multiple random variables [4].

Several point processes have been also suggested. Among these, the most frequently and famous used one is the homogeneous PPP. PPP is commonly used as a mathematical model across numerous disciplines. It simplifies the analysis and provides insights about the operation of networks. On the other side, PPP fails to represent some network configurations study, like

hotspot, heterogenous cellular networks, and other network configurations or scenarios that contains some clustering properties or needed minimum distance between nodes [5].

Many researches have applied stochastic geometry tools in wireless networks. Such works are present in cellular clustered networks [6][7], narrowband and ultra-wideband wireless nodes [8], cognitive radio [9][10], femtocells [11][12] and relay networks [13][14]. The authors in [15] and [16] provided a wide overview about stochastic geometry for wireless networks. They presented a comprehensive survey for stochastic geometry models for single-tier as well as multi-tier and cognitive cellular wireless networks. Also, different important techniques for modeling interference are presented in general. This has been complemented by the analysis and modeling of interference in different works [17][18].

Analytically speaking, a good analysis for coverage and rate in downlink for cellular networks is presented in [19]. The authors used PPP to model the BS locations by deriving quickly-computable integrals for SINR and desired received signal power distribution. Some of the works like in [20] evaluated the uplink cellular networks. In uplink analysis, the locations of the mobile users are modeled as PPP and then the BSs corresponding to each mobile user is located uniformly in its Voronoi cell. Compared to the downlink analysis, the uplink differs in many key features. For example, the dependence between user and BSs point process is different.

A simple Poisson Tree model for analyzing a hierarchical backhaul of a hyper-dense heterogeneous network is introduced in [21]. The model contains traffic concentrators, BSs (Macro and small) and users. The aim of the model is to study the impact of the finite user density (load) on the network performance and the distribution of the SINR. A key element here is modeling the impact of the backhaul on the network. The distributional properties of the interference are derived in [22] using PCP (Matern and Thomas). The Interference complementary cumulative distribution function CCDF is obtained for different path loss

models and different types of fading using Monte Carlo Simulation. The authors also showed that when the transmitter-receiver distance is large, the success probability is greater than that of a Poisson arrangement. In addition, [23] and [24] presented an analysis for the coverage analysis for the scenario of BS-centric user clustering using MCP. The aim was to account for the influence of BS-centric user clustering in small cells.

A tractable framework for SINR analysis in downlink heterogeneous cellular networks with flexible cell association policies is developed in [25]. What is remarkable in this work is that the authors assumed the user connects to the BS that offers the maximum long-term averaged received power (with biasing), and not the BS that offers the highest SINR. Moreover, simple approximate approaches to the SIR distribution of general heterogeneous cellular networks are presented [26].

PPP and hexagonal model are compared in [27] with real cellular networks in urban areas; the data used for the comparison is taken from OpenCellID community project [28]. This project consists a collaborative community project that collects GPS positions of cell towers, available for commercial and private purposes free of charge. The data supplied may have some limitations compared to data obtained from network operators, but is very useful and can be used many works. Results showed that PPP model is more accurate than the hexagonal grid model. Recently, it has been shown [29] that heavy tailed distributions can most precisely fit the actual BS spatial density distribution. Among many distributions (Poisson, Lognormal, Generalized Pareto, etc), α -stable distribution was the best distribution that can fit for the density of BSs and matches the empirical PDF. These results were obtained based on realistic deployment information of BSs from on-operating cellular networks. Another study was done in [30] on data for real deployed BS across urban, rural, and coastal zones. The results have shown that the BS spatial distributions follow α -stable distribution in urban scenarios, and Lognormal and Weibull distributions in rural and coastal scenarios. Furthermore, the authors

in [32] considered two realistic case studies from a European country (one urban and one rural). Then, they computed the spatial distribution of the BSs and they fit the candidate distributions to the real data. They take into account Poisson, Pareto, Lognormal, Weibull and α -Stable as possible candidates. Results showed that lognormal is the best distribution in a rural scenario, while the α -Stable is the most realistic one in an urban case.

CHAPTER II

DENSITY DISTRIBUTION OF BASE STATIONS

In this chapter, we take data for the Evolved NodeB (eNB) locations from real deployed LTE networks in specific areas containing highly populated urban cities. We start our analysis by obtaining the spatial density distribution of these eNBs. Then, we try to fit this distribution with candidate distributions, in which we determine the distribution that best fits and gives the lowest Root Mean Square Error (RMSE). The aim from this procedure is to use this fitted density distribution in a framework that derives a general performance metrics for the whole huge studied area. These metrics give a general idea for the network operators about how the spatial density distribution can affect the network in general.

A. Density Distribution

We present some statistical analysis for the spatial density distribution for real deployed LTE networks of Evolved NodeB (eNB). These networks are deployed in urban areas and contain big cities. To conduct the analysis, we use an open source code in [29][30], and data taken from the OpenCellID community project [28]. The aim from this analysis is to check some of the distributions used for modeling the density of Base Stations (BS) in a cellular network and to shed the light on the importance of the spatial density distribution in network study. With this intention, the main problem here turns out to find the best suitable Probability Density Function (PDF) of the spatial density distribution in each network. Then, this information can be used to develop a network model that considers the density distribution.

To achieve this, we take the locations of eNBs in three main areas, two of them contain big city with high population. We start the analysis by calculating the densities in a randomly chosen $2 \times 2 \text{ km}^2$ regions in each area. As seen in the dimension, the regions are of square

shape, where we take 10000 randomly chosen regions with random boundaries that can be any boundary inside the studied area. The reason for choosing the size of the region as $2 \times 2 \text{ km}^2$ is that we see it as a good size to account for the non-negligible interference signals for a typical user located at the center of the region taken in the cellular network. Then, the resulted densities are compared to potential candidate distributions. Mainly, and coupled with the literature we consider the following candidates: α -stable, Poisson, lognormal, Generalized Pareto, and Weibull distribution.

1. Area 1

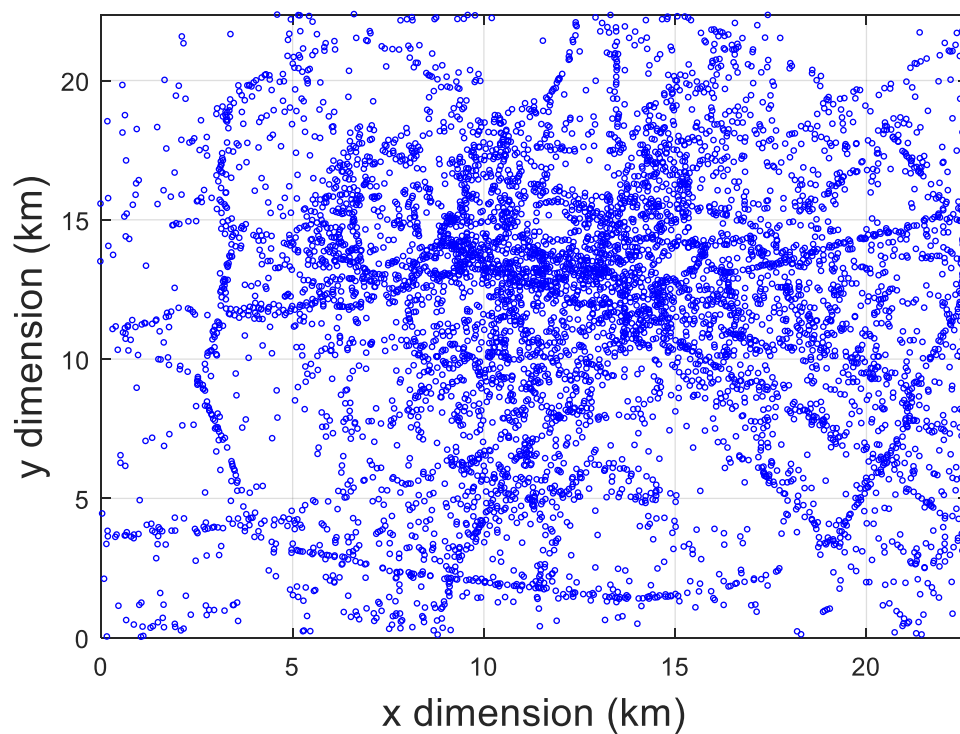


Figure 2.1: BS towers across area 1.

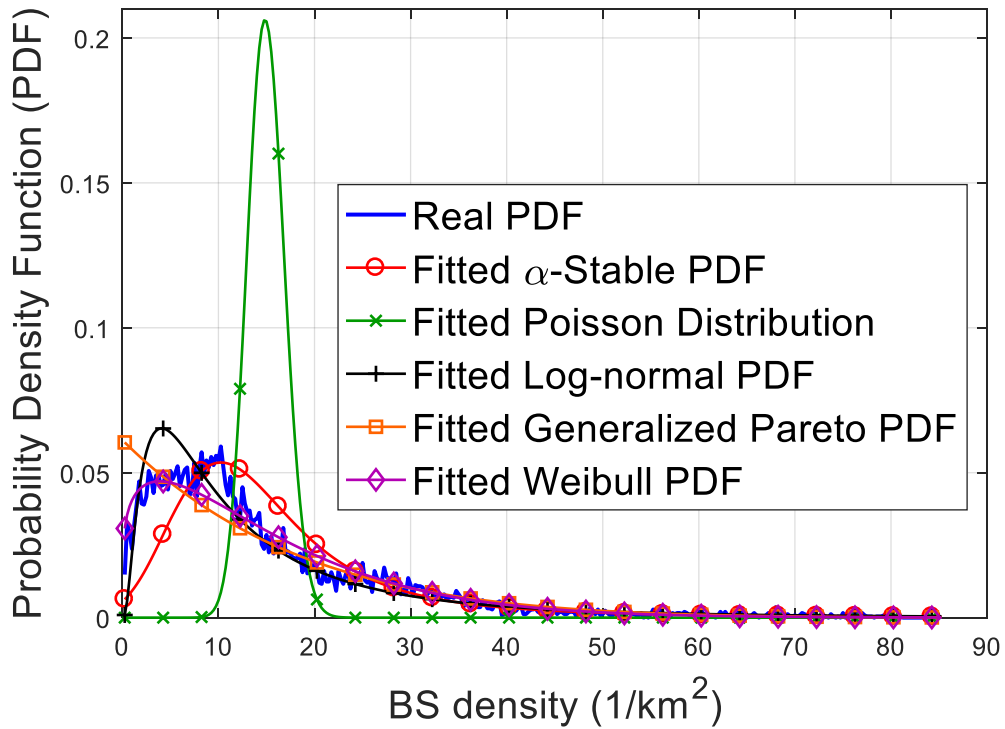


Figure 2.2: BS density distribution in area 1 for $2 \times 2 \text{ km}^2$ randomly chosen regions.

We have considered the area shown in Figure 2.1, while the results of the BS density distribution, according to the described scenario, are shown in Figure 2.2. From the graph, the Weibull distribution gives the best fitting shape for this area. Thus, on average, we can assume that a developed model using Weibull for the spatial density will better fit as a representation for this area. Obviously, this result is clearly seen by analyzing the Root Mean Square Error (RMSE) between the data and the fitted distribution, where the Weibull distribution has the smallest RMSE. In Table 2.1, we show different RMSE values with the corresponding distribution fitted parameters.

Legend	α -Stable	PPP	Lognormal	GPareto	Weibull
RMSE	0.007463	0.037801	0.004999	0.006096	0.003889
Fitted Parameters	$\alpha = 1.321487$ $\beta = 1$ $\gamma = 5.321872$ $\delta = 21.163042$	$\lambda = 59.9031$	<i>mean</i> $= 2.325125$ <i>std. deviation</i> $= 0.95672$	<i>tail index (shape)</i> $= -0.108722$ <i>scale</i> $= 16.578036$	<i>scale</i> $= 16.034311$ <i>shape</i> $= 1.217128$

Table 2.1: RMSE results for different distributions for area 1.

2. Area 2

We continue our analysis for another area of bigger size that contains lower density regions and many empty locations.

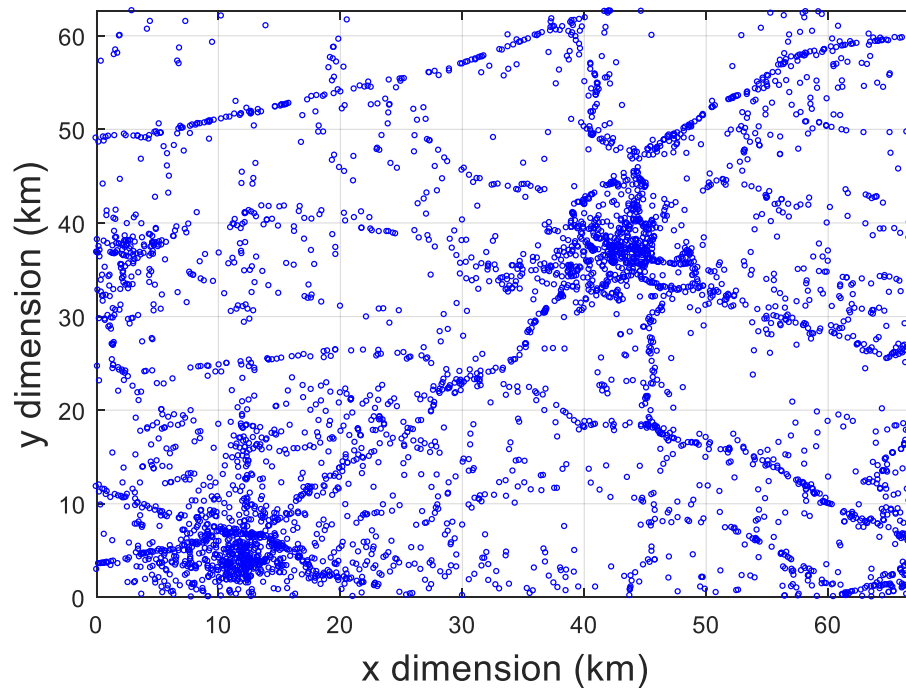


Figure 2.3: BS towers across area 2.

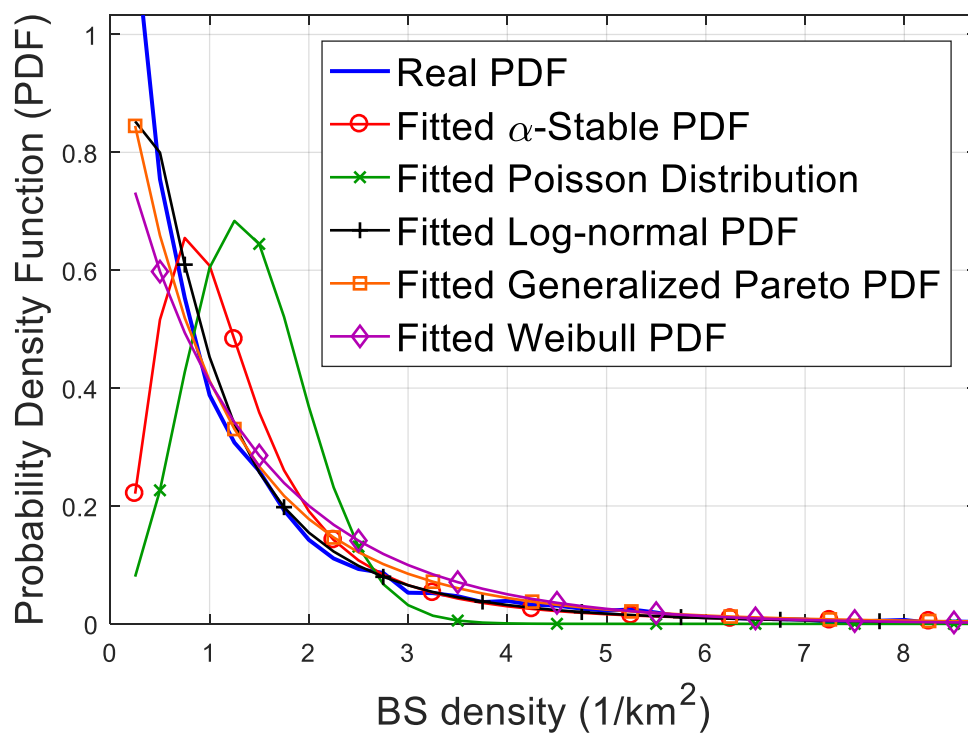


Figure 2.4: BS density distribution in area 2 for $2 \times 2 \text{ km}^2$ randomly chosen regions.

Again, by analyzing Figure 2.4 and the RMSE in Table 2.2, we can see that the Lognormal and Generalized Pareto are the most accurate among the other distributions. Moreover, we can see that most of the candidate distributions are giving higher RMSE values than area 1.

Legend	α -Stable	PPP	Lognormal	GPareto	Weibull
RMSE	0.115955	0.159556	0.036942	0.038822	0.054487
Fitted Parameters	$\alpha = 1.146562$ $\beta = 1$ $\gamma = 0.440456$ $\delta = 2.819257$	$\lambda = 5.656916$	<i>mean</i> = -0.175598 <i>std. deviation</i> = 0.975887	<i>tail index (shape)</i> = 0.196047 <i>scale</i> = 1.130071	<i>scale</i> = 1.391299 <i>shape</i> = 0.969809

Table 2.2: RMSE results for different distributions for area 2.

3. Area 3

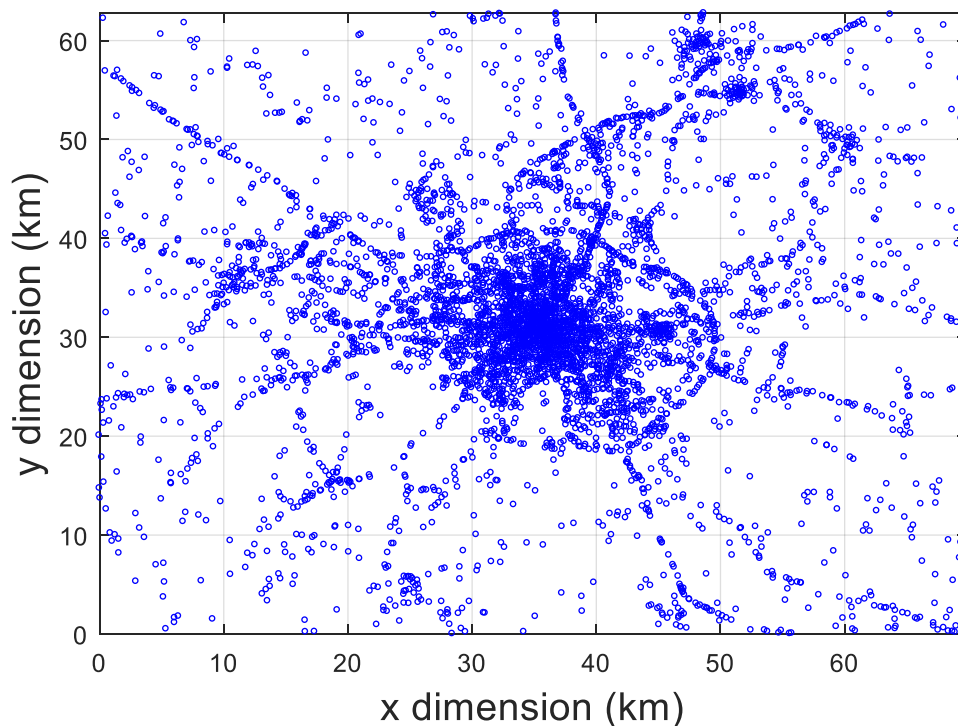


Figure 2.5: BS towers across area 3.

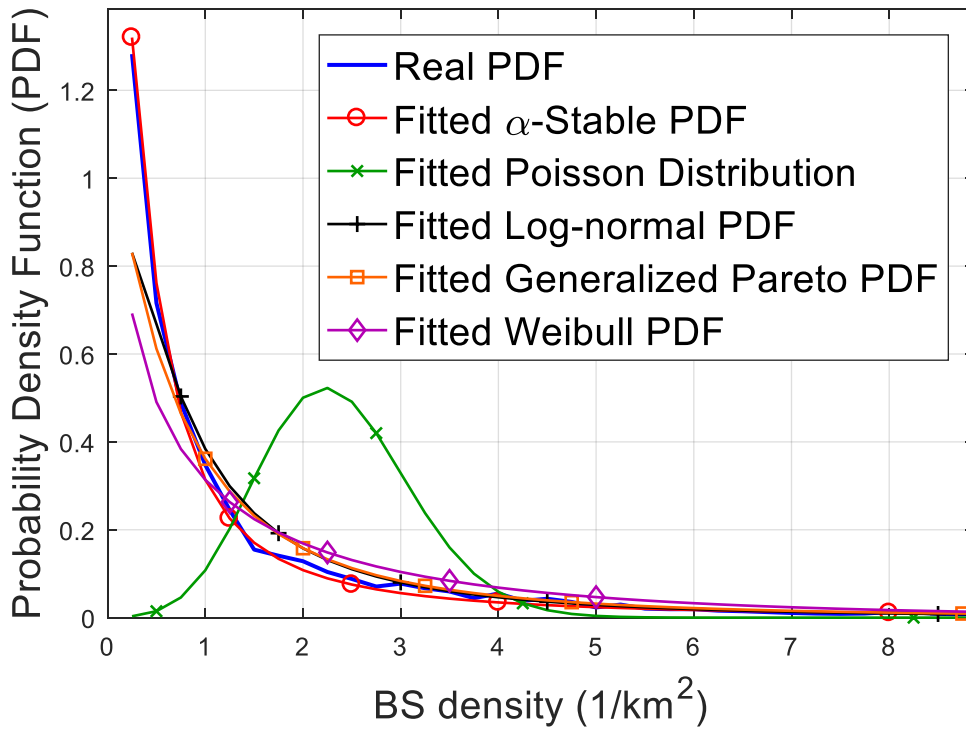


Figure 2.6: BS density distribution in area 3 for $2 \times 2 \text{ km}^2$ randomly chosen regions.

In the third analyzed area, the fitted shape and the RMSE in Table 2.3 show the accuracy of the α -stable distribution. Undoubtedly, the fitted parameters for this distribution are very close to the subclass of the α -stable distribution, which is called the Lévy distribution which has the parameters $\alpha = 0.5$ and $\beta = 1$.

This simple analysis shows that the BS density does not necessarily have the same distribution in all the networks of different sizes, type (urban, rural, ...) and studied regions. Also, it shows that the information about the density distribution is important to give an accurate model for a whole network (not just a small area). This means that a deeper analysis of the different situations should be done. This will be achieved in the next sections.

Legend	α -Stable	PPP	Lognormal	GPareto	Weibull
RMSE	0.004780	0.090961	0.024048	0.024370	0.033486
Fitted Parameters	$\alpha = 0.643739$ $\beta = 1$ $\gamma = 0.309647$ $\delta = -0.145156$	$\lambda = 9.399914$	<i>mean</i> $= -0.059201$ <i>std. deviation</i> $= 1.195194$	<i>tail index (shape)</i> $= 0.544306$ <i>scale</i> $= 1.062577$	<i>scale</i> $= 1.779881$ <i>shape</i> $= 0.730365$

Table 2.3: RMSE results for different distributions for area 3.

B. Analysis: Coverage and Rate

In the previous section, we have seen the importance of the spatial density distribution and we have shed the light on some candidate distributions that can be used to model the density. Hence, we use this information about the best fitted distributions in a network model to study the performance of such network.

1. Network Model

Modeling the same scenario described in the previous section is a complex operation. As an illustration, the interference experienced by a user located in a specific region will depend on many things related to this region, like its shape, size, density and the location of the user within this region. Besides, many questions arise. How many regions should we consider and what about their boundaries, should we choose them with overlaps or not? Also, in a developed mathematical model, should we consider the interference from the neighboring regions or assume it totally negligible? However, this imposes an important disadvantage of such developed model according to this specific scenario. This disadvantage is that such model is not stationary in space, so the different performance metrics depend on the spatial location of the user. Consequently, the notion of “typicality” of the user does not apply. For that, we propose to use a different model for the locations of the BSs. This model uses PPP but with a random density, which is a good representation for the average performance of the network. Given these points, we suppose that the average density of the network is a non-negative number taken from a specific distribution. Such a network model is a PPP conditioned on the intensity measure, and is referred to as a Cox process or doubly stochastic Poisson process [2].

We consider a baseline bi-directional cellular network with BSs arranged as a Poisson Point Process (PPP) $\Phi \subset \mathbb{R}^2$ with density λ_i . Additionally, we use three candidate distributions

to model the density of the PPP. More precisely, we consider the Lévy distribution (a specific case of the α -Stable distribution), Generalized Pareto distribution and the Weibull distribution. We note that the α -Stable distribution does not have a closed form expression for its PDF, but it contains a family of distributions for specific parameters that have PDF closed form such as the Lévy distribution. Moreover, we assume that each BS is using the same transmit power P , and the BSs are using omnidirectional antennas, with a single transmit and single receive antenna. Furthermore, the users are associated with the nearest BS that is at distance r and is called the serving BS and denoted by BS_0 .

2. Signal to Interference plus Noise Ratio

The SINR of a typical user located at the origin and at a random distance r from its associated BS can be expressed as:

$$SINR = \frac{S}{P_n + I_r} = \frac{P_t L_p h r^{-\eta}}{P_n + P_t L_p \sum_{i \in \Phi / BS_0} g_i R_i^{-\eta}} \quad (2.1)$$

where S, P_n and I_r are the received signal, noise and interference powers respectively. The cumulative effect of fading in the signal power domain is denoted by h . In our work, we focus on the case when the signal S experiences Rayleigh fading, which means h follows exponential distribution with mean $1/\mu$. I_r is the aggregate interference from the other BSs having distances R_i to the typical user. We assume a simple or a singular path loss model, η is the PLE such that $\eta > 2$, and g_i is the fading value for the interfering signals from the BSs. P_t is the transmit power of the BSs, and L_p is a constant that depends on the characteristics of the transmitter, receiver and the frequency used. Since each user communicates with the closest BS, no other BS can be closer than r . So, to get the PDF of r , we first express the Complementary Cumulative Distribution Function (CCDF) using the null probability of a 2-D PPP in a small area A_i with density λ_i .

$$P[r > R/\lambda = \lambda_i] = P[\text{no BS closer than } R/\lambda = \lambda_i] = e^{-\lambda_i \pi R^2} \quad (2.2)$$

Then, we can write:

$$p(r > R) = \int f(x/y_i) f(y_i) = \int p(r > R/\lambda = \lambda_i) p(\lambda = \lambda_i) d\lambda \quad (2.3)$$

a. Lévy Distribution:

The Lévy distribution is a subclass of the α -Stable distribution family, and it is a distribution that has four parameters, that are the stability $\alpha = 0.5$, skewness $\beta = 1$, scale $\gamma \in (0, \infty)$ and location parameter $\delta \in (-\infty, \infty)$. Moreover, the Lévy distribution has a closed form expression for the PDF, which is defined as follows:

$$f(\lambda) = \sqrt{\frac{\gamma}{2\pi}} \frac{1}{(\lambda - \delta)^{3/2}} \exp\left(-\frac{\gamma}{2(\lambda - \delta)}\right) \quad (2.4)$$

For our calculations, we will use the Lévy distribution with $\delta = 0$ to represent the density distribution. Thus, the CCDF becomes:

$$\begin{aligned} P[r > R] &= \int_0^\infty e^{-\lambda \pi R^2} p(\lambda = \lambda_i) d\lambda = \int_0^\infty e^{-\lambda \pi R^2} \sqrt{\frac{\gamma}{2\pi}} \frac{1}{\lambda^{3/2}} \exp\left(-\frac{\gamma}{2\lambda}\right) = \\ &= \frac{e^{-\pi \delta R^2}}{2} \left[e^{-\sqrt{2\gamma\pi}R} \left(\operatorname{erf}\left(\frac{-2\sqrt{\pi}R\lambda + \sqrt{2\gamma}}{2\sqrt{\lambda}}\right) + 1 \right) + e^{\sqrt{2\gamma\pi}R} \left(\operatorname{erf}\left(\frac{2\sqrt{\pi}R\lambda + \sqrt{2\gamma}}{2\sqrt{\lambda}}\right) - 1 \right) \right]_0^\infty = \\ &= e^{-\sqrt{2\gamma\pi}R} \end{aligned} \quad (2.5)$$

where $\operatorname{erf}(z) = \frac{2}{\sqrt{\pi}} \int_0^z e^{-t^2} dt$ is the error function.

The CDF is given by:

$$P[r \leq R] = F_r(R) = 1 - CCDF = 1 - e^{-\sqrt{2\gamma\pi}R}$$

This leads to the PDF:

$$f_r(r) = \frac{dF_r(r)}{dr} = \sqrt{2\pi\gamma} e^{-\sqrt{2\gamma\pi}r} \quad (2.6)$$

b. Generalized Pareto Distribution:

The PDF of the GPareto distribution is defined as follows:

$$f(\lambda) = \frac{1}{\gamma} \left(1 + k \left(\frac{\lambda - \theta}{\gamma} \right) \right)^{-1 - \frac{1}{k}} \quad (2.7)$$

where $\theta \in (-\infty, \infty)$ is the location (or the threshold) of the distribution, $\gamma \in (0, \infty)$ is the scale parameter, and $k \in (-\infty, \infty)$ is the shape parameter. In our analysis, the density of the transmitters can't be negative, so the threshold θ is set to zero.

Applying the same calculations where $\theta = 0$, we get the following PDF for the distance r :

$$f_r(r) = \frac{1}{\gamma} \left[\frac{2\gamma^2(k+1)\pi^{\frac{1}{k}} r e^{-\frac{\pi\gamma r^2}{k}} \left(\frac{\gamma r^2}{k}\right)^{\frac{1}{k}-1} \Gamma\left(-\frac{k+1}{k}, \frac{\pi r^2 \gamma}{k}\right)}{k^4} - \frac{2\gamma^2(k+1)r \left(\frac{\gamma r^2}{k}\right)^{-2}}{\pi k^3} + \frac{2\gamma^2(k+1)\pi^{\frac{1}{k}+1} r e^{-\frac{\pi\gamma r^2}{k}} \left(\frac{\gamma r^2}{k}\right)^{\frac{1}{k}} \Gamma\left(-\frac{k+1}{k}, \frac{\pi r^2 \gamma}{k}\right)}{k^3} + \frac{2}{\pi r^3} \right] \quad (2.8)$$

c. Weibull Distribution:

The PDF of the Weibull distribution is defined as:

$$f(\lambda) = \begin{cases} \frac{n}{m} \left(\frac{\lambda}{m}\right)^{n-1} \exp\left(-\left(\frac{\lambda}{m}\right)^n\right), & \lambda \geq 0 \\ 0, & \lambda < 0 \end{cases} \quad (2.9)$$

where $m \in (0, \infty)$ is the scale of the distribution and $n \in (0, \infty)$ is the shape of the distribution.

Working with the distribution with variables m and n alongside with our calculations leads to unsolvable mathematical formulas. For that, in our calculations we assume the shape $n = 1$ and variable scale m .

Hence, the PDF for the distance r :

$$f_r(r) = \frac{2\pi mr}{(1+\pi mr^2)^2} \quad (2.10)$$

C. Network Coverage

The probability of coverage for a typical user located in the network is defined as the probability of the user receiving SINR greater than a threshold value T . The threshold value determines the starting value at which the received signal is considered useful so that the user can decode and use it. If the received signal is below the threshold, it is considered not useful and the sent data will be unreadable. The threshold depends on the type of services delivered in the system, the ability of the receiver to extract the signal and the needed system performance. The probability of coverage is defined as follows:

$$p_c = \mathbb{E}_r[\mathbb{P}[SINR > T|r]] \quad (2.11)$$

In Table 2.4, we provide the probability of coverage for a typical user located at the center of the network. In this table, we are assuming that the fading coefficient g has an arbitrary distribution.

Density Distribution	Coverage Probability for the case of an arbitrary fading distribution
Lévy	$p_c(T, \gamma, \delta = 0, \eta, \mu, \sigma) \quad (2.12)$ $= \sqrt{2\pi\gamma} \int_0^{\infty} \exp\left(-\mu \frac{T}{P_t L_p} r^\eta P_n - \sqrt{2\pi\gamma} r - \sqrt{2\gamma}(\xi_1)^{1/2}\right) dr$ <p>with $\xi_1 = \pi r^2 - \frac{2\pi(\mu T)^{2/\eta} r^2}{\eta} \int_0^{\infty} g^{2/\eta} \left[\Gamma\left(-\frac{2}{\eta}, gT\mu\right) - \Gamma\left(-\frac{2}{\eta}\right) \right] f(g) dg$</p>

GPareto	$p_c(T, \gamma, k, \eta, \mu, \sigma) \tag{2.13}$ $= \frac{1}{\gamma^2} \int_0^\infty e^{-\mu \frac{T}{\gamma L_p} r^\eta P_n} \left[\frac{1}{\xi_1} - \frac{\gamma(k+1)e^{\frac{\gamma \xi_1}{k}} \left(\frac{\gamma}{k} \xi_1\right)^{\frac{1}{k}} \Gamma\left(-\frac{k+1}{k}, \frac{\gamma}{k} \xi_1\right)}{k^2} \right] \left[-\frac{2\gamma^2(k+1)r \left(\frac{\gamma r^2}{k}\right)^{-2}}{\pi k^3} + \frac{2\gamma^2(k+1)\pi^{\frac{1}{k}} r e^{\frac{\pi \gamma r^2}{k}} \left(\frac{\gamma r^2}{k}\right)^{\frac{1}{k}-1} \Gamma\left(-\frac{k+1}{k}, \frac{\pi r^2 \gamma}{k}\right)}{k^4} + \frac{2\gamma^2(k+1)\pi^{\frac{1}{k}+1} r e^{\frac{\pi \gamma r^2}{k}} \left(\frac{\gamma r^2}{k}\right)^{\frac{1}{k}} \Gamma\left(-\frac{k+1}{k}, \frac{\pi r^2 \gamma}{k}\right)}{k^3} + \frac{2}{\pi r^3} \right] dr$
Weibull	$p_c(T, a, \eta, \mu, \sigma) = \int_0^\infty e^{-\mu \frac{T}{\gamma L_p} r^\eta P_n} \left(\frac{1}{1+a \xi_1} \right) \frac{2\pi a r}{(1+\pi a r^2)^2} dr \tag{2.14}$

Table 2.4: Probability of coverage for the different considered density distributions for an arbitrary distribution for g .

Proof: See Appendix II.A.

When the interfering signals experience Rayleigh fading, i.e. power of the fading follows exponential distribution of mean $1/\mu$, the terms for the fading become:

$$\xi_1 = \pi r^2 T^{2/\eta} \int_{T^{-2/\eta}}^\infty \frac{1}{y^{\eta/2} + 1} dy \tag{2.15}$$

This can be also verified by re-solving the Laplace transform of the interference in which we have $\mathbb{E}_g[\exp(-sgR_i^{-\eta})] = \frac{\mu}{\mu + sR_i^{-\eta}}$.

D. Mean Achievable Rate

The average data rate is another important metric related to system performance. It is indeed related to the density and location of the transmitters. We derive the formula for the data rate for each user such that they achieve the Shannon bound for their instantaneous SINR. Thus, we study the mean achievable rate for a typical user, which is an outage-based metric used in stochastic geometry. The mean achievable rate is defined as:

$$\tau = \mathbb{E}[\ln(1 + SINR)] \quad (2.16)$$

In Table 2.5, we present the mean achievable for the network model with location of BSs arranged as PPP with random λ . The results are for the Rayleigh fading case i.e. exponential distribution for fading power.

Density Distribution	Mean achievable rate for the case of Rayleigh fading
Lévy	$\tau = \sqrt{2\pi\gamma} \int_0^\infty \int_0^\infty \exp\left(-\mu \frac{P_n}{P_t L_p} r^\eta (e^t - 1) - \sqrt{2\pi\gamma} r - \sqrt{2\gamma}(\xi_2)^{1/2}\right) dt dr \quad (2.17)$ <p>With $\xi_2 = \pi r^2 (e^t - 1)^{2/\eta} \int_{(e^t - 1)^{-2/\eta}}^\infty \frac{1}{y^{\eta/2 + 1}} dy$</p>
GPareto	$\tau = \frac{1}{\gamma^2} \int_0^\infty \left[\frac{2\gamma^2(k+1)\pi^{\frac{1}{k}} r e^{\frac{\pi\gamma r^2}{k}} \left(\frac{\gamma r^2}{k}\right)^{\frac{1}{k}-1} \Gamma\left(-\frac{k+1}{k}, \frac{\pi r^2 \gamma}{k}\right)}{k^4} - \frac{2\gamma^2(k+1)r \left(\frac{\gamma r^2}{k}\right)^{-2}}{\pi k^3} \right. \quad (2.18)$ $+ \frac{2\gamma^2(k+1)\pi^{\frac{1}{k+1}} r e^{\frac{\pi\gamma r^2}{k}} \left(\frac{\gamma r^2}{k}\right)^{\frac{1}{k}} \Gamma\left(-\frac{k+1}{k}, \frac{\pi r^2 \gamma}{k}\right)}{k^3}$ $+ \frac{2}{\pi r^3} \int_0^\infty e^{-\mu r^\eta \frac{P_n}{P_t L_p} (e^t - 1)} \left[\frac{1}{\xi_2} \right.$ $\left. - \frac{\gamma(k+1)e^{\frac{\gamma \xi_2}{k}} \left(\frac{\gamma}{k} \xi_2\right)^{\frac{1}{k}} \Gamma\left(-\frac{k+1}{k}, \frac{\gamma}{k} \xi_2\right)}{k^2} \right] dt dr$
Weibull	$\tau = \int_0^\infty \frac{2\pi a r}{(\pi a r^2 + 1)^2} \int_0^\infty \frac{\exp\left(-\mu r^\eta \frac{P_n}{P_t L_p} (e^t - 1)\right)}{1 + a \xi_2} dt dr \quad (2.19)$

Table 2.5: Mean achievable rate for the different considered density distributions when interference experiences Rayleigh fading.

Proof: See Appendix II.B.

E. Numerical Results

From the simulation in section II, we can see that the Generalized Pareto distribution is the most accurate among the candidates in area 2 (classified as rural or a mixed urban-rural area as it contains empty regions). The other two distributions were the best in areas 1 and 2, classified as urban dense areas. In this section, we present some simulation results to give an

overview about the changes in the performance metrics. Unless specified in the figures, the evaluation is done using the simulation parameters specified in Table 2.6:

Parameter	Value
P_t	15 dBm
f, G_t, G_r	1800 MHz, 10 dB, 5 dB
L_p	$\frac{G_t G_r}{(4\pi)^2} \left(\frac{c}{f}\right)^2$
P_n	-20 dBm
μ	1

Table 2.6: Common simulation parameters; unless specified.

where G_t and G_r are the gains of the BS and the typical user respectively, f is the operating frequency, and c is the speed of light.

We note that for the Generalized Pareto case, the mean data rate does not simulate because it requires huge amount of computation time. For the other two models, we have simulated different use cases for both the coverage probability and the mean achievable rate for different η . In Figure 2.7, we plot the probability of coverage when the density follows Levy distribution for $\gamma = 0.3$ and $\gamma = 1.2$ (dashed). The distribution parameters are near the values for the fitted α -stable distribution in Area 3 in Section II. Comparatively, we see how the coverage increases with γ . This increase is less observable at lower noise power P_n , because when there is no noise, the distance from the user to serving BS and to the nearest interferer both scales and cancel each other (increasing the density also increases the interference power). This is better observed when we plot the mean achievable rate which, at small P_n , does not change with the density. Important to realize, this is consistent with the literature about the models using the homogeneous PPP network model. However, surely this result is not the case for a single studied user at a specific fixed distance to their serving BS independent from the density of the BSs.

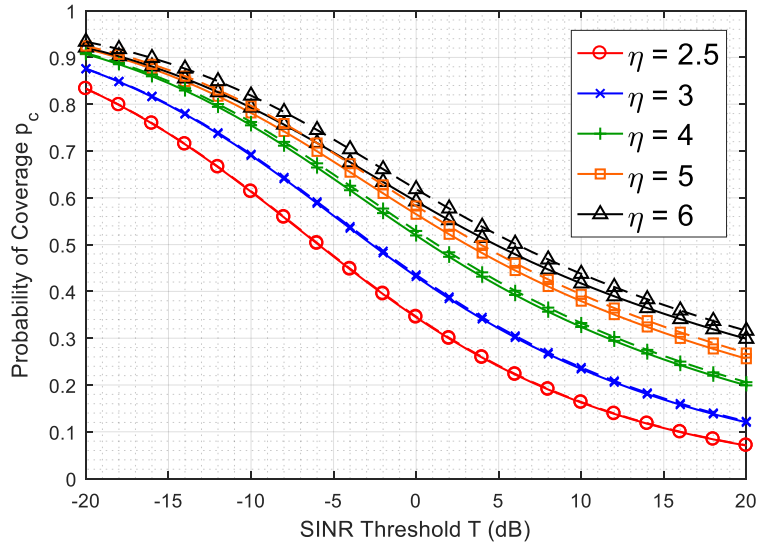


Figure 2.7: Probability of coverage when the density follows Levy distribution, and the interference experiences Rayleigh fading. Normal plot ($\gamma = 0.3$), dashed ($\gamma = 1.2$).

Similarly, we plot the coverage probability when the density follows the Weibull distribution in Figure 2.8. The figure shows the increase in the coverage when m increases from 0.5 to 20. Moreover, in Figure 2.9 we show the results when the density follows the Generalized Pareto distribution. The parameters' values are near those obtained in the fitting in Section II. As seen in the figures, the coverage shape changed because we have changed two parameters for the distribution.

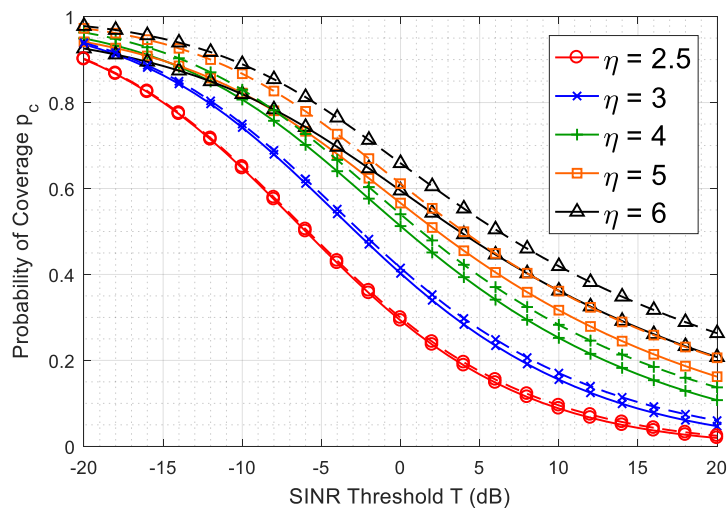


Figure 2.8: Probability of coverage when density follows Weibull distribution (shape $n=1$), and the interference experiences Rayleigh fading. Normal plot ($m = 0.5$), dashed ($m = 20$).

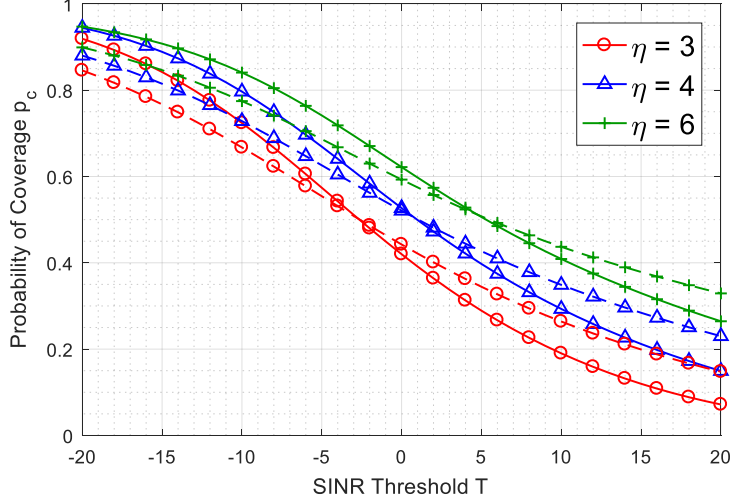


Figure 2.9: Probability of coverage when the density follows Generalized Pareto distribution, and the interference experiences Rayleigh fading. Normal plot ($\gamma = 1, k = 0.54$), dashed ($\gamma = 1.2, k = 2$).

As for the mean achievable rate, we observe that when there is no noise (at very small noise power), the mean data rate does not depend on the density distribution parameters, which is consistent with the literature about PPP. As seen in the mean rate figures, for the no noise (small noise) case, the mean achievable rate in the Lévy case is $1.7116 \text{ nats/Hz} = 2.4693 \text{ bits/Hz}$ and $2.6502 \text{ nats/Hz} = 3.8235 \text{ bits/Hz}$ for $\eta = 3$ and $\eta = 4$ respectively. As for the Weibull case, it is $1.2119 \text{ nats/Hz} = 1.7484 \text{ bits/Hz}$ and $1.967 \text{ nats/Hz} = 2.8378 \text{ bits/Hz}$ for $\eta = 3$ and $\eta = 4$ respectively. Notably, the Lévy case gives higher mean achievable rate than that of the Weibull case, and higher than that of the uniform PPP model available in literature [19], which was 1.49 nats/Hz for $\eta = 4$ and no noise. Also, in reference [64], the author claimed that the mean data rate is 2.45 nats/sec/Hz in an Matérn Cluster Process (MCP) network, with no noise, $\eta = 4$, and two-tier network with two parent cells and 20 daughter nodes in each of them. Hence for this specific configuration of MCP model, the mean data rate for the Levy case is higher while the Weibull case is lower. This shows that for the studied areas that the MCP could be an underestimate for the average metrics for the deployment of Figure 2.5 and overestimate for that in Figure 2.1.

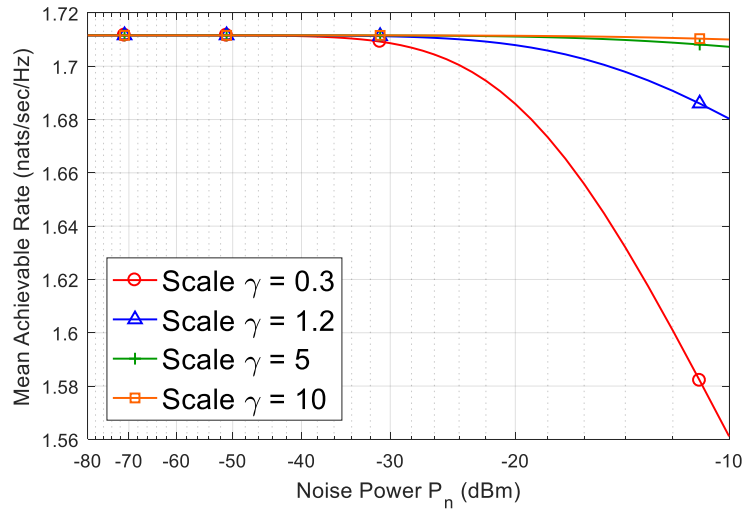


Figure 2.10: Mean data rate when $\eta = 3$ the density follows Levy distribution, and the interference experiences Rayleigh fading.

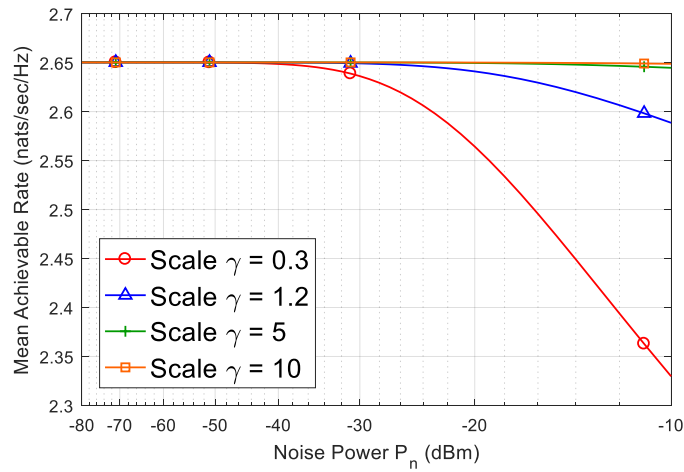


Figure 2.11: Mean data rate when $\eta = 4$, the density follows Levy distribution, and the interference experiences Rayleigh fading.

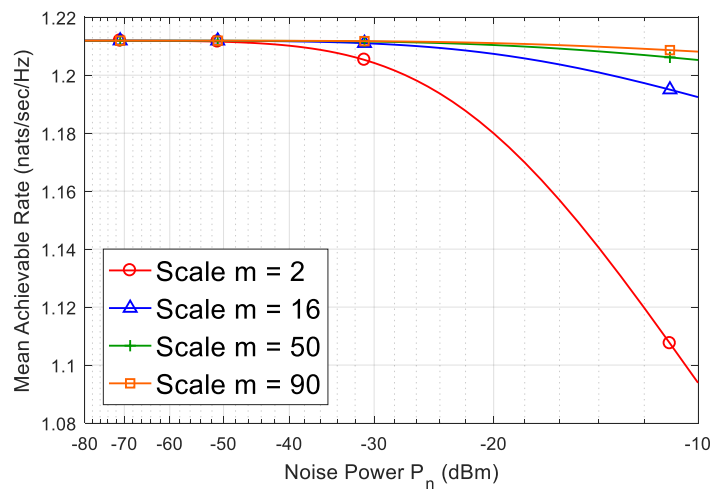


Figure 2.12: Mean data rate when $\eta = 3$, the density follows Weibull distribution (shape $b=1$), and the interference experiences Rayleigh fading.

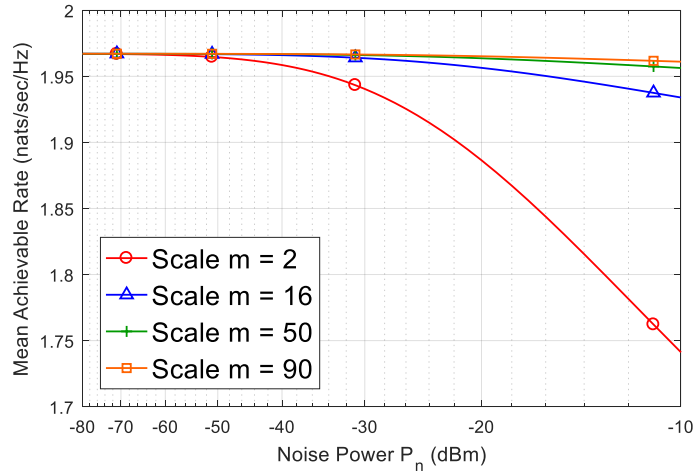


Figure 2.13: Mean data rate when $\eta = 4$, the density follows Weibull distribution (shape $b=1$), and the interference experiences Rayleigh fading.

F. Conclusion

As a conclusion, we have analyzed the spatial density distribution in three network areas. We have determined the best fitted distributions for the densities in these areas among several candidate distributions. Then, we have used these distributions to obtain the probability of coverage and the mean achievable rate for such areas when we model them using a Cox Process. Mainly for the density, we have considered the Lévy, Weibull and the Generalized Pareto distribution.

CHAPTER III

PROBABILITY DENSITY FUNCTION OF THE INTERFERENCE POWER IN PPP NETWORKS

In this chapter, we provide closed form expressions for the probability density functions (PDF) of the interference power in a network whose transmitters are arranged according to the Poisson Point Process (PPP). These expressions apply for any integer path loss exponent η greater than 2. Using the stretched exponential or Kohlrausch function, we show that the PDF formulas can be obtained as long as the Laplace transform (LT) for the PDF follows a specific common (exponential) formulation. Also, as the obtained PDF formulas are complex, we propose to approximate them using the Generalized Extreme Value (GEV) distribution, whose parameters can be determined through Maximum Likelihood, or Probability Weighted Moments. Simulations and numerical analysis validated the proposed analytical derivations and showed that the GEV gives good approximations.

In wireless networks, operators spend huge efforts on their network planning in order to provide better services and performance to their customers. Nonetheless, these efforts are more effective when the operators have reliable analytical formulation for the network performance metrics. The derivation of the interference analytical models, distribution, and characteristics, will therefore give network planners the needed tools for deriving the network performance in different scenarios and conditions. Additionally, as the wireless networks are becoming increasingly denser and experiencing higher traffic load, as defined by the connection density and area traffic capacity in the requirements of 5G access technologies [33], the need to characterize interference becomes more critical.

In stochastic geometry, the LT for the interference power distribution is used extensively to get many performance metrics for the network [15], where it is commonly employed as a tool for network evaluation (coverage, data rate, etc). On the other hand, the PDF gives an extensible method for the network operators to understand interference behavior and trends (distribution shape, lower-bound, upper bound, and other possible statistics). Most of the works that analyzed interference stated that no closed form expressions for the PDF of the interference power has been found, except for the specific case of path loss exponent (PLE) [17]. This is clearly seen in the PPP network, the most common model in network analysis using stochastic geometry. The authors of [34] gave a summary of the main approaches for approximating the PDF of the aggregate interference and showed that the approximations are wide varying between normal, log-normal, gamma, etc. To the best of the authors' knowledge, the general PDF of the interference power in PPP networks has not been addressed, that is, except for the case mentioned above and given in [17].

In this chapter, we state that exact closed form PDF expressions for interference power exist as long as we can write their formulas in the Laplace domain in a specific exponential structure. Our main contribution lies in showing that the stretched exponential function is a suitable choice for obtaining the formulas of the interference distribution. We illustrate that this distribution can be written in terms of a modified Lévy distribution, a specific type of alpha-stable functions. We also show how the Generalized Extreme Value (GEV) distribution can be used as an approximation for the interference power.

The work we present is important for performing further analysis of the network performance, and specifically for directly obtaining the interference statistics and thus deriving the signal to interference and noise ratio (SINR) in PPP networks. This in turn helps in understanding network enhancement techniques that can better tune the interference distribution. Besides, a compact closed form expression allows for plugging parameters and

deriving network performance measures in an infinite number of scenarios. This is the first work dealing with exact expressions of the interference PDFs for any integer value of the PLE.

A. Mathematical Background

The stretched exponential function, which is the Kohlrausch function, or the Kohlrausch-Williams-Watts (KWW) function [35][36], is defined as:

$$F_{\beta}(s) = e^{-s^{\beta}} \quad (3.1)$$

It is directly related to the Laplace domain of the Lévy distribution as:

$$L_{f_{\beta}}(s) = \int_0^{\infty} e^{-sI} f_{\beta}(I) dI = e^{-s^{\beta}} \quad (3.2)$$

where $f_{\beta}(I)$ is a stable PDF having a stretching exponent for $0 < \beta < 1$, where $\beta = \frac{\beta_1}{\beta_2}$ is usually assumed and whose the two fraction terms are integers. For $\beta_1 = 1$ and $\beta_2 = 2$, we have the simplest case:

$$f_{\frac{1}{2}}(I) = \frac{\exp\left(-\frac{1}{4I}\right)}{2\sqrt{\pi}I^{\frac{3}{2}}} \quad (3.3)$$

which is the PDF of a subclass of stable distributions called the Lévy distribution¹. The random variable I is a random variable with a Lévy distribution having the following parameters: *stability* $\alpha = 0.5$, *skewness* $\epsilon = 1$, *scale* $\sigma = 0.5$ and *location* $l = 0$.

The Lévy distribution and its scaled Laplace version $e^{-ts^{\beta}}$ are very important in different fields, particularly the Inverse unilateral Laplace Transform (ILT) for $e^{-ts^{\beta}}$ which could be directly obtained from a simple scaling weight, as defined in the Laplace properties.

Hence, the main problem is to derive the ILT of $e^{-s^{\beta}}$ for different β values, which is not an easy task to achieve. This will be elaborated later.

¹ Some authors use Lévy distribution for all sum stable laws

In the literature, and mainly in wireless communications using stochastic geometry approaches, the use of KWW functions is very useful, although the analysis has been limited to $\beta = 1/2$. The ILT for the KWW with different β values was not considered due to the lack of closed form expressions. This chapter fills that gap, where we use a transitive property to obtain the ILT for other β values.

Property 3.1: the PDF $f_{\{\beta_a, \beta_b\}}(I)$ can be obtained from f_{β_a} and f_{β_b} through a simple integration given by [37]:

$$f_{\{\beta_a, \beta_b\}}(I) = \int_0^\infty \frac{1}{t^{\beta_a}} f_{\beta_a} \left(\frac{I}{t^{\beta_a}} \right) f_{\beta_b}(t) dt = \int_0^\infty \frac{1}{t^{\beta_b}} f_{\beta_b} \left(\frac{I}{t^{\beta_b}} \right) f_{\beta_a}(t) dt \quad (3.4)$$

where β_a and β_b are two lower order stable distributions that follow the same rules of β . This equation becomes very useful when getting different values for β . For example, $\beta = \frac{1}{4}$ can be obtained by setting $\beta_a = \frac{1}{2}$ and $\beta_b = \frac{1}{2}$ which are given by (3.3), and then substituting them in (3.4). The step-by-step derivations of the PDF for different β values are out of scope of this letter but can be simply obtained by combining KWW and Laplace properties from one side and the expression in (3.4) from the other side. Using this strategy, we provide in Table 3.1 some important formulas for the sake of their applications in interference power analysis in PPP networks.

β	PDF of I
$\frac{1}{2}$	$\frac{1}{t^2} \rho_{\frac{1}{2}} \left(\frac{I}{t^2} \right) = \frac{1}{t^2} \frac{\exp(-\frac{t^2}{4I})}{2\sqrt{\pi} \left(\frac{I}{t^2} \right)^{\frac{3}{2}}} = \frac{t \exp(-\frac{t^2}{4I})}{2\sqrt{\pi} I^{\frac{3}{2}}}$
$\frac{1}{3}$	$\frac{1}{t^3} \rho_{\frac{1}{3}} \left(\frac{I}{t^3} \right) = \frac{t^{\frac{3}{2}}}{3\pi I^{\frac{3}{2}}} K_{\frac{1}{3}} \left(\frac{2}{3\sqrt{\frac{3I}{t^3}}} \right)$ Where $K_\nu(z)$ is the modified Bessel function of the second kind.

$\frac{2}{3}$	$\frac{1}{t^2} \rho_{\frac{2}{3}} \left(\frac{I}{t^2} \right) = \frac{2\sqrt{3}t^3}{27\pi I^3} \exp \left(-\frac{2t^3}{27I^2} \right) \left(K_{\frac{1}{3}} \left(\frac{2t^3}{27I^2} \right) + K_{\frac{2}{3}} \left(\frac{2t^3}{27I^2} \right) \right)$ $= \frac{\Gamma \left(\frac{2}{3} \right) t}{\sqrt{3}\pi I^{\frac{5}{3}}} {}_1F_1 \left(\frac{5}{6}; \frac{2}{3}; -\frac{2^2 t^3}{I^2} \right) + \frac{2}{9} t^2 \frac{{}_1F_1 \left(\frac{7}{6}; \frac{4}{3}; -\frac{2^2 t^3}{I^2} \right)}{\Gamma \left(\frac{2}{3} \right) I^{\frac{7}{3}}}$ <p>Where ${}_pF_q(a_1, \dots, a_p; b_1, \dots, b_q; x)$ is the generalized hypergeometric function.</p>
$\frac{1}{4}$	$\frac{1}{t^4} \rho_{\frac{1}{4}} \left(\frac{I}{t^4} \right) = \frac{t^3}{64\pi I^{\frac{7}{4}}} \left(\frac{8\sqrt{2}I}{t^2} \Gamma \left(\frac{1}{4} \right) {}_0F_2 \left(; \frac{1}{2}, \frac{3}{4}; -\frac{t^4}{256I} \right) \right.$ $\left. - \sqrt{2} \Gamma \left(\frac{-1}{4} \right) {}_0F_2 \left(; \frac{5}{4}, \frac{3}{2}; -\frac{t^4}{256I} \right) - 16\sqrt{\pi} \frac{I^{\frac{1}{4}}}{t} {}_0F_2 \left(; \frac{3}{4}, \frac{5}{4}; -\frac{t^4}{256I} \right) \right)$
$\frac{1}{5}$	$\frac{1}{t^5} \rho_{\frac{1}{5}} \left(\frac{I}{t^5} \right) = \frac{1}{t^5} \sum_{m=1}^4 \frac{b_m(5,1)}{\left(\frac{I}{t^5} \right)^{1+\frac{m}{5}}} {}_2F_5 \left(\left[1, \Delta \left(1, 1 + \frac{m}{5} \right) \right]; \left[\Delta(5, 1 + m) \right]; \frac{t^5}{5^5 I} \right)$ <p>Where $\Delta(a, b) = \frac{b}{a}, \frac{b+1}{a}, \dots, \frac{b+a-1}{a}$ and</p> $b_1(5,1) = \frac{\sqrt{5}\Gamma \left(\frac{1}{5} \right)}{20\pi \sin \left(\frac{2\pi}{5} \right)}$ $b_2(5,1) = \frac{-\sqrt{5}\Gamma \left(\frac{2}{5} \right)}{20\pi \sin \left(\frac{\pi}{5} \right)}$ $b_3(5,1) = \frac{\sqrt{5}\Gamma \left(\frac{3}{5} \right)}{40\pi \sin \left(\frac{\pi}{5} \right)}$ $b_4(5,1) = \frac{-\sqrt{5}\Gamma \left(\frac{4}{5} \right)}{120\pi \sin \left(\frac{2\pi}{5} \right)}$
$\frac{2}{5}$	$\frac{1}{t^2} \rho_{\frac{2}{5}} \left(\frac{I}{t^2} \right) = \frac{1}{t^2} \sum_{m=1}^4 \frac{b_m(5,2)}{\left(\frac{I}{t^2} \right)^{1+\frac{2m}{5}}} {}_3F_5 \left(1, \Delta \left(2, 1 + \frac{2m}{5} \right); \Delta(5, 1 + m); \frac{2^2}{5^5 \left(\frac{I}{t^2} \right)^2} \right)$ <p>Where</p> $b_1(5,2) = \frac{2^{\frac{2}{5}} \sqrt{5} \Gamma \left(\frac{1}{5} \right)}{10\sqrt{\pi} \Gamma \left(\frac{3}{10} \right) \sin \left(\frac{2\pi}{5} \right)}$ $b_2(5,2) = \frac{-2^{\frac{4}{5}} \sqrt{5} \Gamma \left(\frac{2}{5} \right)}{10\sqrt{\pi} \Gamma \left(\frac{1}{10} \right) \sin \left(\frac{\pi}{5} \right)}$

	$b_3(5,2) = \frac{-2^{\frac{1}{5}}\sqrt{5}\Gamma\left(\frac{3}{5}\right)}{100\sqrt{\pi}\Gamma\left(\frac{9}{10}\right)\sin\left(\frac{\pi}{5}\right)}$ $b_4(5,2) = \frac{2^{\frac{3}{5}}\sqrt{5}\Gamma\left(\frac{4}{5}\right)}{100\sqrt{\pi}\Gamma\left(\frac{7}{10}\right)\sin\left(\frac{2\pi}{5}\right)}$
$\frac{1}{6}$	$\frac{1}{t^6}\rho_{\frac{1}{6}}\left(\frac{I}{t^6}\right) = \frac{2^{-\frac{1}{3}}3^{-\frac{3}{2}}\sqrt{\pi}t}{\left(\Gamma\left(\frac{2}{3}\right)\right)^2 I^{\frac{7}{6}}} {}_0F_4\left(\left[\right]; \frac{1}{3}, \frac{1}{2}, \frac{2}{3}, \frac{5}{6}; -\frac{t^6}{6^6 I}\right)$ $- \frac{t^2}{6\Gamma\left(\frac{2}{3}\right) I^{\frac{4}{3}}} {}_0F_4\left(\left[\right]; \frac{1}{2}, \frac{2}{3}, \frac{5}{6}, \frac{7}{6}; -\frac{t^6}{6^6 I}\right)$ $+ \frac{t^3}{12\sqrt{\pi}I^{\frac{3}{2}}} {}_0F_4\left(\left[\right]; \frac{2}{3}, \frac{5}{6}, \frac{7}{6}, \frac{4}{3}; -\frac{t^6}{6^6 I}\right)$ $- \frac{\sqrt{3}t^4\Gamma\left(\frac{2}{3}\right)}{72\pi I^{\frac{5}{3}}} {}_0F_4\left(\left[\right]; \frac{5}{6}, \frac{7}{6}, \frac{4}{3}, \frac{3}{2}; -\frac{t^6}{6^6 I}\right)$ $+ \frac{3^{-\frac{3}{2}}t^5\left(\Gamma\left(\frac{2}{3}\right)\right)^2}{2^{\frac{17}{3}}\pi^{\frac{3}{2}}I^{\frac{11}{6}}} {}_0F_4\left(\left[\right]; \frac{7}{6}, \frac{4}{3}, \frac{3}{2}, \frac{5}{3}; -\frac{t^6}{6^6 I}\right)$

Table 3.1: Inverse Laplace for scaled KWW $F(s) = \exp(-ts^\beta)$ for mostly needed β indexes

B. Interference Power PDF Analysis

The analysis of the interference Laplace transformations in different PPP environments concludes that it can be written as a KWW, hence the importance of the formulas in Table 3.1. For this purpose, we consider two particular cases for interference analysis. The first is the common interference model in PPP [19], while the second considers the case when the base station (BS) distribution has a random density λ . Here, we are interested in obtaining the PDF of the interference power when fading is Rayleigh (i.e., fading power is exponential), while a typical user is connected to the nearest BS in the network. We start from the common system model given in [19] where the probability of coverage defined as $P_c = P_r(\text{SINR} > T)$ is given in terms of $L_{I_r}(s)$; the LT of the aggregate interference power I_r defined by:

$$I_r = \sum_{i \in \Phi \setminus Tx_{serving}} g_i R_i^{-\eta} \quad (3.5)$$

where Φ represents the locations of the BSs that are modeled as a PPP with density λ , η is the PLE, T is the SINR threshold to guarantee the coverage, g_i is the fading channel coefficient for the Rayleigh fading case, R_i is the distance from the user to the interfering BSs. It should be noted that P_c is averaged over all channel coefficients g_i , the distance r to the serving BS, and then over the interference I_r . The probability of coverage (which depends on T) is then given in terms of $L_{I_r}(s)$, where $s = \mu T r^\eta$, as:

$$P_c = \mathbb{E}_r[\mathbb{P}[g > Tr^\eta(\sigma^2 + I_r)|r, I_r]] = \mathbb{E}_r[\exp(-\mu T r^\eta \sigma^2) L_{I_r}(s)|r] \quad (3.6)$$

where $1/\mu$ is the mean of the fading power, σ^2 is the noise power. The PDF of the aggregate interference can be obtained using the ILT of $L_{I_r}(s)$. In this work, we consider the cases where the LT is written as modified KWW function. This is a common case in stochastic geometry, in which β is related to the PLE η as seen in the next subsection. However, as $L_{I_r}(s)$ depends on T , the PDF of the aggregate interference will be conditioned on T , i.e., it can be written as:

$$f_{I_r}(I_r) = P_r(I_r | SINR > T) \quad (3.7)$$

Hence, the problem reduces to finding the PDF of the aggregate interference independently of T . To do so, we use a property from the conditional expectation theory.

Property 3.2: if $\mathbb{E}[X/Y] = 0$, i.e., if the conditional expectation of the random term X is the same for all terms of the population Y , then X and Y are independent.

Using Property 2 in (3.6), the PDF of interference becomes independent of T , i.e., deconditioned on T , if and only if the expectation becomes zero, i.e. when T tends to ∞ . Note that in this work, we provide the PDF of the general case of the interference including those conditioned on T . In summary, the PDF of the interference can be obtained from the ILT of

interference power using Table 3.1, conditioned on the SINR threshold T . When T tends to ∞ , the PDF of the interference becomes independent of T .

In order to verify our analytical derivations, we provide in this work a numerical solution given by Talbot's method, widely used in the literature to get numerical values of ILT [38]. Talbot's method is one of the best approaches to compute the ILT by deforming the standard contour in the Bromwich inversion integral. The reader might refer to [38][17] for more details. We also summarize the simulation parameters used in the analysis in Table 3. 2:

Parameter	Definition	Case 1 (Fig 3.1)	Case 2 (Fig 3.2)
η	Path loss exponent	3	6
μ	$1/\mu$ is the mean of the fading power	1	1
λ	Density of PPP	2	Not used
γ	Scale parameter of Lévy distribution	Not used	0.4
β	Index of scaled KWW	2/3	1/6

Table 3. 2: Simulation Parameters

1. *The PDF of the Interference Power in Homogeneous PPP*

In a network whose transmitters are distributed according to homogeneous PPP, the LT of the interference power is [19]:

$$L_{I_r}(s) = \exp \left(-\pi\lambda \left(\frac{s}{\mu} \right)^{\frac{2}{\eta}} \int_{T^{-2/\eta}}^{\infty} \frac{1}{y^{\frac{2}{\eta}} + 1} dy \right) \quad (3.8)$$

Equation (3.8) can be written as KWW function where t is the scaling factor of s and $\beta = 2/\eta$. Hence, its ILT (i.e. PDF) will be a simple plugin in Table 3.1, depending on η .

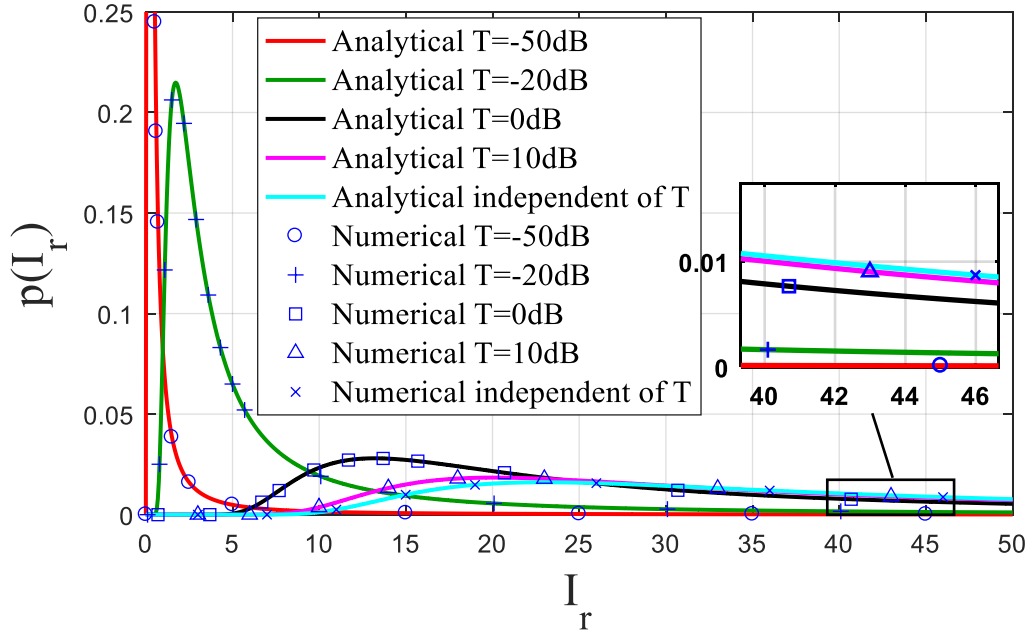


Figure 3.1: Interference power PDF (conditioned and decondition on T).

In Figure 3.1, we provide and compare the results of the PDF of the interference power obtained analytically as in Table 3.1, and numerically from the ILT numerical Talbot's method for $\eta = 3$. To get the analytical PDF, t can be obtained by solving the inner integral in (3.8), and inserting the result in the third row of Table 3.1 (case $\beta = 2/3$). It is given by:

$$t = \frac{\lambda\pi}{3\mu^{\frac{2}{3}}} \left(\sqrt{3}\pi + 2\sqrt{3} \tan^{-1} \left(\frac{-2 + T^{\frac{1}{3}}}{\sqrt{3}T^{\frac{1}{3}}} \right) + \ln \left(\frac{T^{\frac{2}{3}} + 2T^{\frac{1}{3}} + 1}{T^{\frac{2}{3}} - T^{\frac{1}{3}} + 1} \right) \right) \quad (3.9)$$

It is clear from this equation that the interference PDF depends on T . When $T = \infty$, $t = \frac{\lambda\pi}{3\mu^{\frac{2}{3}}} \left(\sqrt{3}\pi + 2\sqrt{3} \tan^{-1} \left(\frac{1}{\sqrt{3}} \right) \right)$, which gives the PDF of the interference deconditioned on T for $\eta = 3$.

By following the same approach for $\eta = 4$, it can be easily verified that the exact analytical expression of the interference PDF [17] where $t = \frac{\pi^2\lambda}{2\sqrt{\mu}}$ is obtained. Hence, we claim that our approach tackles the general case of the aggregate interference PDF as long as the LT can be expressed as a KWW form, i.e., $\exp(-ts^\beta)$.

2. The PDF of the Interference Power in a Cox Process

In this section, we suppose that the average density of the network is a non-negative number taken from a specific distribution. Such a network model is a PPP conditioned on the intensity measure, and is referred to as a Cox process [2]. For a reliable study, this random distribution must mostly characterize the spatial density statistics of the transmitters across the network, such as the work done in [29], where it has been shown that the density follows a stable distribution. Also, from our fitting results for the density distribution done in CHAPTER II, we have showed the parameters for the fitted alpha-stable, where in some studied areas it was near a subclass of alpha-stable distribution, which is the Lévy distribution. Without loss of generality, assuming that the realized random density λ is taken from a Lévy distribution with location parameter = 0 (a special case of the stable distribution), the LT of the average interference experienced by a random user in the network with Rayleigh fading is:

$$L_{I_r}(I_r) = \exp\left(-\sqrt{2\gamma\pi}\left(\frac{S}{\mu}\right)^{\frac{1}{\eta}}\left(\int_{T^{-2/\eta}}^{\infty}\frac{1}{y^{\frac{2}{\eta}}+1}dy\right)^{\frac{1}{2}}\right) \quad (3.10)$$

where γ is the scale parameter for the distribution of λ .

Proof: it was done in CHAPTER II.

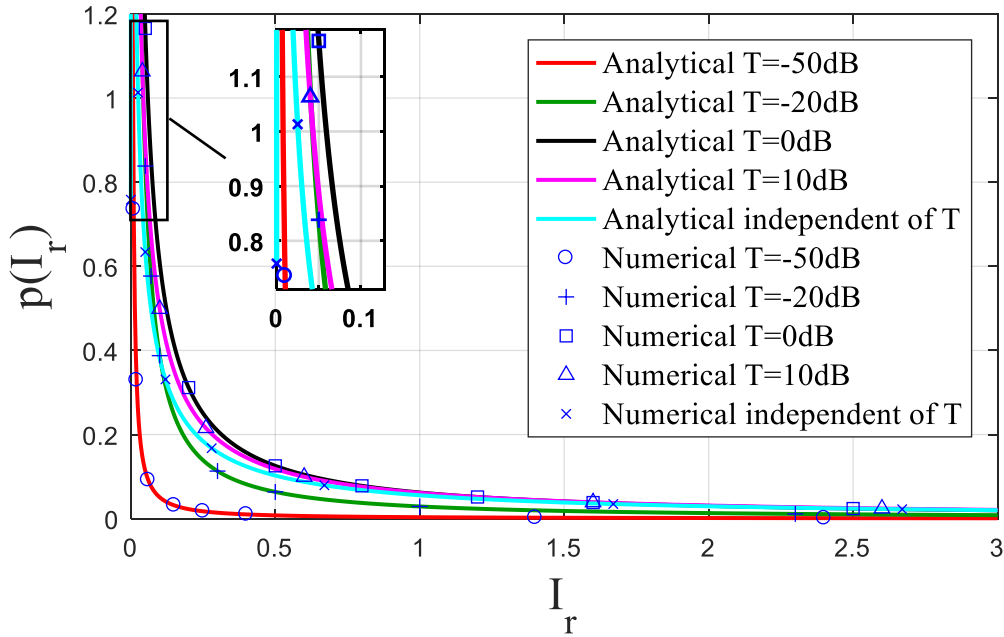


Figure 3. 2: PDF when density follows Levy distribution.

Again, it is very clear that in this particular case, the LT of the interference power distribution can be written as a scaled KWW function (similar to (3.1)). Hence, we can get its ILT from Table 3.1. Figure 3. 2 sketches the PDF at $\eta = 6$ obtained analytically and numerically through Talbot's method for accuracy comparison. The PDF of the aggregate interference independent of T is shown ($T = \infty$ case).

C. Approximating interference PDF using GEV

In the previous sections, we provided the exact formulas for the interference distributions in different network environments. However, as Table 3.1 shows, these formulas may still be complex to use, as they include Hypergeometric or Bessel functions. Hence, to simplify their use, we propose to approximate them with the Generalized Extreme Value (GEV) distribution, which is normally used to model the maximum or minimum of a series of i.i.d. random variables. In a PPP network and in an interference limited scenario (which is the case of our network), the use of GEV approximation could be justified by the fact that in order

to get an SINR greater than a threshold T , and for a fixed signal and noise power, the interference must be upper-bounded within a confidence interval. The GEV PDF is:

$$f_X(x) = \frac{1}{\sigma} u(x)^{\xi+1} e^{-u(x)} \quad (3.11)$$

where

$$u(x) = \begin{cases} \left(1 + \xi \left(\frac{x-l}{\sigma}\right)\right)^{-1/\xi}, & \xi \neq 0 \\ e^{-\left(\frac{x-l}{\sigma}\right)}, & \xi = 0 \end{cases} \quad (3.12)$$

and shape $\xi \in \mathbb{R}$, scale $\sigma > 0$ and location $l \in \mathbb{R}$.

To prove the feasibility in using GEV for approximating the interference power PDF, we propose both the maximum likelihood (ML) and the probability weighted moments (PWMs) methods. ML works by maximizing the GEV log-likelihood function with the sample data for the interference, while the PWMs give a simple generalization of the weighted moments of a distribution, but are less accurate in fitting. In fact, the defined PWMs method is more accurate for $-0.5 < \xi < 0.5$ with $\xi \neq 0$. The PWMs are defined in [39]:

$$w_i = \frac{1}{1+i} \left[1 - \frac{\sigma}{\xi} \left(1 - (1+i)^\xi \Gamma(1-\xi) \right) \right], i = 0,1,2 \quad (3.13)$$

They can be obtained from the ordered interference power variable I_j :

$$\hat{w}_i = \frac{1}{n} \sum_{j=1}^n I_j \left(\frac{j}{n}\right)^i \quad (3.14)$$

Once obtained, the estimated parameters for the fitted GEV can be calculated as follows:

$$\frac{3\hat{w}_2 - \hat{w}_0}{2\hat{w}_1 - \hat{w}_0} = \frac{3^{\hat{\xi}} - 1}{2^{\hat{\xi}} - 1} \quad (3.15)$$

$$2\hat{w}_1 - \hat{w}_0 = \frac{\hat{\sigma}}{\hat{\xi}} [\Gamma(1-\hat{\xi})(2^{\hat{\xi}} - 1)] \quad (3.16)$$

$$\hat{l} = \hat{w}_0 + \frac{\hat{\sigma}}{\hat{\xi}} [1 - \Gamma(1 - \hat{\xi})] \quad (3.17)$$

The results show that GEV provides a small root mean square error (RMSE) with the true distribution of the interference, as shown for this particular example $T = 0$ dB. **Figure 3.3** shows different fittings for the PPP interference power for $\eta = 3$ and $\eta = 5$. Both cases show a good fitting. For the case of $\eta = 3$, we have an RMSE of 2.6331×10^{-4} (ML) and 1.5989×10^{-3} (PWMs), with ML giving better performance. The PWMs fitting performance is limited because the shape ξ is not within the needed boundaries to apply the PWM approximations [39]. But, as a general result, we observe that GEV fits well for many different system configurations with a small error, which makes it an effective candidate for approximating the interference power distribution.

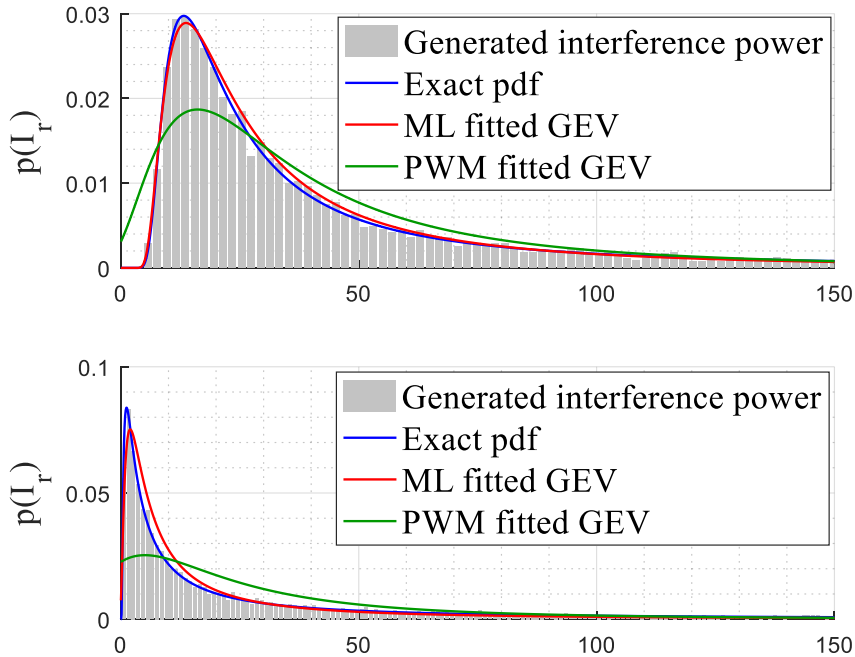


Figure 3.3: Fitting interference power distribution in a PPP network with GEV distribution when $\mu = 1$ and $\lambda = 2$. (Upper) Case $\eta = 3, T = 0$ dB. ML: $\xi = 0.84296, \sigma = 17.2143, l = 21.9015$, PWMs: $\xi = 0.53143, \sigma = 22.4888, l = 24.6996$. (Lower) Case $\eta = 5, T = 0$ dB. ML: $\xi = 1.29279, \sigma = 9.53744, l = 6.80689$, PWMs: $\xi = 0.49147, \sigma = 18.5028, l = 11.7603$.

D. Conclusion

In this chapter, we have shown that the distribution of interference power in a stochastic geometry framework does have exact closed forms, as long as its LT could be written as a KWW function. We have presented the closed form expressions for different path loss exponents when the interference experiences Rayleigh fading, and evaluated the accuracy of the formulas using numerical analysis. Finally, we have shown that the interference power PDF could be also approximated by the GEV distribution, which may be used for simplicity.

CHAPTER IV

IN-BAND FULL-DUPLEX (IBFD) SHARED CHANNEL ACCESS

A. Introduction:

In this chapter, we study the performance of users operating at IBFD in a cellular network. We assume that this network uses Fractional Frequency Reuse (FFR) and that the resources used by the users are not totally isolated nor orthogonal between each other. That is, there is some sort of shared channel resources i.e. non-orthogonal transmissions between the users such as Non-Orthogonal Multiple Access (NOMA). Markedly, the use of shared network resources is aligned with the vision for future networks. With this intention, we analyze the performance of a network configuration using two approaches and we show the effect of using such configuration on different networks parameters. The first approach is achieved by tweaking the PPP network analysis while the second approach is based on inner-city model which is the reverse model of the Poisson Hole Process (PHP). For multiple reusability, we try to keep the presented system model as abstract as possible. Thus, we do not restrict it with a specific resource allocation scheme, but we illustrate and give an example on how the network model and calculations can be used for a specific scheme. We show that the SINR degrades due to IBFD in both core and edge users while a gain in system throughput is obtained. We provide extensive simulation results in terms of SINR outage threshold, full duplex region, throughput, etc. We also show, as expected, how FFR can mitigate this decrease for the cell edge users.

B. In-Band Full-Duplex:

IBFD has emerged as a technology to increase the throughput and the spectral efficiency for users. It is a key potential technology that is expected to be part of the future enhancements applied on the next generation mobile cellular networks. Particularly, it is considered as an advanced technology for increasing the spectral efficiency. Nodes operating at IBFD are expected to transmit and receive simultaneously at the same time/frequency resource blocks, without the need to orthogonalize the Uplink/Downlink (UL/DL) frequency bands. Transceivers using IBFD must be able to route incoming and outgoing signals and transmit them at the same network resources thus potentially doubling the capacity of the wireless channel. The basic advantage from using IBFD is its ability to increase the throughput and to reduce the transmission feedback and the end-to-end delay. This technology has been applied for a long time in radar systems [40], but it is still not deployed in wireless communication systems like mobile cellular or WiFi systems.

Yet, the application of IBFD in wireless communication systems faces challenges related to the design of a transmission system that can receive and transmit frames at the same channel resource (a principle known as reciprocity). Other important challenges are related to the design of the used protocols, access layer and transmission scheduling and management. Besides, systems using IBFD experiences self-interference. The latter occurs when the signal being transmitted by the node is received by its own receiver thus causing interference. Such problem can't be avoided in IBFD, but it can be suppressed using Self-Interference Cancellation SIC techniques, equalization, physical separation of Tx and Rx antennas (if possible) and beamforming-based self-interference nulling [41]-[44].

SIC techniques can be divided into three types [45] related to the domain that they work on. The first type works on the propagation domain isolation and it uses combinations of

separate antenna systems, cross-polarization, antenna directionality and antenna cancellation [46]. The second works on the analog circuit domain in which the self-interference is suppressed before it passes through an analog to digital converter, and it includes circulators, circuits that tap and cancel the interfering transmit signal and some antenna isolation methods. These circuits can be divided into channel-aware and channel-unaware. The third type works on the digital domain, and it includes applying the needed gain/phase/delay adjustments digitally based on the knowledge of the transmitted signal, digital signal processing techniques, and other physical layer algorithms and equalizations. For more details, the readers can refer to [47].

Applying IBFD in cellular systems is even more challenging due to longer distances between the transmitter and the receiver node. Moreover, as the network is larger, the effect of interference is more significant. This challenge increases also with shared resources scenario, which decreases the effectiveness of SIC techniques. Anyhow, IBFD definitely includes additional interference to the end-user hence its application may not be a good solution for users receiving weak signal, such as the users far from their serving Base Station (BS).

C. Fractional Frequency Reuse:

FFR is a non-conventional Inter-Cell Interference Coordination (ICIC) technique that aims to reduce the interference within and between the network cells. FFR provides better spectral efficiency for the network than conventional frequency reuse. Mainly, FFR divides a cell into edge and core regions, and applies different frequency reuse schemes for these regions, i.e. FFR divides the users into cell-edge users U_e and cell-core user U_c . Then, different FFR schemes are applied so that interference is reduced between the two user types and mainly for the cell-edge users U_e .

Notable types of FFR schemes are Strict-FFR (St-FFR) and Soft-FFR (So-FFR). In Figure 4.1 (left), we depict the St-FFR scheme with a reuse factor $N = 3$. The users U_c are allocated a common part of the band B_1 , while the edge-users U_e take the remaining bandwidth divided across the neighboring cells according to the reuse factor N . This means for $N = 3$, the three neighboring cells will not be using the same bands to serve the U_e . Thus, a typical U_e in cell 1, will not experience neither interference from the BSs in cells 2 and 3, nor interference from any U_e operating at IBFD in the bands of cells 2 and 3. On the other side, Figure 4.1 (right) depicts the So-FFR scheme, where we can observe that So-FFR requires less bandwidth than St-FFR leading to a better spectral efficiency, but it suffers from larger interference levels. In So-FFR, the users U_c can share the bandwidth with the edge users U_e from the neighboring cells, but they transmit with a lower power than U_e . This is done through power control schemes. In this work, we will consider only St-FFR, but the work can be easily extended to So-FFR.

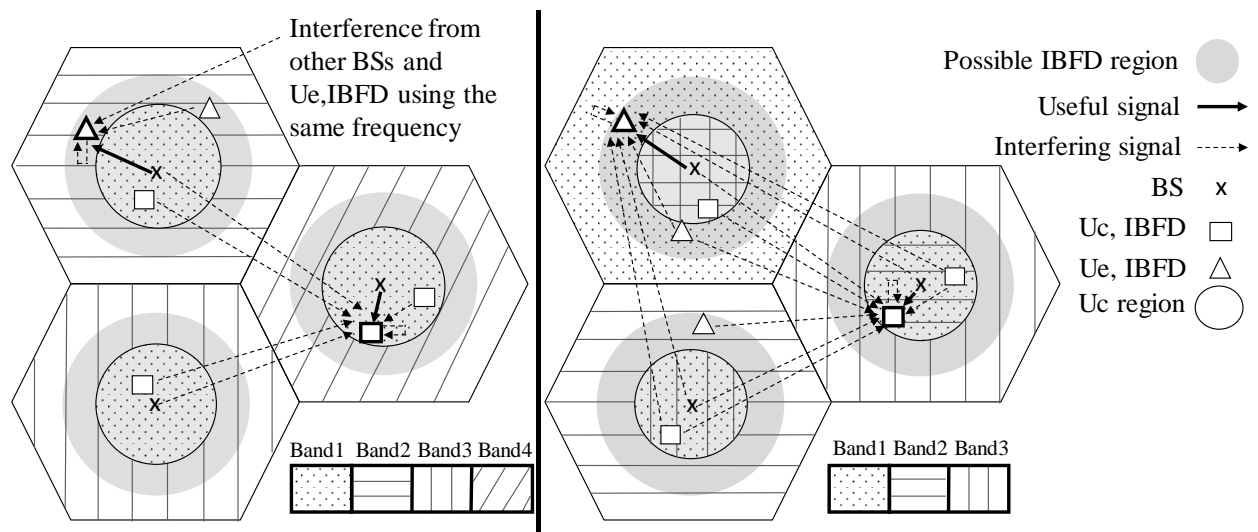


Figure 4.1: Left: St-FFR. Right: So-FFR. Possible interference experienced by a typical user operating at IBFD (core $U_{c,IBFD}$, edge $U_{e,IBFD}$) in a network implementing FFR schemes with $N = 3$ reuse factor in a hexagonal cell. Frequency Plans are also shown for different schemes. Note: Typical studied users are shown in bold.

D. Related Work:

Different full-duplex schemes and models have been investigated in stochastic geometry. Using stochastic geometry tools, the authors in [48] studied the throughput in a wireless network that contains both IBFD and half-duplex nodes. The network model supposed that a node may operate at IBFD with some probability. A novel duplexing scheme for IBFD targeting cellular networks is studied in [49]. The scheme assumed that there is a partial overlap between the DL and UL frequency bands, and showed that the optimal overlap depends on the network parameters and the design objective. The authors in [50] investigated the performance of a basic OFDM based cellular system that is using IBFD and proposed a scheduling algorithm that enhances its performance. Moreover, [51] proposed a power and user allocation schemes with a manageable signaling overhead to improve capacity.

The authors of [52] proposed a coupled and decoupled user association schemes for IBFD to improve the transmission rate. In [53], IBFD operation for device-to-device (D2D) communication is studied. The work in [54] analyzed IBFD in a network where nodes are using perfect/imperfect carrier sensing and RTS/CTS signaling. The use of IBFD in small cells has been also studied. The authors in [55] analyzed the performance of IBFD in small cells with some multiple antennas configuration, in which the performance has been compared with half-duplex. Also, [56] studied IBFD in backhauling small cells to macro cells over the wireless network.

On the other hand, the effect of the FFR has been analyzed in stochastic geometry. The authors in [57] analyzed the effect for using two FFR schemes (strict and soft) in a single tier cellular network, and showed the advantages of each scheme. Similarly, [58] analyzed the performance of a specific FFR scheme in a heterogeneous cellular network. In the literature, the results showed that the strict FFR provides better coverage and achievable rate for users.

On the contrary, the soft FFR provides better spectrum efficiency. Moreover, [59] studied the effect of FFR alongside with using Multiple Input Multiple Output (MIMO) technology. Likewise, the authors of [60] studied the effect of using FFR in Femto-cells, in which a novel metric is used to determine the optimal inner region radius and frequency allocation. Furthermore, [61] studied an adaptation process that better tunes the FFR scheme (inner region radius and frequency allocation) for a better performance and cell throughput.

E. General Network Model:

We present a cellular network model in which the BS are arranged according to a uniform PPP Φ_{BS} with a density λ_{BS} on \mathbb{R}^2 . Also, we assume that the mobile users in this network are arranged according to another PPP Φ_U with a density λ_U on \mathbb{R}^2 . Both Φ_{BS} and Φ_U are considered independent with $\lambda_U > \lambda_{BS}$ so that at least one user is connected to each BS. Besides, each user is connected to the nearest BS that is the serving BS denoted as BS_0 . In addition, we assume that all users have SIC capabilities and can operate in IBFD mode. Since operating at IBFD causes more interference especially in the presence of shared channel resources between the users, it is preferred to make users who are near their serving BS use IBFD. Thus, we define IBFD regions around each BS, and the users inside these regions will be operating at IBFD. For simplicity, we define these regions as disks with radius d_F around each BS. This definition can be also translated into the user having a specific long-term average power received (APR) which depends mainly on the distance to its BS_0 .

In the network, there will be some users operating at IBFD and others using half-duplex. In this general network model, we assume that there exist non-orthogonal transmissions between IBFD users, so these users are using some sort of shared channel resources. This is aligned with novel resources allocation schemes proposed in 5G networks. For the st-FFR

scheme a user U_e uses one of the total available sub-bands reserved for the edge users, where a served user takes a frequency band n_0 , and experiences new interference value I' with new fading value g' . The BSs other than the serving one can use the band n_0 of that U_e depending on the reuse threshold N in St-FFR scheme. When $N = 1$, all BSs use n_0 , and when $N > 1$, one BS in each BS-cluster of size N uses n_0 . We define two SINR thresholds; T_{edge} which is the threshold required to separate between U_c or U_e i.e. user $\in U_c$ if $SINR > T_{edge}$ else it is considered U_e [57]. The second threshold is the detection threshold T to consider the user connected i.e. any user receiving $SINR > T$ is considered receiving useful signal and covered by the network.

Depending on the network configuration, we may have U_c using either IBFD or half-duplex, or U_e using either IBFD or half-duplex. So, there is no user considered U_e and U_c at the same time, and no user operating at IBFD and Half-duplex at the same time. So, these modes are mutually exclusive. In Figure 4.2, we show a PPP representation for this model, in which the users are connected to the nearest BS, which consists a Voronoi tessellation coverage areas. Moreover, in Figure 4.1, we show the St-FFR scheme and some of the different possible interference sources due to IBFD operation and the shared network resources model. As stated, in this model we are using the St-FFR scheme.

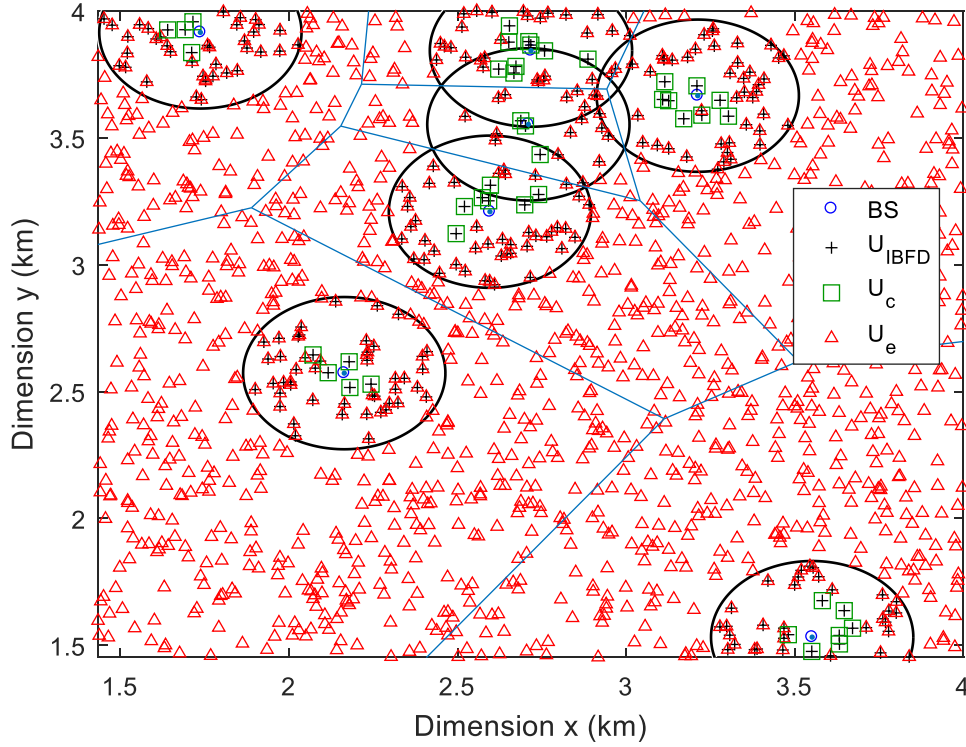


Figure 4.2: Network Model for $\lambda_{BS} = 0.5 \text{ BS/km}^2$, $\lambda_U = 200 \text{ users/km}^2$, $d_F = 0.3 \text{ km}$, $T_{\text{edge}} = -1 \text{ dB}$

In Table 4.1, we present the summary for the different notations used in this chapter for the sake of clarification:

Notation	Meaning
$\phi_{BS}; \lambda_{BS}$	PPP modeling the locations of the BSs; density of ϕ_{BS}
$\phi_U; \lambda_U$	PPP modeling the locations of the users; density of ϕ_U
$P_{s1}, P_{s2}; P_n$	Transmit power of: BSs, users; power of noise
$h, g_i; \mu$	Exponential fading power with mean $1/\mu$ (Rayleigh fading case)
L_{p1}, L_{p2}	Constant that depends on the transmitter, receiver characteristics and frequency
R_i	Distance from a typical user to the interfering BS i
η	Path loss exponent > 2
β	A coefficient that determines the efficiency of the self-interference cancellation (SIC) technique used. It is between 0 (best SIC) and 1 (no SIC).
U_e, U_c	Cell-edge user, Cell-core user

$U_{IBFD}, U_{e,IBFD}, U_{c,IBFD}$	All users operating at IBFD, U_e operating at IBFD, U_c operating at IBFD
I_x'	Interference experienced by U_e from source x due to the FFR scheme (notice the prime sign on I)

Table 4.1: Notations used

In the sequel, we define the IBFD regions defined as disks of radius d_F around each BS. Any user inside these disks will be operating at IBFD.

Definition 1: Let us consider the following random set which represents the germ-grain model [2] for a union of all disks of radius d_F centered at a point of ϕ_{BS} :

$$\mathcal{E} \triangleq \cup \{x \in \Phi_{BS} : b(x, d_F)\}$$

The users $\phi_{U_{IBFD}}$ using IBFD, and the users Φ_{U_H} using half duplex are defined as:

$$\Phi_{U_{IBFD}} = \{x \in \Phi_U : x \in \mathcal{E}\} = \Phi_U \cap \mathcal{E}$$

$$\Phi_{U_H} = \{x \in \Phi_U : x \notin \mathcal{E}\} = \Phi_U \setminus \mathcal{E}$$

By this we get both the so called inner-city model and the Poisson Hole Process (PHP), each having an intensity given by:

$$\lambda_{U_{IBFD}} = \lambda_U (1 - \exp(-\lambda_{BS} \pi d_F^2)) \quad (4.1)$$

$$\lambda_{U_H} = \lambda_U \exp(-\lambda_{BS} \pi d_F^2) \quad (4.2)$$

A further verification can be done by setting d_F to 0 and ∞ and checking the output. When studying the performance for the IBFD users we use the inner-city model. This model represents all the points of Φ_U that are inside the disks created by \mathcal{E} .

This definition alongside the FFR scheme leads to these three possible interference sources shown in Figure 4.3, depending on the users that may be sharing resources with the typical user.

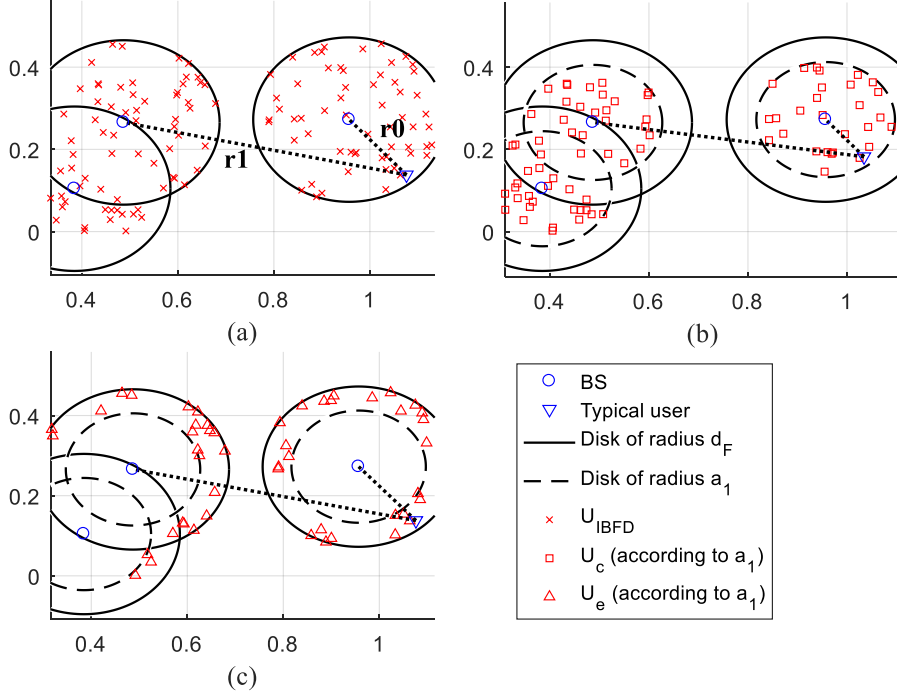


Figure 4.3: Schema showing different possible types of interference sources from the users operating at IBFD, and the distance from a typical user to the serving BS and the other nearest BS. (a) IBFD users, (b) core users operating at IBFD, (c) edge users operating at IBFD.

F. Coverage of Users Operating at IBFD:

In this section, we study the probability of coverage for a typical user operating at IBFD in the general network model. Then, we analyze this model using two approaches briefly explained thereafter. Then, a possible use case is considered. It allows providing different transmission metrics and schemes depending on the SINR. To sum up, the aim here is to develop a general model for different use-cases offering a wider range of network performance evaluation hence the importance of this work.

1. Cell-Edge Users:

Without loss of generality, we analyze the network performance of a typical user taken as the reference user, located at the origin. According to Slivnyak's theorem [2], any other

location in the space has an identical statistical behavior to the origin. Due to the FFR scheme, the users are identified as either U_e or U_c , where different interference is experienced in each case. As we stated, the classification of the user as U_e or U_c is dependent on having $SINR_1$ less than or greater than T_{edge} respectively. Then, we define the probability of coverage or the success probability for U_e operating at IBFD, as the user having an $SINR > T$ given it is an edge user U_e . For that, we use a common condition to classify users as U_e or U_c operating at IBFD, given by:

$$SINR_1 = \frac{S}{N + I_1 + I_2 + SI} = \frac{P_{s_1} h_2 L_{p_1} r^{-\eta}}{P_n + P_{s_1} L_{p_1} I_{BS} + P_{s_2} L_{p_2} I_{U_{IBFD}} + \beta P_{s_2}} \quad (4.3)$$

The notations of (4.3) are available in Table 4.1. $SINR_1$ is defined as the ratio of the received signal power over the sum of the following: the noise power N ; the interference I_1 from the BSs other than the serving one before applying the FFR scheme (user still not identified as U_e or U_c); the interference from all the users operating at IBFD I_2 and sharing the same resources i.e. inside the IBFD regions; and the remaining self-interference SI . Our definition differs from [57] because of the different interference sources found. Besides, to simplify the calculations, all the power and constant terms ($P_{s_i} L_{p_i}$) are kept outside the interference definitions I_{BS} and $I_{U_{IBFD}}$ terms. The latter are defined as:

$$I_{BS} = \sum_{i \in \Phi_{BS} \setminus \{BS_0\}} g_i R_i^{-\eta}, I_{U_{IBFD}} = \sum_{i \in \Phi_{U_{IBFD}} \setminus \text{typical user}} g_i R_i^{-\eta}$$

Thus, the probability of coverage for U_e operating at IBFD is defined as:

$$p_{U_e}^{\text{st-FR}} = \mathbb{P} \left(\frac{P_{s_1} h_1 L_{p_1} r^{-\eta}}{P_n + P_{s_1} L_{p_1} I_{BS}' + P_{s_2} L_{p_2} I_{U_e, IBFD}' + \beta P_{s_2}} > T \mid SINR_1 < T_{edge} \right) = \frac{\int_{r>0} E_1 f_r(r) dr}{\int_{r>0} E_2 f_r(r) dr} \quad (4.4)$$

where $f_r(r)$ is the widely known pdf of the distance r between the user and its serving BS. It is derived according to the null probability of a 2D Poisson process and equals:

$$f_r(r) = 2\pi\lambda_{BS}r e^{-\pi\lambda_{BS}r^2} \quad (4.5)$$

The two functions E_1 and E_2 are defined by:

E_1

$$= e^{-\mu \frac{r^\eta T (P_n + \beta P_{S_2})}{P_{S_1} L_{p_1}}} L_{I_{BS}'}(\mu r^\eta T) L_{I_{U_e, IBFD}'} \left(\mu \frac{P_{S_2} L_{p_2} r^\eta T}{P_{S_1} L_{p_1}} \right) \\ - e^{-\mu \frac{r^\eta ((P_n + \beta P_{S_2})T + (P_n + \beta P_{S_2})T_{edge})}{P_{S_1} L_{p_1}}} L_{I_{BS}', I_{BS}}(\mu r^\eta T, \mu r^\eta T_{edge}) \cdot L_{I_{U_e, IBFD}', I_{U_{IBFD}}} \left(\mu \frac{P_{S_2} L_{p_2} r^\eta}{P_{S_1} L_{p_1}} T, \mu \frac{P_{S_2} L_{p_2} r^\eta}{P_{S_1} L_{p_1}} T_{edge} \right)$$

$$E_2 = 1 - e^{-\mu \frac{r^\eta T_{edge} (P_n + \beta P_{S_2})}{P_{S_1} L_{p_1}}} L_{I_{BS}}(\mu r^\eta T_{edge}) L_{I_{U_{IBFD}}} \left(\mu \frac{P_{S_2} L_{p_2} r^\eta}{P_{S_1} L_{p_1}} T_{edge} \right)$$

The LT of the interference terms will be defined later due to their complexity.

In our network, as power allocation schemes are not assigned, a user U_e takes a sub-band n_0 with uniform probability $\frac{1}{N}$, according to the FFR strategy. This user U_e experiences fading power and out-of-cell interference denoted by g' and I_{BS}' respectively. $I_{U_e, IBFD}'$ is the interference from all the U_e operating at IBFD and using the FFR scheme.

In order to define the LTs above, i.e. $L_{I_{BS}', I_{BS}}$ and $L_{I_{U_e, IBFD}', I_{U_{IBFD}}}$, the following s domains are defined:

$$S_1 = \mu \frac{P_{S_1} L_{p_1} r^\eta}{P_{S_1} L_{p_1}} T, S_2 = \mu \frac{P_{S_1} L_{p_1} r^\eta}{P_{S_1} L_{p_1}} T_{edge}, S_3 = \mu \frac{P_{S_2} L_{p_2} r^\eta}{P_{S_1} L_{p_1}} T, S_4 = \mu \frac{P_{S_2} L_{p_2} r^\eta}{P_{S_1} L_{p_1}} T_{edge}.$$

Proof: See Appendix IV.A

2. Cell-Core Users:

The probability of coverage for the users U_c operating at IBFD is defined as:

$$p_{U_c}^{\text{st-FR}} = \mathbb{P}\left(\frac{P_{s_1} h_1 L_{p_1} r^{-\eta}}{P_n + P_{s_1} L_{p_1} I_{BS} + P_{s_2} L_{p_2} I_{U_c,IBFD} + \beta P_{s_2}} > T | \text{SINR}_1 > T_{\text{edge}}\right) = \frac{\int_{r>0} E_3 f_r(r) dr}{\int_{r>0} E_4 f_r(r) dr} \quad (4.6)$$

where

$$E_3 = e^{-\mu \frac{r^\eta ((P_n + \beta P_{s_2})(\max\{T, T_{\text{edge}}\} + T_{\text{edge}}))}{P_{s_1} L_{p_1}}} L_{I_{BS}}(\mu r^\eta (\max\{T, T_{\text{edge}}\} + T_{\text{edge}})) L_{I_{U_c,IBFD}, I_{U_{IBFD}}}\left(\mu \frac{P_{s_2} L_{p_2} r^\eta}{P_{s_1} L_{p_1}} \max\{T, T_{\text{edge}}\}, \mu \frac{P_{s_2} L_{p_2} r^\eta}{P_{s_1} L_{p_1}} T_{\text{edge}}\right)$$

$$E_4 = e^{-\mu \frac{r^\eta T_{\text{edge}} (P_n + \beta P_{s_2})}{P_{s_1} L_{p_1}}} L_{I_{BS}}(\mu r^\eta T_{\text{edge}}) L_{I_{U_{IBFD}}}\left(\mu \frac{P_{s_2} L_{p_2} r^\eta}{P_{s_1} L_{p_1}} T_{\text{edge}}\right)$$

where I_{BS} is the interference from all BSs in the network as they share the same resources for the cell-core users, as shown in Figure 4.1. $I_{U_c,IBFD}$ is the interference from all the U_c operating at IBFD.

Proof: See Appendix IV.B.

To analyze the probability of coverage, we need to characterize the LT of the different interference signals experienced by the typical user, either core or edge.

As the different schemes are too complicated to be analytically evaluated, we propose in this work two different approaches:

- 1- Approach I: it approximates the IBFD regions $\Phi_{U_{IBFD}}$ as a PPP with a modified density value derived from the inner-city model i.e., PPP with a density $\lambda_{U_{IBFD}}$.
- 2- Approach II: it uses the actual inner-city model, but gives lower and upper bounds for the probability of coverage. This is because getting the exact formula for such model is very hard and can result in un-tractable results as we will see later.

It is worth mentioning that the BSs distributions are not changing for any approach, hence the LTs of the interferences I_{BS} and I_{BS}' are derived according to PPP as long as their density is updated accordingly. The joint LT of I_{BS}', I_{BS} :

$$L_{I_{BS}', I_{BS}}(s_1, s_2) = \exp \left(-2\pi\lambda_{BS}r^2 \int_1^\infty \left(1 - \frac{1}{1 + \frac{P_{s_1}L_{p_1}T_{edge}}{P_{s_1}L_{p_1}}y^{-\eta}} \left(1 - \frac{1}{N} \left(1 - \frac{1}{1 + \frac{P_{s_1}L_{p_1}T}{P_{s_1}L_{p_1}}y^{-\eta}} \right) \right) \right) y dy \right) \quad (4.7)$$

Proof: See Appendix IV.C.

The LT of I_{BS}' is given by:

$$L_{I_{BS}'}(s_1) = \exp \left(-\frac{\pi\lambda_{BS}}{N} r^2 \left(\frac{P_{s_1}L_{p_1}T}{P_{s_1}L_{p_1}} \right)^{2/\eta} \int_{\left(\frac{P_{s_1}L_{p_1}T}{P_{s_1}L_{p_1}} \right)^{-2/\eta}}^\infty \frac{1}{1 + y^{\eta/2}} dy \right) \quad (4.8)$$

This equation can be viewed as a thinning operation on PPP, in which the density became $\frac{\lambda_{BS}}{N}$.

Proof: See Appendix IV.D.

The Laplace of I_{BS} :

$$L_{I_{BS}} \left(\mu \frac{P_{s_1}L_{p_1}r^\eta}{P_{s_1}L_{p_1}} T_{edge} \right) = \exp \left(-\pi\lambda_{BS}r^2 (T_{edge})^{\frac{2}{\eta}} \int_{T_{edge}^{-2/\eta}}^\infty \left(\frac{1}{y^{\eta/2} + 1} \right) dy \right) \quad (4.9)$$

Proof: this formula is derived similarly to the conventional LT in a homogenous PPP.

3. Approach I:

In approach I, we approximate the IBFD regions by a PPP with density $\lambda_{U_{IBFD}}$. This approximation is optimistic because in the inner-city model the distances between the different interferers increase (including the condition to classify the user as U_e or U_c).

i. Coverage for edge users operating at IBFD:

We start with the LT of $I_{U_{IBFD}}$, using the inner-city model with a PPP of density $\lambda_{U_{IBFD}}$, updated as per the conventional homogeneous PPP model. It is given by:

$$L_{I_{U_{IBFD}}}\left(\mu \frac{P_{s_2} L_{p_2} r^\eta}{P_{s_1} L_{p_1}} T_{edge}\right) = \exp\left(-\pi \lambda_{U_{IBFD}} r^2 \left(\frac{P_{s_2} L_{p_2} T_{edge}}{P_{s_1} L_{p_1}}\right)^{\frac{2}{\eta}} \int_0^\infty \frac{dy}{1+y^{\eta/2}}\right) \quad (4.10)$$

Proof: It is like the proof of I_{BS} except that we are evaluating at a different s and the integral starts at 0 in the Probability Generating Functional (PGFL) of the PPP.

Thus, we can write the term found in the denominator of $p_{U_e}^{st-FR}$ as:

$$\begin{aligned} \int_{r>0} E_2 f_r(r) dr &= 1 - p_{c_2} = 1 - \int_0^\infty f_r(r) e^{-\mu \frac{r^\eta T_{edge} (P_n + \beta P_{s_2})}{P_{s_1} L_{p_1}}} L_{I_{BS}}(\mu r^\eta T_{edge}) L_{I_{U_{IBFD}}}\left(\mu \frac{P_{s_2} L_{p_2} r^\eta}{P_{s_1} L_{p_1}} T_{edge}\right) dr \\ &= 1 - 2\pi \lambda_{BS} \int_0^\infty r e^{-\mu \frac{r^\eta T_{edge} (P_n + \beta P_{s_2})}{P_{s_1} L_{p_1}} - \pi \lambda_{BS} r^2} \left(1 + \left(\frac{P_{s_1} L_{p_1} T_{edge}}{P_{s_1} L_{p_1}}\right)^{\frac{2}{\eta}} \int_{T_{edge}}^\infty \frac{dy}{1+y^{\eta/2}}\right) e^{-\pi \lambda_{U_{IBFD}} r^2 \left(\frac{P_{s_2} L_{p_2} T_{edge}}{P_{s_1} L_{p_1}}\right)^{\frac{2}{\eta}} \int_0^\infty \frac{dy}{1+y^{\eta/2}}} dr \end{aligned}$$

where p_{c_2} is the probability of having $SINR_1$ greater than T_{edge} . It will be used to get the other interference terms experienced by the typical user. For example, p_{c_2} can be used to get the percent of the possible U_c users, as we see later in the joint LT for $I_{U_{e,IBFD}'}, I_{U_{IBFD}}$:

The joint LT for $I_{U_{e,IBFD}'}, I_{U_{IBFD}}$ is given by:

$$\begin{aligned}
L_{I_{U_e,IBFD}',I_{IBFD}} \left(\mu \frac{P_{s_2} L_{p_2} r^\eta}{P_{s_1} L_{p_1}} T, \mu \frac{P_{s_2} L_{p_2} r^\eta}{P_{s_1} L_{p_1}} T_{edge} \right) & \quad (4.11) \\
= \exp \left(-2\pi\lambda_{U_{IBFD}} r^2 \int_0^\infty \left(1 \right. \right. & \\
- \frac{1}{1 + \frac{P_{s_2} L_{p_2} T_{edge}}{P_{s_1} L_{p_1}} y^{-\eta}} \left. \left. \left(1 - \frac{1 - \exp\left(-\frac{\lambda_{BS}}{N} \pi d_F^2\right)}{1 - \exp(-\lambda_{BS} \pi d_F^2)} \right) (1 - p_{c2}) \left(1 - \frac{1}{1 + \frac{P_{s_2} L_{p_2} T}{P_{s_1} L_{p_1}} y^{-\eta}} \right) \right) \right) y dy &
\end{aligned}$$

Proof: See Appendix IV.E.

The LT of $I_{U_e,IBFD}'$ is given by:

$$\begin{aligned}
L_{I_{U_e,IBFD}'} \left(\mu \frac{P_{s_2} L_{p_2} r^\eta}{P_{s_1} L_{p_1}} T \right) & \quad (4.12) \\
= \exp \left(-\pi\lambda_{U_{IBFD}} \left(\frac{1 - \exp\left(-\frac{\lambda_{BS}}{N} \pi d_F^2\right)}{1 - \exp(-\lambda_{BS} \pi d_F^2)} \right) (1 \right. & \\
- p_{c2}) r^2 \left(\frac{P_{s_2} L_{p_2} T}{P_{s_1} L_{p_1}} \right)^{2/\eta} \int_0^\infty \frac{dy}{1 + y^{\eta/2}} &
\end{aligned}$$

Proof: It is similar to 4.10 and available in Appendix IV.F.

This concludes the probability of coverage for edge-user operating at IBFD:

$$p_{Ue}^{st-FR} = \frac{p_{c1} - p_{c3}}{1 - p_{c2}} \quad (4.13)$$

with

$$\begin{aligned}
p_{c1} & \\
= 2\pi\lambda_{BS} r \int_0^\infty e^{-\mu \frac{r^\eta T (P_n + \beta P_{s_2})}{P_{s_1} L_{p_1}} - \pi\lambda_{BS} r^2 \left(1 + \frac{1}{N} T^{2/\eta} \int_T^\infty \rho_1 \right) - \pi\lambda_{U_{IBFD}} \left(\frac{1 - e^{-\frac{\lambda_{BS}}{N} \pi d_F^2}}{1 - e^{-\lambda_{BS} \pi d_F^2}} \right) (1 - p_{c2}) r^2 \left(\frac{P_{s_2} L_{p_2} T}{P_{s_1} L_{p_1}} \right)^{2/\eta} \int_0^\infty \frac{dy}{1 + y^{\eta/2}}} & dr
\end{aligned}$$

$$p_{c2} = 2\pi\lambda_{BS}r \int_0^\infty e^{-\mu \frac{r^\eta T_{edge}(P_n + \beta P_{s2})}{P_{s1}L_{p1}} - \pi\lambda_{BS}r^2 \left(1 + T_{edge} \frac{2}{\eta} \int_{T_{edge}}^\infty \frac{dy}{1+y^{\eta/2}}\right) - \pi\lambda_{UBFD}r^2 \left(\frac{P_{s2}L_{p2}T_{edge}}{P_{s1}L_{p1}}\right)^{\frac{2}{\eta}} \int_0^\infty \frac{dy}{1+y^{\eta/2}}} dr$$

$$p_{c3} = 2\pi\lambda_{BS}r \int_0^\infty e^{-\mu \frac{r^\eta ((P_n + \beta P_{s2})T + (P_n + \beta P_{s2})T_{edge})}{P_{s1}L_{p1}} - \pi\lambda_{BS}r^2 (1 + 2\rho 1_{(P_{s1}L_{p1}, T, T_{edge})}) - 2\pi\lambda_{UBFD}r^2 \rho 2_{(P_{s2}L_{p2}, T, T_{edge})}} dr$$

$$\rho 1_{(P_{s_j}L_{p_j}, T, T_{edge})} = \int_1^\infty \left(1 - \frac{1}{1 + \frac{P_{s_j}L_{p_j}T_{edge}}{P_{s1}L_{p1}} y^{-\eta}} \left(1 - \frac{1}{N} \left(1 - \frac{1}{1 + \frac{P_{s_j}L_{p_j}T}{P_{s1}L_{p1}} y^{-\eta}} \right) \right) \right) y dy \text{ for } j \in \{1, 2\}$$

$$\rho 2_{(P_{s_j}L_{p_j}, T, T_{edge})} = \int_0^\infty \left(1 - \frac{1}{1 + \frac{P_{s_j}L_{p_j}T_{edge}}{P_{s1}L_{p1}} y^{-\eta}} \left(1 - \left(\frac{1 - e^{-\frac{\lambda_{BS}\pi d_F^2}{N}}}{1 - e^{-\lambda_{BS}\pi d_F^2}} \right) (1 - p_{c2}) \left(1 - \frac{1}{1 + \frac{P_{s_j}L_{p_j}T}{P_{s1}L_{p1}} y^{-\eta}} \right) \right) \right) y dy \text{ for } j \in \{1, 2\}$$

ii. Coverage for core users operating at IBFD:

For the U_c the LT of I_{BS} is evaluated at $s = \mu \frac{P_{s1}L_{p1}r^\eta}{P_{s1}L_{p1}} (\max\{T, T_{edge}\} + T_{edge})$, thus the formula is:

$$\begin{aligned} L_{I_{BS}} \left(\mu \frac{P_{s1}L_{p1}r^\eta}{P_{s1}L_{p1}} (\max\{T, T_{edge}\} + T_{edge}) \right) & \quad (4.14) \\ = \exp \left(-\pi\lambda_{BS}r^2 \left(\frac{P_{s1}L_{p1}(\max\{T, T_{edge}\} + T_{edge})}{P_{s1}L_{p1}} \right)^{\frac{2}{\eta}} \int_{\left(\frac{P_{s1}L_{p1}(\max\{T, T_{edge}\} + T_{edge})}{P_{s1}L_{p1}} \right)^{-2/\eta}}^\infty \frac{dy}{1+y^{\eta/2}} \right) \end{aligned}$$

Also, in St-FFR we don't apply the frequency scheme on the core users, thus bands for core-user are used by all BSs. So, the core user will not experience a new interference I_{BS}' .

To get $L_{I_{UC,IBFD}, I_{UBFD}}$, the same approximation for the inner-city model is followed using a density λ_{IBFD} . We have

$$\begin{aligned}
L_{I_{Uc,IBFD},I_{U,IBFD}} \left(\mu \frac{P_{s_2} L_{p_2} r^\eta}{P_{s_1} L_{p_1}} \max\{T, T_{edge}\}, \mu \frac{P_{s_2} L_{p_2} r^\eta}{P_{s_1} L_{p_1}} T_{edge} \right) &= \mathbb{E}_{I_r} [\exp(-s_5 I_{Uc,IBFD} - s_4 I_{U,IBFD})] \\
&= (a) \mathbb{E}_{\phi_{U,IBFD}, g_i', g_i} \left[\prod_{i \in \phi_{U,IBFD} \setminus U_0} \exp(-s_4 g_i R_i^{-\eta}) (1 - \mathbb{E}[\mathbf{1}(U_i \in Uc, IBFD)] (1 - \exp(-s_5 g_i' R_i^{-\eta}))) \right]
\end{aligned}$$

Thus

$$\begin{aligned}
L_{I_{Uc,IBFD},I_{U,IBFD}} \left(\mu \frac{P_{s_2} L_{p_2} r^\eta}{P_{s_1} L_{p_1}} \max\{T, T_{edge}\}, \mu \frac{P_{s_2} L_{p_2} r^\eta}{P_{s_1} L_{p_1}} T_{edge} \right) & \quad (4.15) \\
&= (b) \exp \left(-2\pi\lambda_{U,IBFD} r^2 \int_0^\infty \left(1 - \frac{1}{1 + \frac{P_{s_2} L_{p_2} T_{edge}}{P_{s_1} L_{p_1}} y^{-\eta}} \left(1 - p_{c2} \left(1 - \frac{1}{1 + \frac{P_{s_2} L_{p_2} \max\{T, T_{edge}\}}{P_{s_1} L_{p_1}} y^{-\eta}} \right) \right) \right) y dy \right)
\end{aligned}$$

with

$$s_5 = \mu \frac{P_{s_2} L_{p_2} r^\eta}{P_{s_1} L_{p_1}} \max\{T, T_{edge}\}$$

The indicator function $\mathbf{1}(U_i \in Uc, IBFD)$ in (a) is present because only the core users generate interference (not all of them). (b) is obtained by substituting the expectation of the indicator function which is the probability to have $SINR_1 > T_{edge}$.

This concludes the probability of coverage for core-user operating with IBFD:

$$p_{Uc}^{st-FR} = \frac{p_{c4}}{p_{c2}} \quad (4.16)$$

With

$$\begin{aligned}
&p_{c4} \\
&= 2\pi\lambda_{BS} r \int_0^\infty e^{-\mu \frac{r^\eta ((P_n + \beta P_{s_2}) (\max\{T, T_{edge}\} + T_{edge}))}{P_{s_1} L_{p_1}}} - \pi\lambda_{BS} r^2 \left(1 + (\max\{T, T_{edge}\} + T_{edge})^{\frac{2}{\eta}} \int_{(\max\{T, T_{edge}\} + T_{edge})}^\infty \frac{dy}{(1+y)^{\eta/2}} \right) - 2\pi\lambda_{U,IBFD} r^2 \rho_3 \quad dr
\end{aligned}$$

where

$$\rho_3 = \int_0^\infty \left(1 - \frac{1}{1 + \frac{P_{s_2} L_{p_2} T_{edge}}{P_{s_1} L_{p_1}} y^{-\eta}} \left(1 - p_{c2} \left(1 - \frac{1}{1 + \frac{P_{s_2} L_{p_2} \max\{T, T_{edge}\}}{P_{s_1} L_{p_1}} y^{-\eta}} \right) \right) \right) y dy$$

4. Approach II:

In this section, we adopt a more realistic model where an overlap between the IBFD regions (disks) might exist. This is because the BSs PPP model (the centers of the disks) does not have a minimum separating distance between the BSs, and is independent from the radius of the IBFD disks d_F . Henceforth, we derive tight lower and upper bounds of the LT interference. To tackle this problem, we extend the work in [63] based on the PHP where the typical user is outside the disks. However, contrarily to [63], the users of interest are within the IBFD disks and adapt those techniques accordingly.

Before we define the lower and the upper bounds, we use Figure 4.4 to clarify the terms used in the upper bound definition (definition 2). In the figure, we show the two nearest disks that contain the users causing interference on the typical user. The first disk center is at distance r_0 from the typical user and of radius d_F , and the second is at r_1 and with same radius d_F .

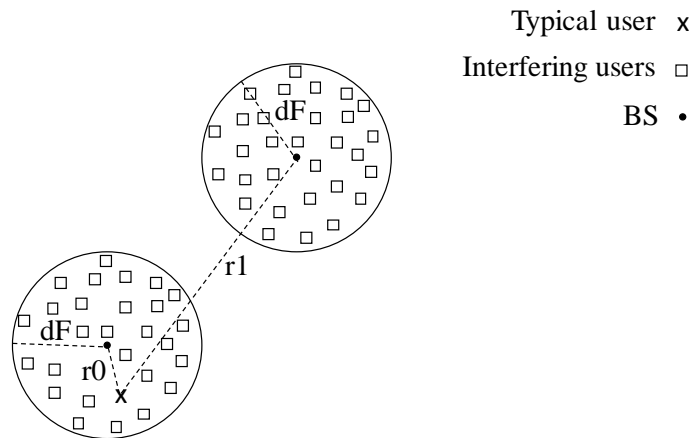


Figure 4.4: Upper bound for LT of interference. For case 1, we consider one disk $b(r_0, d_F)$, and for case 2 we consider two disks $b(r_0, d_F)$ and $b(r_1, d_F)$.

Definition 2, Upper Bound for the LT: In an inner-city model, we have the upper bound for the LT of the interference when we are underestimating the interference. An easy underestimate for the interference is to consider only n finite number of disks that contain the interfering sources rather considering them all. These finite disks are the n nearest ones to the typical user, so they have the strongest interference effect due to the lower path loss. However, this creates a problem in the approximation due to the possible overlapping regions among the interfering sources. More importantly, for $n > 1$, the interference from the overlapped region should be considered once. If we do not do this, we will be taking the interference in the overlapped regions two\many times depending on the number of the overlapped disks. This means that the definition will not be valid if the possible overlapped regions are not handled. As we will see later, an easy solution is to just avoid the possible overlap between the disks, and this still holds as an underestimate for the interference. In our analysis, to calculate the LT of the different interferences ($I_{U,IBFD}, I_{U_e,IBFD}', I_{UC,IBFD}$), we take two cases for the upper bound. The first version or case (**case 1**) is to consider the interference source only from the same disk where the typical user is located ($n = 1$) (consider the disk of radius r_0 in Figure 4.4). Similarly, the second case (**case 2**) is to consider these sources from the same disk $b(r_0, d_F)$ and from the nearest disk $b(r_1, d_F)$ i.e. ($n = 2$). The second case gives a tighter bound, and can be easily extended to n points, but requires more time to evaluate.

Definition 3, Lower Bound for the LT: the lower bound for the LT is when we overestimate the interference. A simple overestimate is to consider all the IBFD disks without canceling the possible overlap. So, the interference sources in the overlapped regions, if it exists, will be calculated many times depending on the number of the overlapped disks. Such definition can give the exact formula for the LT if the network model input is configured so that no overlap between disks exists; this is particularly true when we have both small density λ_{BS} and small IBFD radius d_F .

i. Coverage for edge users operating at IBFD:

As a summary, we provide the upper and the lower bound for the LTs of the different interferences in the network in the following table:

LT Term	Expression
$L_{I_{U_{IBFD}}}(s_4)$ upper bound case 1	$L_{I_{U_{IBFD}}}(s_4) \leq \int_0^{\infty} 2\pi\lambda_{BS}r_0 \exp(-\pi\lambda_{BS}r_0^2) \exp(-2\lambda_U A_1(s_4, r_0, d_F)) dr_0 \quad (4.17)$ <p>with $A_1(s_4, r_0, d_F) = \int_{r_0-d_F}^{r_0+d_F} \frac{\cos^{-1}\left(\frac{x^2+r_0^2-d_F^2}{2r_0x}\right)}{1+\frac{\mu x^\eta}{s_4}} x dx$</p> <p>where r_0 is the center of the same disk that the typical user exists in and contains users causing interference.</p>
$L_{I_{U_{IBFD}}}(s_4)$ upper bound case 2	$L_{I_{U_{IBFD}}}(s_4) \leq \int_0^{\infty} \int_{r_0}^{\infty} (2\pi\lambda_{BS})^2 r_0 r_1 \exp(-\pi\lambda_{BS}r_1^2) \exp(-2\lambda_U (A_1(s_4, r_0, d_F) + A_2(s_4, r_1, d_F, r_0))) dr_1 dr_0 \quad (4.18)$ <p>with $A_2(s_4, r_1, d_F, r_0) = \int_{\max(r_1-d_F, r_0+d_F)}^{r_1+d_F} \frac{\cos^{-1}\left(\frac{x^2+r_1^2-d_F^2}{2r_1x}\right)}{1+\frac{\mu x^\eta}{s_4}} x dx$</p> <p>$r_1$ is the center of the nearest disk (other than the same disk) that contains users causing interference, and the boundaries of the area A_2 are set to avoid any possible overlap between the two disks.</p>
$L_{I_{U_{IBFD}}}(s_4)$ lower bound	$L_{I_{U_{IBFD}}}(s_4) \geq \exp\left[-2\pi\lambda_{BS} \int_0^{\infty} (1 - \exp(-2\lambda_U A_1(s_4, y, d_F))) y dy\right] \quad (4.19)$
$L_{I_{U_e,IBFD}}'(s_3)$ upper bound case 1	$L_{I_{U_e,IBFD}}'(s_3) \leq \int_0^{\infty} 2\pi \frac{\lambda_{BS}}{N} r_0 \exp\left(-\pi \frac{\lambda_{BS}}{N} r_0^2\right) \exp\left(-2\lambda_U (A_1(s_3, r_0, d_F) - A_1(s_3, r_0, a_1))\right) dr_0 \quad (4.20)$

	<p>with $a_1 = p_{c2}'d_F = d_F \frac{\mathbb{P}[SINR_1 > T_{edge}, r < d_F]}{\mathbb{P}[r < d_F]} = d_F \frac{2\pi\lambda_{BS}r}{1 - \exp(-\pi\lambda_{BS}d_F^2)} \times$</p> $\int_0^{d_F} e^{-\mu \frac{r^\eta T_{edge} (P_n + \beta P_{s2})}{P_{s1} L_{p1}} - \pi\lambda_{BS}r^2 \left(1 + (T_{edge})^{\frac{2}{\eta}} \int_{T_{edge}}^{\infty} \frac{dy}{1+y^{\eta/2}}\right) - \pi\lambda_{U_{IBFD}} r^2 \left(\frac{P_{s2} L_{p2} T_{edge}}{P_{s1} L_{p1}}\right)^{\frac{2}{\eta}} \int_0^{\infty} \frac{dy}{1+y^{\eta/2}}} dr$ <p>For simplification, we have approximated the region of the edge users as a circular region.</p>
<p>$L_{I_{U_{e,IBFD}}}'(\mathbf{s}_3)$ upper bound case 2</p>	$L_{I_{U_{e,IBFD}}}(\mathbf{s}_3) \tag{4.21}$ $\leq \int_0^{\infty} \int_{r_0}^{\infty} \left(2\pi \frac{\lambda_{BS}}{N}\right)^2 r_0 r_1 \exp\left(-\pi \frac{\lambda_{BS}}{N} r_1^2\right) \exp\left(-2\lambda_U(A_1(\mathbf{s}_3, r_0, d_F) - A_1(\mathbf{s}_3, r_0, a_1))\right) \exp\left(-2\lambda_U(A_2(\mathbf{s}_3, r_1, d_F, r_0) - A_3(\mathbf{s}_3, r_1, a_1, r_0, d_F))\right) dr_1 dr_0$ <p>With $A_3(\mathbf{s}_3, r_1, a_1, r_0, d_F) = \int_{\max(r_1 - a_1, r_0 + d_F)}^{\max(r_1 + a_1, r_0 + d_F)} \frac{\cos^{-1}\left(\frac{x^2 + r_1^2 - a_1^2}{2r_1x}\right)}{1 + \frac{\mu}{s_3} x^\eta} x dx$</p>
<p>$L_{I_{U_{e,IBFD}}}'(\mathbf{s}_3)$ lower bound</p>	$L_{I_{U_{e,IBFD}}}'(\mathbf{s}_3) \geq \mathbb{E}_{\phi_{BS}} \left[\prod_{y \in \phi_{BS}} \exp\left(-2\lambda_U(A_1(\mathbf{s}_3, y, d_F) - A_1(\mathbf{s}_3, y, a_1))\right) \right] \tag{4.22}$ $= \exp\left[-2\pi \frac{\lambda_{BS}}{N} \int_0^{\infty} \left(1 - \exp\left(-2\lambda_U(A_1(\mathbf{s}_3, y, d_F) - A_1(\mathbf{s}_3, y, a_1))\right)\right) y dy\right]$
<p>$L_{I_{U_{e,IBFD}}}'(\mathbf{s}_3, \mathbf{s}_4)$ upper bound case 1</p>	$L_{I_{U_{e,IBFD}}}'(\mathbf{s}_3, \mathbf{s}_4) \tag{4.23}$ $\leq \int_0^{\infty} 2\pi\lambda_{BS}r_0 \exp(-\pi\lambda_{BS}r_0^2) \exp(-2\lambda_U A_1(\mathbf{s}_4, r_0, d_F)) \left[1 - \frac{1}{N} \left(1 - \exp\left(-2\lambda_U(A_1(\mathbf{s}_3, r_0, d_F) - A_1(\mathbf{s}_3, r_0, a_1))\right)\right)\right] dr_0$

$L_{I_{U_e,IBFD}}, I_{U,IBFD}}(s_3, s_4)$ upper bound case 2	$L_{I_{U_e,IBFD}}, I_{U,IBFD}}(s_3, s_4) \tag{4.24}$ $\leq \int_0^\infty \int_{r_0}^\infty (2\pi\lambda_{BS})^2 r_0 r_1 \exp(-\pi\lambda_{BS}r_1^2) \exp(-2\lambda_U(A_1(s_4, r_0, d_F) + A_2(s_4, r_1, d_F, r_0))) \left[1 - \frac{1}{N} \left(1 - \exp(-2\lambda_U(A_1(s_3, r_0, d_F) - A_1(s_3, r_0, a_1) + A_2(s_3, r_1, d_F, r_0) - A_3(s_3, r_1, a_1, r_0, d_F))) \right) \right] dr_1 dr_0$
$L_{I_{U_e,IBFD}}, I_{U,IBFD}}(s_3, s_4)$ lower bound	$L_{I_{U_e,IBFD}}, I_{U,IBFD}}(s_3, s_4) \geq \exp \left[-2\pi\lambda_{BS} \int_0^\infty (1 - \xi(y)) y dy \right] \tag{4.25}$ <p>Where $\xi(y) = \exp(-2\lambda_U A_1(s_4, y, d_F)) \left[1 - \frac{1}{N} \left(1 - \exp(-2\lambda_U (A_1(s_3, y, d_F) - A_1(s_3, y, a_1))) \right) \right]$</p>

Table 4.2: Upper and lower bounds of the LT of the different interference evaluated using Approach 2.

Proof: See Appendix IV.G.

In Figure 4.5, we depict the lower and upper bounds for the LT of $L_{I_{U_e,IBFD}}(s_3)$ including noise

i.e. we plot $e^{-\mu \frac{r^\eta T(P_n + \beta P_{s_2})}{P_{s_1} L_{p_1}}} L_{I_{U_e,IBFD}}(s_3)$ at a specific d_F and distance r to the serving BS. It is very clear that the lower and upper bounds are tight from one side and case 2 is even tight as the interference is considered from two different disks.

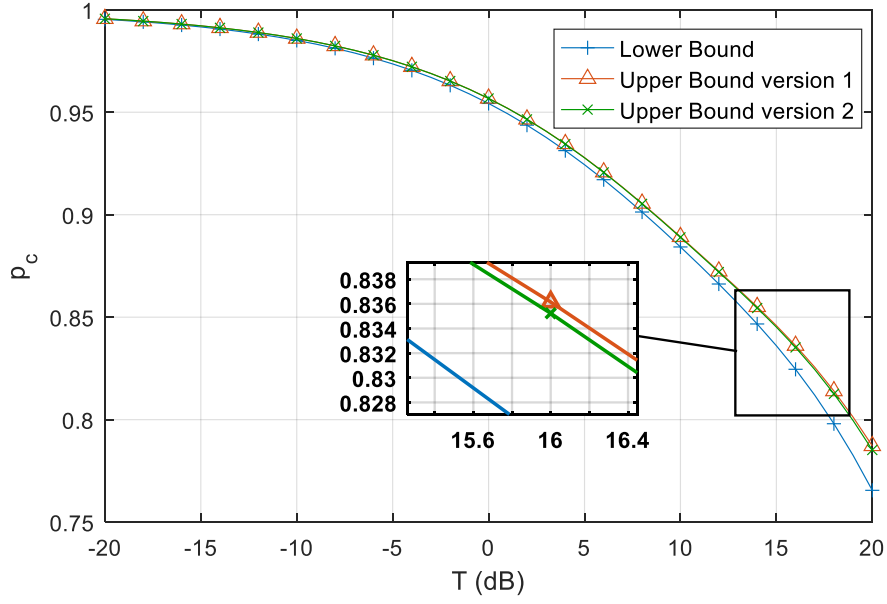


Figure 4.5: Lower and upper bounds for the LT of $L_{U_e,IBFD}'(s_3)$ plus noise. The more disks we take the tighter the upper bound becomes.

The probability of coverage can be deduced from the different LTs provided earlier. The lower bound of the probability of coverage of an edge user U_e is then given by:

$$\begin{aligned}
 p_{U_e}(r) & \quad (4.26) \\
 & \geq \frac{e^{-\mu \frac{r^\eta T (P_n + \beta P_{s_2})}{P_{s_1} L_{p_1}}} L_{I_{BS}'}(\mathbf{s}_1) L_{I_{U_e,IBFD}'}^{lower}(\mathbf{s}_3)}{1 - e^{-\mu \frac{r^\eta T_{edge} (P_n + \beta P_{s_2})}{P_{s_1} L_{p_1}}} L_{I_{BS}}(\mathbf{s}_2) L_{I_{U_{IBFD}}}^{upper}(\mathbf{s}_4)} \\
 & = \frac{e^{-\mu \frac{r^\eta ((P_n + \beta P_{s_2})T + (P_n + \beta P_{s_2})T_{edge})}{P_{s_1} L_{p_1}}} L_{I_{BS}',I_{BS}}(\mathbf{s}_1, \mathbf{s}_2) \cdot L_{I_{U_e,IBFD}'}^{upper}(\mathbf{s}_3, \mathbf{s}_4)}{1 - e^{-\mu \frac{r^\eta T_{edge} (P_n + \beta P_{s_2})}{P_{s_1} L_{p_1}}} L_{I_{BS}}(\mathbf{s}_2) L_{I_{U_{IBFD}}}^{upper}(\mathbf{s}_4)}
 \end{aligned}$$

The upper bound of the probability of coverage can be also deduced by inverting the lower and the upper bounds for the LTs expressions in the formulation above.

ii. Coverage for core users operating at IBFD:

For the core user, we need to additionally write the formula for the joint LT of $I_{U_c, IBFD}, I_{U_{IBFD}}$, which is the joint LT between the core users operating at IBFD and between all the IBFD users.

Different from approach I, we now use the definitions 2 and 3 to compute this LT:

LT Term	Expression
$L_{I_{U_c, IBFD}, I_{U_{IBFD}}}(s_5, s_4)$ upper bound case 1	$L_{I_{U_c, IBFD}, I_{U_{IBFD}}}(s_5, s_4) \quad (4.27)$ $\leq \int_0^{\infty} 2\pi\lambda_{BS}r_0 \exp(-\pi\lambda_{BS}r_0^2) \exp(-2\lambda_U(A_1(s_5, r_0, a_1) + A_1(s_4, r_0, d_F))) dr_0$
$L_{I_{U_c, IBFD}, I_{U_{IBFD}}}(s_5, s_4)$ upper bound case 2	$L_{I_{U_c, IBFD}, I_{U_{IBFD}}}(s_5, s_4) \quad (4.28)$ $\leq \int_0^{\infty} \int_{r_0}^{\infty} (2\pi\lambda_{BS})^2 r_0 r_1 \exp(-\pi\lambda_{BS}r_1^2) \exp(-2\lambda_U(A_1(s_5, r_0, a_1) + A_2(s_5, r_1, a_1, r_0) + A_1(s_4, r_0, d_F) + A_2(s_4, r_1, d_F, r_0))) dr_1 dr_0$
$L_{I_{U_c, IBFD}, I_{U_{IBFD}}}(s_5, s_4)$ lower bound	$L_{I_{U_c, IBFD}, I_{U_{IBFD}}}(s_5, s_4) \quad (4.29)$ $\geq \exp\left[-2\pi\lambda_{BS} \int_0^{\infty} \left(1 - \exp(-2\lambda_U(A_1(s_5, y, a_1) + A_1(s_4, y, d_F)))\right) y dy\right]$

Table 4.3: Upper and lower bounds of the joint LT of $I_{U_c, IBFD}, I_{U_{IBFD}}$ interference using Approach 2.

Proof: See Appendix IV.H.

Using Table 4.3, the lower bound for the probability of coverage for U_c is:

$$p_{U_c}(r) \geq \frac{e^{-\mu \frac{r^\eta((P_n + \beta P_{s_2})(\max\{T, T_{edge}\} + T_{edge}))}{P_{s_1} L_{p_1}}} L_{I_{BS}}(s_5) L_{I_{U_c}, I_{U_{IBFD}}}^{lower}(s_6, s_4)}{e^{-\mu \frac{r^\eta T_{edge}(P_n + \beta P_{s_2})}{P_{s_1} L_{p_1}}} L_{I_{BS}}(s_2) L_{I_{U_{IBFD}}}^{upper}(s_4)} \quad (4.30)$$

with $s_5 = \mu r^\eta (\max\{T, T_{edge}\} + T_{edge})$ and $s_6 = \mu \frac{P_{s_2} L_{p_2} r^\eta}{P_{s_1} L_{p_1}} \max\{T, T_{edge}\}$

The upper bound is similarly obtained by using the upper bound for the LT of $L_{I_{U_c}, I_{U_{IBFD}}}$ in the numerator and the lower bound for the LT of $L_{I_{U_{IBFD}}}$ in the denominator.

5. A Use Case for the General Model:

In this section, we present a general model including both IBFD and FFR schemes. The target here is an easy generalization of the different resource sharing schemes. We show the use case model for the channel resources scheme in Table 4.4.

Bands	Frequencies # in each band $f_{\#}^{band}$	Codes for UL	Codes for DL
Band 1	$f_1^1, f_2^1, \dots, f_n^1$	C_1	C_2, C_3, \dots, C_m
Band 2	$f_1^2, f_2^2, \dots, f_n^2$	C_1	C_2, C_3, \dots, C_m
Band 3	$f_1^3, f_2^3, \dots, f_n^3$	C_1	C_2, C_3, \dots, C_m
Band 4	$f_1^4, f_2^4, \dots, f_n^4$	C_1	C_2, C_3, \dots, C_m

Table 4.4: Use case channel resources allocation.

To illustrate, we give in Figure 4.6 an example about the resources distributed in a cell:

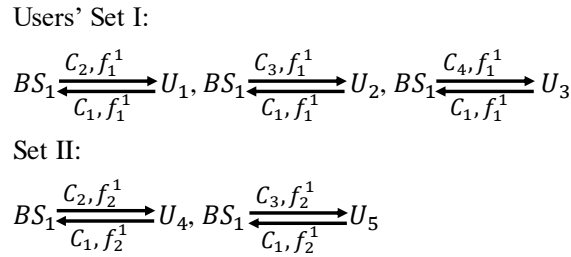


Figure 4.6: Resources allocation example in cell 1; same scheme is used in each N^{th} neighbor cell according to the FFR.

We assume that the condition to classify the user as U_e or U_c still holds. the number of the used frequencies and the orthogonal codes will determine the density of the users that are causing interference which will be used in the LT of $I_{U_e, IBFD}'$. This scheme protects the uplink from the

downlink by using different orthogonal codes, so the downlink and the uplink analysis are different. An uplink analysis will lead to the following SINR, where the LT formulas are already calculated in the general model:

$$p_{Ue}^{\text{st-FR}} = \mathbb{P}\left(\frac{P_{s_2} h_1 L_{p_1} r^{-\eta}}{P_n + P_{s_2} L_{p_2} I_{Ue,IBFD}' + \beta P_{s_2}} > T | \text{SINR}_1 < T_{edge}\right) \quad (4.31)$$

G. Mean Achievable Rate:

IBFD increases the spectral efficiency and thus the data rate for a specific user due to the simultaneous use of the band in both UL and DL. On the other side, users operating at IBFD experience higher interference than those operating at Half-duplex resulting in a degraded SINR values hence reduced capacity. Hence, appropriate definition of the IBFD regions should be found. This will be a compromise between the probability of coverage loss and capacity increase. In this section, we study the mean achievable rate for a typical user, which is an outage-based metric.

The achievable rate is defined as:

$$\tau = \mathbb{E}[\ln(1 + \text{SINR}_{H\text{-duplex}})] \quad (4.32)$$

For a typical user operating at IBFD, it is defined by:

$$\begin{aligned} \tau &= \mathbb{E}[2 \ln(1 + \text{SINR}_{IBFD})] \quad (\text{nats/Hz}) \quad (4.33) \\ \tau &= \mathbb{E}[2 \ln(1 + \text{SINR}_{IBFD})] = \int_0^{\infty} 2\pi\lambda_{BS}r e^{-\pi\lambda_{BS}r^2} \mathbb{P}\left[\ln(1 + \text{SINR}_{IBFD}) > \frac{t}{2}\right] dr \\ &= \int_0^{\infty} 2\pi\lambda_{BS}r e^{-\pi\lambda_{BS}r^2} \int_0^{\infty} \mathbb{P}\left[\text{SINR}_{IBFD} > e^{\frac{t}{2}} - 1\right] dt dr \\ &= \int_0^{\infty} \int_0^{\infty} 2\pi\lambda_{BS}r e^{-\pi\lambda_{BS}r^2} \mathbb{P}\left[\text{SINR}_{IBFD} > e^{\frac{t}{2}} - 1\right] dr dt \end{aligned}$$

Similarly to the probability of coverage, the mean achievable rate for an edge user operating at IBFD:

$$\begin{aligned}
\tau_{U_e} &= \mathbb{P} \left[SINR_{IBFD} > e^{\frac{t}{2}-1} \right] \\
&= \mathbb{P} \left(\frac{P_{s_1} h_1 L_{p_1} r^{-\eta}}{P_n + P_{s_1} L_{p_1} I_{BS}' + P_{s_2} L_{p_2} I_{U_e,IBFD}' + \beta P_{s_2}} \right. \\
&\quad \left. > e^{\frac{t}{2}-1} \mid \frac{P_{s_1} h_2 L_{p_1} r^{-\eta}}{P_n + P_{s_1} L_{p_1} I_{BS} + P_{s_2} L_{p_2} I_{U,IBFD} + \beta P_{s_2}} < T_{edge} \right) \\
&= \frac{\mathbb{P} \left(\frac{P_{s_1} h_1 L_{p_1} r^{-\eta}}{P_n + P_{s_1} L_{p_1} I_{BS}' + P_{s_2} L_{p_2} I_{U_e,IBFD}' + \beta P_{s_2}} > e^{\frac{t}{2}-1}, \frac{P_{s_1} h_2 L_{p_1} r^{-\eta}}{P_n + P_{s_1} L_{p_1} I_{BS} + P_{s_2} L_{p_2} I_{U,IBFD} + \beta P_{s_2}} < T_{edge} \right)}{\mathbb{P} \left(\frac{P_{s_1} h_2 L_{p_1} r^{-\eta}}{P_n + P_{s_1} L_{p_1} I_{BS} + P_{s_2} L_{p_2} I_{U,IBFD} + \beta P_{s_2}} < T_{edge} \right)} \\
\tau_{U_e} &= \int_0^{\infty} \frac{p_{c1}(t) - p_{c3}(t)}{1 - p_{c2}} dt \tag{4.34}
\end{aligned}$$

In this expression, we replaced T by $e^{\frac{t}{2}-1}$.

Similarly, for the core user operating at IBFD we have:

$$\tau_{U_c} = \int_0^{\infty} \frac{p_{c4}(t)}{p_{c2}} dt \tag{4.35}$$

H. Simulation Results:

In this section, we numerically simulate the derived formulas and we show how the network performance changes with respect to the different network configurations. We also compare the performance of the network to that of the model found in [57] that uses the FFR for simple half-duplex users. Unless mentioned in the figures, we present in Table 4.5 the general simulation parameters, where the terms L_{p_1} and L_{p_2} were defined as follows: $L_{p_1} = L_{p_2} =$

$$G_t G_r \left(\frac{c}{4\pi f} \right)^2.$$

Parameter	Value
$P_{s_1}; P_{s_2}; P_n$	37 dBm; 17 dBm; -104 dBm
$G_t; G_r; f$	20 dB; 5 dB; 1800 MHz
N	3
d_F	0.2 km
$\lambda_{BS}; \lambda_U$	2; 100
η	4
T_{edge}	1 dB
β	0.1
μ	1

Table 4.5: Simulation Parameters.

In Figure 4.7, and using approach 1, we present the probability of coverage p_c for the typical edge user U_e operating at IBFD versus the SINR threshold T . As d_F increases, the probability of coverage p_c decreases because higher interference from the edge users is experienced by the typical edge users. Moreover, we can see that p_c saturates as d_F increases. Indeed, increasing d_F does not result in an increase in the number of interfering users. Furthermore, setting d_F to a very small value gives the same p_c of edge users in a network using only half duplex ($st - FFR, U_e, H$). In Figure 4.8, we present p_c for a core user operating at IBFD. In Figure 4.9, we compare the p_c for the edge and core users' cases. As seen, the p_c for core users is higher than that of the edge users, and for the edge users it is increasing with the BS density. As for the core users, it is not always increasing with the BS density, the reason for this may be related to the fact that the strict FFR scheme is giving better ICIC to the edge user than that of the core that is benefiting less from the strict FFR scheme.

Additionally, in Figure 4.10 we show the effect of increasing the reuse factor N on the probability of coverage for the edge user. We can see how FFR is beneficial for the edge users. On the other hand, the strict FFR scheme increases the coverage for the core users by separating

them from the edge users, but does not give them benefits, because N applies only for the edge users.

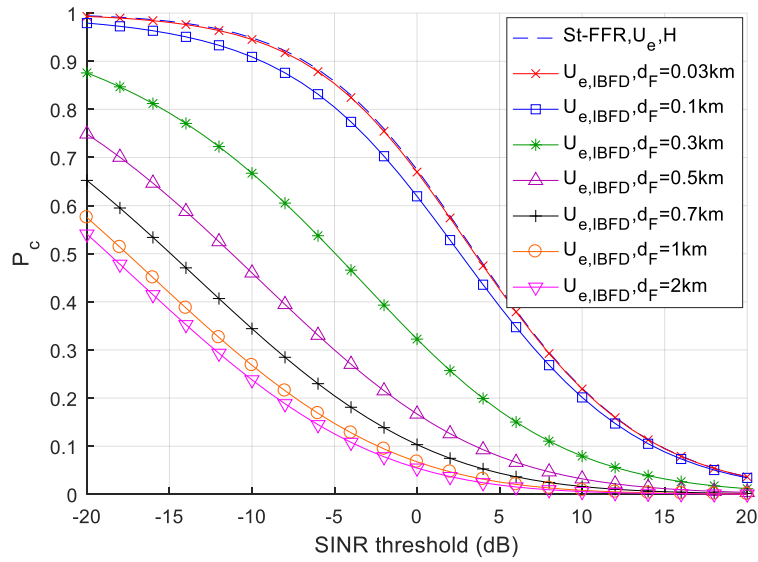


Figure 4.7: Coverage probability using approach 1 for U_e operating at IBFD at different d_F , and for half-duplex U_e .

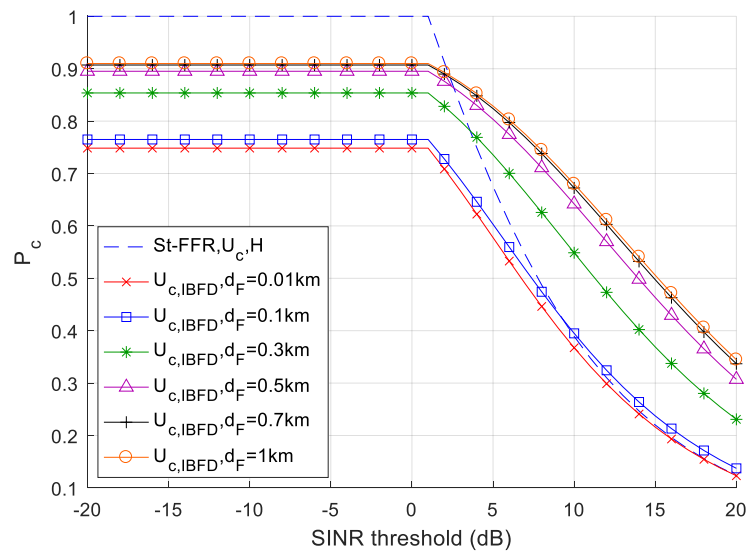


Figure 4.8: Coverage probability using approach 1 for U_c operating at IBFD at different d_F , and for half-duplex U_c .

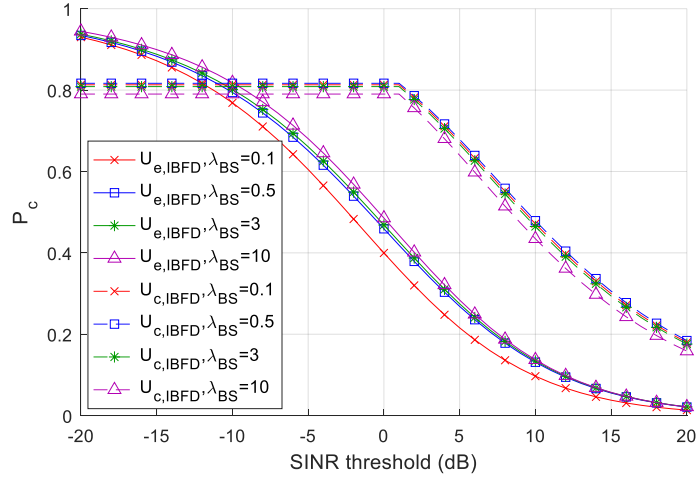


Figure 4.9: Coverage probability using approach 1 comparison between U_e and U_c at different λ_{BS} .

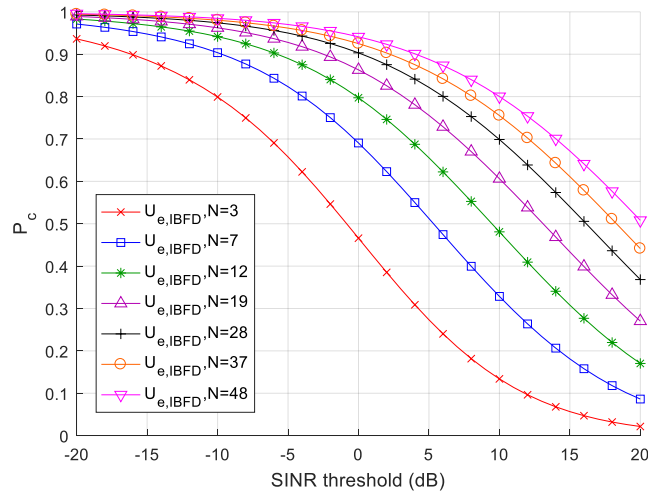


Figure 4.10: Coverage probability using approach 1 for U_e with respect to different N .

In Figure 4.11, we plot the mean achievable rate using Approach 1. The rate for the typical edge user operating at IBFD at $T = -20 \text{ dB}$ is $2.3765 \text{ nats/Hz} = 3.4285 \text{ bits/Hz}$. It is $1.2508 \text{ nats/Hz} = 1.8045 \text{ bits/Hz}$ for the half-duplex case. Thus, operating at IBFD with the shared network resources has increased the mean achievable rate by a factor of 1.71. On higher T , this increase is lower, as expected, by a factor of 1.22 times. As for the core user operating at IBFD at $T = -20 \text{ dB}$, the rate is $1.9442 \text{ nats/Hz} = 2.8049 \text{ bits/Hz}$, while for the core user operating at half-duplex, it is $1.5038 \text{ nats/Hz} = 2.1695 \text{ bits/Hz}$, which means it increased by a factor of 1.29. Besides, at higher T , $T = 20 \text{ dB}$, it increased by

a factor of 1.95. On the other side, when we increase the radius d_F of the IBFD region, we observe a decrease in the mean rate for the edge user. As for the core user, the variation strongly depends on T_{edge} that is used. For the edge user, this decrease was big enough in which their mean rate became lower than that of half duplex users. The reason for this is that the SINR became very low and the user is not benefitting from the IBFD operation, which was reflected on the mean rate. This shows that we should carefully determine the region of IBFD operation which mainly depends on the system inputs, and if we don't do this we will not be benefitting from the IBFD. Moreover, at low T_{edge} , the mean rate for the core user is now greater than the half-duplex core user by a factor of 1.0224 at $T = -20$ dB and a factor of 2.4380 at $T = 20$ dB. This shows that our model can get the best radius for the IBFD region that can be used for a specific network configuration. It also shows the limit of this radius, in which the edge user will not benefitting from IBFD operation.

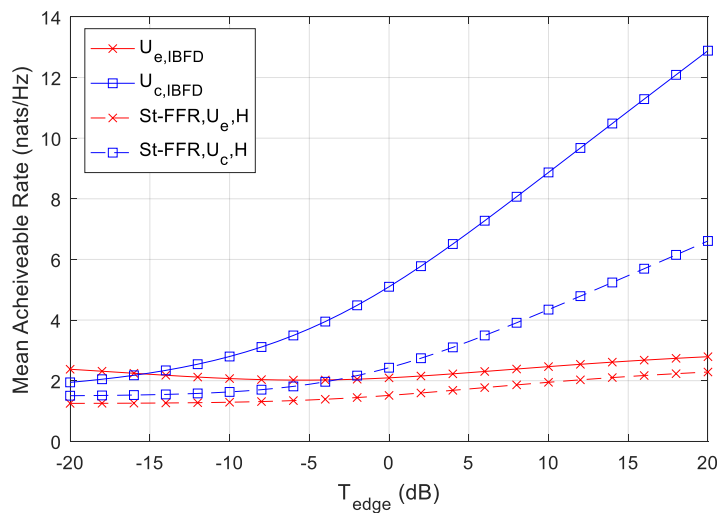


Figure 4.11: Mean achievable rate for U_e and U_c operating at IBFD compared to the half-duplex case without any shared resources.

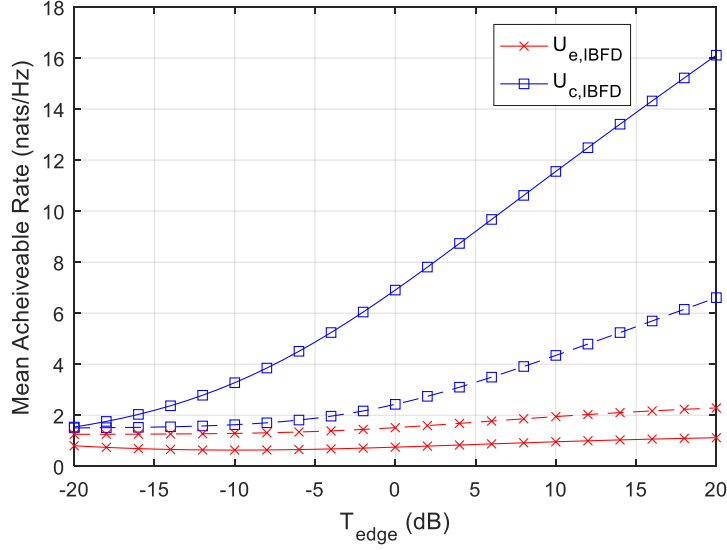


Figure 4.12: Mean achievable rate for U_e and U_c operating at IBFD with $d_f = 0.5$ km compared to the half-duplex case without any shared resources.

In Figure 4.13 and Figure 4.14, we present the probability of coverage expected by the two approaches, with the different used approximations, for an edge and core user respectively. We plot the probability of coverage for a typical user at a specific distance r from its serving BS. This is because for approach 2, the results are quicker to be computed at a specific r and takes much less time than that evaluated at a random r . Equally important, we plot the case 1 of the upper bound which account only for the interferers in the same disk. The case 2 can be obtained, but it needs more evaluation time even at a specific r . In Figure 4.5, we show how case 2 can produce tighter upper bound, similar results can be obtained for each LT and for the entire analysis. The analysis shows that approach 2 succeeds in deriving the probability of coverage in which the lower and upper bounds holds by the definition of the probability of coverage in equations (4.26) and (4.30). Also, it shows the near results of both approach 1 and 2, which concludes the performance of the typical edge and core users operating at IBFD in the abstract system model.

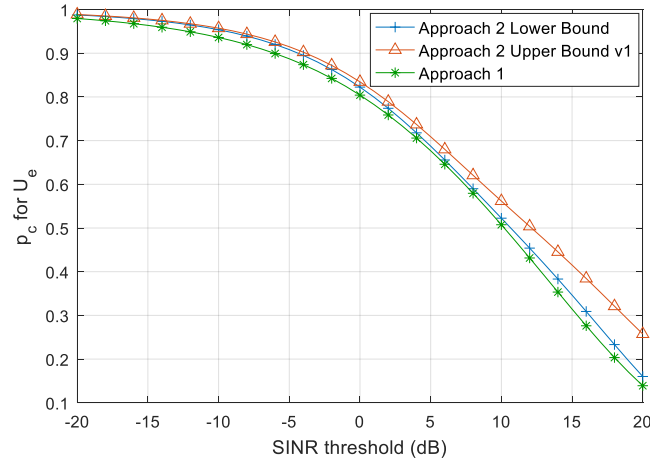


Figure 4.13: Probability of coverage for a typical edge user at distance $r = 0.17 \text{ km} > a_1$ using Approach 1 and 2.

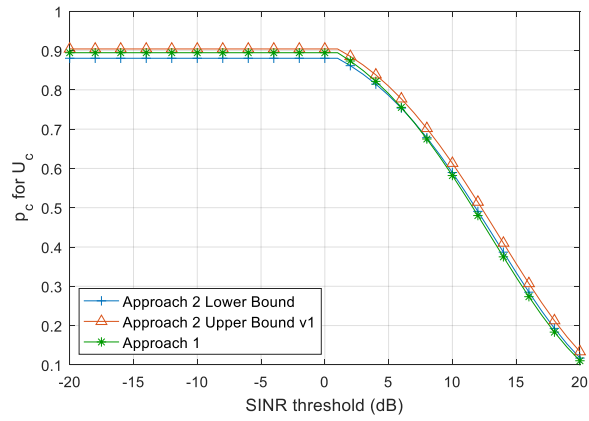


Figure 4.14: Probability of coverage for a typical core user at distance $r = 0.14 \text{ km} < a_1$ using Approach 1 and 2.

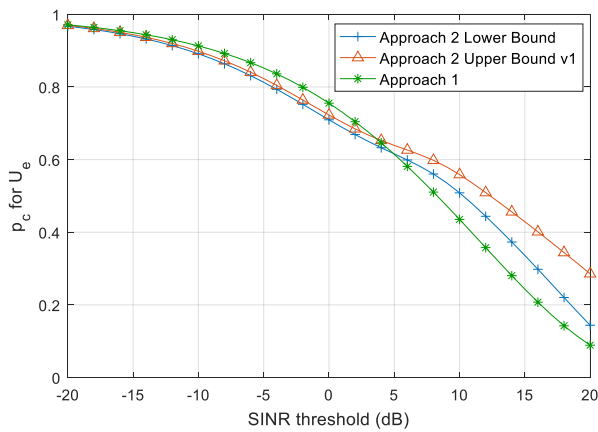


Figure 4.15: Probability of coverage for a typical edge user at distance $r = 0.3 \text{ km} > a_1$, $\lambda_{BS} = 0.5 \text{ BS/km}^2$, $\lambda_U = 50 \text{ users/km}^2$, $dF = 0.4 \text{ km}$ using Approach 1 and 2.

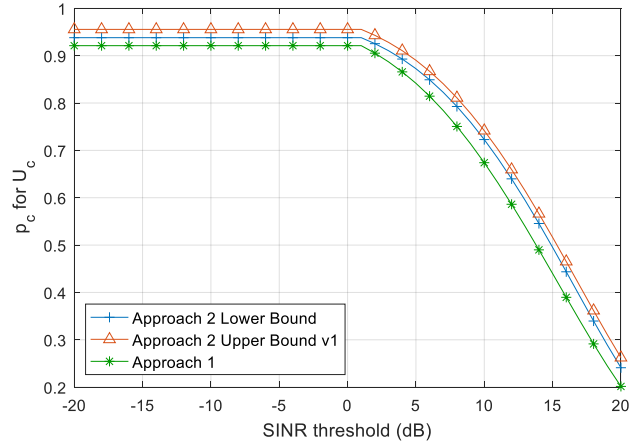


Figure 4.16: Probability of coverage for a typical core user at distance $r = 0.23 \text{ km} < a_1$, $\lambda_{\text{BS}} = 0.5 \text{ BS/km}^2$, $\lambda_{\text{U}} = 50 \text{ users/km}^2$, $dF = 0.4 \text{ km}$ using Approach 1 and 2

I. Conclusion:

We have presented a network model to analyze the performance in a network that uses FFR scheme, and contains users operating at IBFD with some shared resources between the users. We have analyzed this model using two approaches and we have shown the decrease in the coverage probability experienced by the network for the users operating at IBFD. Also, we have shown the increase in the mean achievable gained by these users compared to the half-duplex ones.

CONCLUSION

In this thesis, we have tackled many topics using stochastic geometry tools. We have studied the spatial density distribution of the evolved NodeB (eNB) in LTE networks. Mainly, we compared this distribution in three huge areas to a set of candidate distributions. Using the best fitted distributions, we developed three network models and derived performance metrics for the network. These metrics are the probability of coverage and the mean achievable rate that the network can provide for its users, where we have showed how these metrics change with the different network configuration. As a part of deriving the performance metrics, we analyze the Probability Density Function (PDF) of the interference power in Poisson Point Process (PPP) networks when the fading experienced by the user is Rayleigh fading. By the help of the Koshlrausch-Williams-Watts (KWW) and its properties, we provided closed form expressions for the interference power. In addition to that, the second main part of the thesis was to study the effect of in-Band Full-Duplex (IBFD) in cellular networks. IBFD is a technology that is expected to be used in future networks. We have developed a network model to analyze the performance of users operating at IBFD in a cellular network that uses Fractional Frequency Reuse (FFR). In the developed model, we hadn't restricted ourselves to totally isolated transmissions between the users i.e. we have assumed that there exist shared network resources between the users. Markedly, the use of shared network resources is aligned with the vision for future networks. With this intention, we analyzed the performance of an IBFD network configuration using two approaches and we showed the effect of using such configuration. We derived the performance metrics of users operating at IBFD, and we compared their performance to the half-duplex users. The users operating at IBFD experiences decrease in their received SINR, which is reflected in having lower coverage probability than the half-duplex users, in which we have provided the comparison between these two types of users. On the other side, in the used network configuration, the IBFD users gain throughput and spectral efficiency. As provided by our results, the resulted throughput is not simply the double that of a half-duplex user because the IBFD users experience a decrease in the SINR.

Appendix II.A

The probability of coverage is defined as follows:

$$\begin{aligned} p_c &= \mathbb{E}_r[\mathbb{P}[SINR > T|r]] = \int_0^\infty \mathbb{P}[SINR > T|r]f_r(r)dr = \int_0^\infty \mathbb{P}\left[\frac{P_t L_p h r^{-\eta}}{P_n + I_r} > T|r\right]f_r(r)dr \\ &= \int_0^\infty \mathbb{P}\left[h > \frac{T}{P_t L_p} r^\eta (P_n + I_r)|r\right]f_r(r)dr \end{aligned}$$

where h is the fading coefficient or the power of the fading for the Rayleigh fading case, so we have:

$$\begin{aligned} \mathbb{P}\left[h > \frac{T}{P_t L_p} r^\eta (P_n + I_r)|r\right] &= \mathbb{E}_{I_r}\left[\mathbb{P}\left[h > \frac{T}{P_t L_p} r^\eta (P_n + I_r)|r, I_r\right]\right] \\ &= \mathbb{E}_{I_r}\left[\exp\left(-\mu \frac{T}{P_t L_p} r^\eta (P_n + I_r)\right)|r\right] = e^{-\mu \frac{T}{P_t L_p} r^\eta \sigma^2} L_{\frac{I_r}{P_t L_p}}(\mu T r^\eta) \end{aligned}$$

where $L_{\frac{I_r}{P_t L_p}}(s)$ is the Laplace Transform of the random variable I_r evaluated at s conditioned on the distance to the nearest BS from the origin, and because $P_t L_p$ is a constant we can put it outside the Laplace Transform formula and it will be canceled with the same term found in the signal power S . The density of the PPP follows one of the candidate distributions, so we should also condition the interference on λ . So, the formula for the interference becomes:

$$\begin{aligned} L_{\frac{I_r}{P_t L_p}}(s) &= \mathbb{E}_{\frac{I_r}{P_t L_p}}[e^{-s I_r}] = \mathbb{E}_{\lambda, \Phi, g_i}\left[\exp\left(-s \sum_{i \in \Phi \setminus \{BS_0\}} g_i R_i^{-\eta}\right)\right] \\ &= \mathbb{E}_{\lambda, \Phi, \{g_i\}}\left[\prod_{i \in \Phi \setminus \{BS_0\}} \exp(-s g_i R_i^{-\eta})\right] \\ &= \mathbb{E}_{\lambda, \Phi}\left[\prod_{i \in \Phi \setminus \{BS_0\}} \mathbb{E}_g[\exp(-s g R_i^{-\eta})]\right] \stackrel{(a)}{=} \mathbb{E}_\lambda\left[\mathbb{E}_\Phi\left[\prod_{i \in \Phi \setminus \{BS_0\}} \mathbb{E}_g[\exp(-s g R_i^{-\eta})]\right]\right] \end{aligned}$$

$$\begin{aligned}
&\stackrel{(b)}{=} \mathbb{E}_\lambda \left[\exp \left(-2\pi\lambda_i \int_r^\infty (1 \right. \right. \\
&\quad \left. \left. - \mathbb{E}_g[\exp(-sgx^{-\eta})]x dx \right) \right] \stackrel{(c)}{=} \int_0^\infty \exp \left(-2\pi\lambda \mathbb{E}_g \left[\int_r^\infty (1 \right. \right. \right. \\
&\quad \left. \left. - \exp(-sgx^{-\eta})x dx \right) \right] f_\lambda(\lambda) d\lambda
\end{aligned}$$

where (a) follows from the independence between the variables, and (b) follows from the Probability Generating Functional (PGFL) of PPP, and in (c) we use the definition of the expectation for λ . In a same fashion, to get the final results, (c) is evaluated according to the used distribution for λ , then we substitute $s = \mu T r^\eta$ and apply a change of variable $x^{-\eta} \rightarrow y$. At last, we substitute the formula for the Laplace in the coverage probability formula to get the different results for each density distribution.

Appendix II.B

In a PPP network with random density, the ergodic rate for a typical user depends on the spatial PPP and the fading distribution.

$$\begin{aligned}
\tau &= \mathbb{E}[\ln(1 + SINR)] = \int_{r>0} \mathbb{E} \left[\ln \left(1 + \frac{P_t L_p h r^{-\eta}}{P_n + I_t} \right) \right] f_r(r) dr \\
&= \int_{r>0} f_r(r) \int_{t>0} \mathbb{P} \left[\ln \left(1 + \frac{P_t L_p h r^{-\eta}}{P_n + P_t L_p I_r} \right) > t \right] dt dr \\
&= \int_{r>0} f_r(r) \int_{t>0} \mathbb{P} \left[\frac{P_t L_p h r^{-\eta}}{P_n + P_t L_p I_r} > e^t - 1 \right] dt dr \\
&= \int_{r>0} f_r(r) \int_{t>0} \mathbb{P} \left[h > \frac{r^\eta}{P_t L_p} (P_n + P_t L_p I_r) (e^t - 1) \right] dt dr
\end{aligned}$$

Using the fact that $h \sim \exp(\mu)$, i.e. signal experiences Rayleigh fading.

$$\begin{aligned}\tau &= \int_{r>0} f_r(r) \int_{t>0} \mathbb{E} \left[\exp \left(-\mu \frac{r^\eta}{P_t L_p} (P_n + P_t L_p I_r) (e^t - 1) \right) \right] dt dr \\ &= \int_{r>0} f_r(r) \int_{t>0} e^{-\mu r^\eta \sigma^2 (e^t - 1)} L_{I_r}(\mu r^\eta (e^t - 1)) dt dr\end{aligned}$$

Appendix IV.A

$$\begin{aligned}p_{Ue}^{\text{st-FR}} &= \mathbb{P} \left(\frac{P_{s_1} h_1 L_{p_1} r^{-\eta}}{P_n + P_{s_1} L_{p_1} I_{BS}' + P_{s_2} L_{p_2} I_{Ue,IBFD}' + \beta P_{s_2}} > T \mid \frac{P_{s_1} h_2 L_{p_1} r^{-\eta}}{P_n + P_{s_1} L_{p_1} I_{BS} + P_{s_2} L_{p_2} I_{U,IBFD} + \beta P_{s_2}} < T_{edge} \right) \\ &= \frac{\mathbb{P} \left(\frac{P_{s_1} h_1 L_{p_1} r^{-\eta}}{P_n + P_{s_1} L_{p_1} I_{BS}' + P_{s_2} L_{p_2} I_{Ue,IBFD}' + \beta P_{s_2}} > T, \frac{P_{s_1} h_2 L_{p_1} r^{-\eta}}{P_n + P_{s_1} L_{p_1} I_{BS} + P_{s_2} L_{p_2} I_{U,IBFD} + \beta P_{s_2}} < T_{edge} \right)}{\mathbb{P} \left(\frac{P_{s_1} h_2 L_{p_1} r^{-\eta}}{P_n + P_{s_1} L_{p_1} I_{BS} + P_{s_2} L_{p_2} I_{U,IBFD} + \beta P_{s_2}} < T_{edge} \right)} \\ &= \frac{\int_{r>0} \mathbb{E}_{I_r} \left[\exp \left(-\mu \frac{r^\eta T}{P_{s_1} L_{p_1}} (P_n + P_{s_1} L_{p_1} I_{BS}' + P_{s_2} L_{p_2} I_{Ue,IBFD}' + \beta P_{s_2}) \right) \left(1 - \exp \left(-\mu \frac{r^\eta T_{edge}}{P_{s_1} L_{p_1}} (P_n + P_{s_1} L_{p_1} I_{BS} + P_{s_2} L_{p_2} I_{U,IBFD} + \beta P_{s_2}) \right) \right) \mid r \right] f_r(r) dr}{\int_{r>0} \mathbb{E}_{I_r} \left[1 - \exp \left(-\mu \frac{r^\eta T_{edge}}{P_{s_1} L_{p_1}} (P_n + P_{s_1} L_{p_1} I_{BS} + P_{s_2} L_{p_2} I_{U,IBFD} + \beta P_{s_2}) \right) \mid r \right] f_r(r) dr} \\ &= \frac{\int_{r>0} E_1 f_r(r) dr}{\int_{r>0} E_2 f_r(r) dr}\end{aligned}$$

Where

$$\begin{aligned}E_1 &= \mathbb{E}_{I_r} \left[\exp \left(-\mu \frac{r^\eta T}{P_{s_1} L_{p_1}} (P_n + P_{s_1} L_{p_1} I_{BS}' + P_{s_2} L_{p_2} I_{Ue,IBFD}' + \beta P_{s_2}) \right) - \exp \left(-\mu \frac{r^\eta T}{P_{s_1} L_{p_1}} (P_n + P_{s_1} L_{p_1} I_{BS}' + P_{s_2} L_{p_2} I_{Ue,IBFD}' + \beta P_{s_2}) \right) \exp \left(-\mu \frac{r^\eta T_{edge}}{P_{s_1} L_{p_1}} (P_n + P_{s_1} L_{p_1} I_{BS} + P_{s_2} L_{p_2} I_{U,IBFD} + \beta P_{s_2}) \right) \mid r \right] \\ &= \mathbb{E}_{I_r} \left[e^{-\mu \frac{r^\eta T (P_n + \beta P_{s_2})}{P_{s_1} L_{p_1}}} \exp \left(-\mu \frac{r^\eta T}{P_{s_1} L_{p_1}} (P_{s_1} L_{p_1} I_{BS}' + P_{s_2} L_{p_2} I_{Ue,IBFD}') \right) \right. \\ &\quad \left. - e^{-\mu \frac{r^\eta ((P_n + \beta P_{s_2}) T + (P_n + \beta P_{s_2}) T_{edge})}{P_{s_1} L_{p_1}}} \exp \left(-\mu \frac{r^\eta}{P_{s_1} L_{p_1}} ((P_{s_1} L_{p_1} I_{BS}' + P_{s_2} L_{p_2} I_{Ue,IBFD}') T \right. \right. \\ &\quad \left. \left. + (P_{s_1} L_{p_1} I_{BS} + P_{s_2} L_{p_2} I_{U,IBFD}) T_{edge} \right) \mid r \right] \stackrel{(a)}{=} e^{-\mu \frac{r^\eta T (P_n + \beta P_{s_2})}{P_{s_1} L_{p_1}}} L_{I_{BS}'}(\mu r^\eta T) L_{I_{Ue,IBFD}'} \left(\mu \frac{P_{s_2} L_{p_2} r^\eta T}{P_{s_1} L_{p_1}} \right) \\ &\quad - e^{-\mu \frac{r^\eta ((P_n + \beta P_{s_2}) T + (P_n + \beta P_{s_2}) T_{edge})}{P_{s_1} L_{p_1}}} L_{I_{BS}', I_{BS}}(\mu r^\eta T, \mu r^\eta T_{edge}) \cdot L_{I_{Ue,IBFD}', I_{U,IBFD}} \left(\mu \frac{P_{s_2} L_{p_2} r^\eta}{P_{s_1} L_{p_1}} T, \mu \frac{P_{s_2} L_{p_2} r^\eta}{P_{s_1} L_{p_1}} T_{edge} \right)\end{aligned}$$

And

$$\begin{aligned}E_2 &= \mathbb{E}_{I_r} \left[1 - \exp \left(-\mu \frac{r^\eta T_{edge}}{P_{s_1} L_{p_1}} (P_n + P_{s_1} L_{p_1} I_{BS} + P_{s_2} L_{p_2} I_{U,IBFD} + \beta P_{s_2}) \right) \mid r \right] \\ &= 1 - e^{-\mu \frac{r^\eta T_{edge} (P_n + \beta P_{s_2})}{P_{s_1} L_{p_1}}} L_{I_{BS}}(\mu r^\eta T_{edge}) L_{I_{U,IBFD}} \left(\mu \frac{P_{s_2} L_{p_2} r^\eta}{P_{s_1} L_{p_1}} T_{edge} \right)\end{aligned}$$

Where (a) follows from the independence of ϕ_{BS} and ϕ_U . Each $L_{I_{BS'}, I_{BS}} \left(\mu \frac{P_{s_1} L_{p_1} r^\eta}{P_{s_1} L_{p_1}} T, \mu \frac{P_{s_1} L_{p_1} r^\eta}{P_{s_1} L_{p_1}} T_{edge} \right)$ and $L_{I_{Ue, IBFD'}, I_{IBFD}} \left(\mu \frac{P_{s_2} L_{p_2} r^\eta}{P_{s_1} L_{p_1}} T, \mu \frac{P_{s_2} L_{p_2} r^\eta}{P_{s_1} L_{p_1}} T_{edge} \right)$ are the joint Laplace transforms evaluated at $s_1 = \mu \frac{P_{s_1} L_{p_1} r^\eta}{P_{s_1} L_{p_1}} T, s_2 = \mu \frac{P_{s_1} L_{p_1} r^\eta}{P_{s_1} L_{p_1}} T_{edge}, s_3 = \mu \frac{P_{s_2} L_{p_2} r^\eta}{P_{s_1} L_{p_1}} T, s_4 = \mu \frac{P_{s_2} L_{p_2} r^\eta}{P_{s_1} L_{p_1}} T_{edge}$.

Appendix IV.B

$$\begin{aligned}
p_{Uc}^{\text{st-FR}} &= \mathbb{P} \left(\frac{P_{s_1} h_1 L_{p_1} r^{-\eta}}{P_n + P_{s_1} L_{p_1} I_{BS} + P_{s_2} L_{p_2} I_{Uc, IBFD} + \beta P_{s_2}} > T \mid \frac{P_{s_1} h_2 L_{p_1} r^{-\eta}}{P_n + P_{s_1} L_{p_1} I_{BS} + P_{s_2} L_{p_2} I_{U, IBFD} + \beta P_{s_2}} > T_{edge} \right) \\
&= \frac{\mathbb{P} \left(\frac{P_{s_1} h_1 L_{p_1} r^{-\eta}}{P_n + P_{s_1} L_{p_1} I_{BS} + P_{s_2} L_{p_2} I_{Uc, IBFD} + \beta P_{s_2}} > \max\{T, T_{edge}\}, \frac{P_{s_1} h_2 L_{p_1} r^{-\eta}}{P_n + P_{s_1} L_{p_1} I_{BS} + P_{s_2} L_{p_2} I_{U, IBFD} + \beta P_{s_2}} > T_{edge} \right)}{\mathbb{P} \left(\frac{P_{s_1} h_2 L_{p_1} r^{-\eta}}{P_n + P_{s_1} L_{p_1} I_{BS} + P_{s_2} L_{p_2} I_{U, IBFD} + \beta P_{s_2}} > T_{edge} \right)} \\
&= \frac{\int_{r>0} E_3 f_r(r) dr}{\int_{r>0} E_4 f_r(r) dr}
\end{aligned}$$

Where I_{BS} and $I_{Uc, IBFD}$ are the interference from all other BSs and from all Uc using IBFD respectively, because both are using common band.

Regarding the powers $I_{Uc, IBFD}$ and $I_{U, IBFD}$, These parameters changes with dF. If dF is big enough, $I_{Uc, IBFD} < I_{U, IBFD}$. And for a certain value of dF, the power of $I_{Uc, IBFD} = I_{U, IBFD}$, and this equality will hold for any number bigger than this certain value.

By following the same steps, we get:

$$\begin{aligned}
E_3 &= e^{-\mu \frac{r^\eta ((P_n + \beta P_{s_2}) (\max\{T, T_{edge}\} + T_{edge}))}{P_{s_1} L_{p_1}}} L_{I_{BS}} (\mu r^\eta (\max\{T, T_{edge}\} \\
&\quad + T_{edge})) L_{I_{Uc, IBFD}, I_{U, IBFD}} \left(\mu \frac{P_{s_2} L_{p_2} r^\eta}{P_{s_1} L_{p_1}} \max\{T, T_{edge}\}, \mu \frac{P_{s_2} L_{p_2} r^\eta}{P_{s_1} L_{p_1}} T_{edge} \right)
\end{aligned}$$

Appendix IV.C

$$\begin{aligned}
L_{I_{BS'}, I_{BS}}(s_1, s_2) &= \mathbb{E}_{I_r} [\exp(-s_1 I_{BS'} - s_2 I_{BS})] \\
&= \mathbb{E}_{\phi_{BS}, g_i', g_i} \left[\exp \left(-s_1 \sum_{i \in \phi_{BS} \setminus BS_0} g_i' R_i^{-\eta} \mathbf{1}(n_i = n_0) - s_2 \sum_{i \in \phi_{BS} \setminus BS_0} g_i R_i^{-\eta} \right) \right] \\
&= \mathbb{E}_{\phi_{BS}, g_i', g_i} \left[\exp \left(- \sum_{i \in \phi_{BS} \setminus BS_0} (s_1 g_i' R_i^{-\eta} \mathbf{1}(n_i = n_0) + s_2 g_i R_i^{-\eta}) \right) \right]
\end{aligned}$$

where $\mathbf{1}(n_i = n_0)$ is the indicator function, that takes the value 1 if base station i is transmitting to an edge user on the same sub-band n_0 that the serving BS_0 reserved for the typical user Ue. $\mathbf{1}(\cdot)$ is the indicator function which takes the value 1 if the statement (\cdot) is true and takes the value 0 otherwise.

$$\begin{aligned}
&= \mathbb{E}_{\phi_{BS}, g_i', g_i} \left[\prod_{i \in \phi_{BS} \setminus BS_0} \exp(-(s_1 g_i' R_i^{-\eta} \mathbf{1}(n_i = n_0) + s_2 g_i R_i^{-\eta})) \right] \\
&= \mathbb{E}_{\phi_{BS}, g_i', g_i} \left[\prod_{i \in \phi_{BS} \setminus BS_0} \exp(-s_2 g_i R_i^{-\eta}) (1 - \mathbb{E}[\mathbf{1}(n_i = n_0)](1 - \exp(-s_1 g_i' R_i^{-\eta}))) \right] \\
&= \mathbb{E}_{\phi_{BS}} \left[\prod_{i \in \phi_{BS} \setminus BS_0} \frac{\mu}{\mu + s_2 R_i^{-\eta}} \left(1 - \frac{1}{N} \left(1 - \frac{\mu}{\mu + s_1 R_i^{-\eta}} \right) \right) \right] \\
&= \exp \left(-2\pi\lambda_{BS} \int_r^\infty \left(1 - \frac{\mu}{\mu + s_2 x^{-\eta}} \left(1 - \frac{1}{N} \left(1 - \frac{\mu}{\mu + s_1 x^{-\eta}} \right) \right) \right) x dx \right)
\end{aligned}$$

The results follow from the independence of fading, and the last term from the PGFL of PPP.

Plugging $s_1 = \mu \frac{P_{s_1} L_{p_1} r^\eta}{P_{s_1} L_{p_1}} T$, $s_2 = \mu \frac{P_{s_1} L_{p_1} r^\eta}{P_{s_1} L_{p_1}} T_{edge}$:

$$\begin{aligned}
&L_{I_{BS}', l_{BS}} \left(\mu \frac{P_{s_1} L_{p_1} r^\eta}{P_{s_1} L_{p_1}} T, \mu \frac{P_{s_1} L_{p_1} r^\eta}{P_{s_1} L_{p_1}} T_{edge} \right) \\
&= \exp \left(-2\pi\lambda_{BS} \int_r^\infty \left(1 - \frac{1}{1 + \frac{P_{s_1} L_{p_1} r^\eta}{P_{s_1} L_{p_1}} T_{edge} x^{-\eta}} \left(1 - \frac{1}{N} \left(1 - \frac{1}{1 + \frac{P_{s_1} L_{p_1} r^\eta}{P_{s_1} L_{p_1}} T x^{-\eta}} \right) \right) \right) x dx \right)
\end{aligned}$$

By making changing of variable $r^\eta x^{-\eta} \rightarrow y^{-\eta}$ we get the final result.

Appendix IV.D

$$\begin{aligned}
L_{I_{BS}'}(s_1) &= \mathbb{E}_{I_r}[\exp(-s_1 I_{BS}')] = \mathbb{E}_{\phi_{BS}, g_i'} \left[\prod_{i \in \phi_{BS} \setminus BS_0} (1 - \mathbb{E}[\mathbf{1}(n_i = n_0)](1 - \exp(-s_1 g_i' R_i^{-\eta}))) \right] \\
&= \mathbb{E}_{\phi_{BS}} \left[\prod_{i \in \phi_{BS} \setminus BS_0} \left(1 - \frac{1}{N} \left(1 - \frac{\mu}{\mu + s_1 R_i^{-\eta}} \right) \right) \right] \\
&= \exp \left(-2\pi\lambda_{BS} \int_r^\infty \left(1 - \left(1 - \frac{1}{N} \left(1 - \frac{\mu}{\mu + s_1 x^{-\eta}} \right) \right) \right) x dx \right) \\
&= \exp \left(-2\pi\lambda_{BS} \int_r^\infty \frac{1}{N} \left(1 - \frac{\mu}{\mu + s_1 x^{-\eta}} \right) x dx \right) \\
L_{I_{BS}'} \left(\mu \frac{P_{s_1} L_{p_1} r^\eta T}{P_{s_1} L_{p_1}} \right) &= \exp \left(-2\pi\lambda_{BS} \int_r^\infty \frac{1}{N} \left(1 - \frac{1}{1 + \frac{P_{s_1} L_{p_1} r^\eta T}{P_{s_1} L_{p_1}} x^{-\eta}} \right) x dx \right)
\end{aligned}$$

By making changing of variable $\left(\frac{x}{r \left(\frac{P_{s_1} L_{p_1} T}{P_{s_1} L_{p_1}} \right)^{1/\eta}} \right)^2 \rightarrow y$ we get the final result.

Appendix IV.E

The Laplace transform for the interference from edge users is evaluated in similar fashion, details are below:

$$\begin{aligned}
 L_{I_{U_{e,IBFD}'}, I_{U_{IBFD}}}(s_3, s_4) &= \mathbb{E}_{I_r}[\exp(-s_3 I_{U_{e,IBFD}'} - s_4 I_{U_{IBFD}})] \\
 &= \mathbb{E}_{\phi_{U_{IBFD}}, g_i', g_i} \left[\exp \left(-s_3 \sum_{i \in \phi_{U_{IBFD}} \setminus U_0} g_i' R_i^{-\eta} \mathbf{1}(U_{n_i} = U_{n_0}) - s_4 \sum_{i \in \phi_{U_{IBFD}} \setminus U_0} g_i R_i^{-\eta} \right) \right] \\
 &= (a) \exp \left(-2\pi\lambda_{U_{IBFD}} \int_r^\infty \left(1 - \frac{\mu}{\mu + s_4 x^{-\eta}} \left(1 - \frac{1 - \exp\left(-\frac{\lambda_{BS}}{N} \pi d_F^2\right)}{1 - \exp\left(-\lambda_{BS} \pi d_F^2\right)} \right) (1 - p_{c2}) \left(1 - \frac{\mu}{\mu + s_3 x^{-\eta}} \right) \right) dx \right)
 \end{aligned}$$

With

$$\begin{aligned}
 \mathbb{P}[SINR < T_{edge}] &= 1 - \mathbb{P}[SINR > T_{edge}] = 1 - p_{c2} \\
 &= 1 \\
 &- 2\pi\lambda_{BS} r \int_0^\infty e^{-\mu \frac{r^\eta T_{edge} (P_n + \beta P_{s_2})}{P_{s_1} L_{p_1}} - \pi\lambda_{BS} r^2 \left(1 + (T_{edge})^{\frac{2}{\eta}} \rho_1(P_{s_1} L_{p_1}, T_{edge}) \right) - \pi\lambda_{U_{IBFD}} r^2 \left(\frac{P_{s_2} L_{p_2} T_{edge}}{P_{s_1} L_{p_1}} \right)^{\frac{2}{\eta}} \rho_1(P_{s_2} L_{p_2}, T_{edge})} dr
 \end{aligned}$$

Which comes from the calculated pc2 in the same expression.

$$\text{Where } SINR < T_{edge} = \frac{P_{s_1} h_2 L_{p_1} r^{-\eta}}{P_n + P_{s_1} L_{p_1} I_{BS} + P_{s_2} L_{p_2} I_{U_{IBFD}} + \beta P_{s_2}} < T_{edge}$$

Where (a) follows from the fact that the FFR scheme is making thinning on the λ_{BS} that consists the disks centers of the inner-city model, so the density evaluated on s_3 becomes $\lambda_{U_{IBFD}'} = \lambda_U \left(1 - \exp\left(-\frac{\lambda_{BS}}{N} \pi d_F^2\right) \right) (1 - p_{c2})$. Where the functionality of $(1 - p_{c2})$ is to select only the edge users from those operating at IBFD, and the functionality of the $\frac{\lambda_{BS}}{N}$ term is to select the edge users working on the same FFR bands. And by this, we are approximating the inner-city model $\phi_{U_{IBFD}}$ by a PPP of density $\lambda_U \left(1 - \exp\left(-\frac{\lambda_{BS}}{N} \pi d_F^2\right) \right)$ with choosing only the edge users from this model. This approximation consists an underestimate for the interference, because the distance between the interferers is relaxed.

Appendix IV.F

$$\begin{aligned}
L_{I_{U_{e,IBFD}}}(s_3) &= \mathbb{E}_{I_r}[\exp(-s_3 I_{U_{e,IBFD}})] \\
&= \mathbb{E}_{\phi_{U_{IBFD}, g_i'}} \left[\prod_{i \in \phi_{U_{IBFD}} \setminus U_0} (1 - \mathbb{E}[\mathbf{1}(Un_i = Un_0)](1 - \exp(-s_3 g_i' R_i^{-\eta}))) \right] \\
&= \mathbb{E}_{\phi_{U_{IBFD}}} \left[\prod_{i \in \phi_{U_{IBFD}} \setminus U_0} \left(1 - \left(\frac{1 - \exp\left(-\frac{\lambda_{BS}}{N} \pi d_F^2\right)}{1 - \exp(-\lambda_{BS} \pi d_F^2)} \right) (1 - p_{c2}) \left(1 - \frac{\mu}{\mu + s_3 R_i^{-\eta}} \right) \right) \right] \\
&= (a) \exp \left(-2\pi \lambda_{U_{IBFD}} \int_r^\infty \left(1 - \left(1 - \left(\frac{1 - \exp\left(-\frac{\lambda_{BS}}{N} \pi d_F^2\right)}{1 - \exp(-\lambda_{BS} \pi d_F^2)} \right) (1 - p_{c2}) \left(1 - \frac{\mu}{\mu + s_3 x^{-\eta}} \right) \right) \right) x dx \right)
\end{aligned}$$

Where it is solved similarly to $L_{I_{BS}}\left(\mu \frac{P_{s_1} L_{p_1} r^{\eta\tau}}{P_{s_1} L_{p_1}}\right)$, where (a) the density $\lambda_{U_{IBFD}} = \lambda_U(1 - \exp(-\lambda_{BS} \pi d_F^2))$.

Appendix IV.G

Upper bound for the LT of $I_{U_{IBFD}}$ case 2:

We start by the LT conditioned on the distances r_0 and r_1 . Where r_0 is the distance between the typical user and the center of the same IBFD disk that contains the interfering users i.e. this center is the location of the serving BS. And r_1 is the distance between the typical user and the second BS that forms the center of the second nearest IBFD disk. Figure 4.4 (a) clarifies these distances, where we use the terms $b(r_0, d_F)$ and $b(r_1, d_F)$ to describe these disks.

$$\begin{aligned}
L_{I_{U_{IBFD}}|r_0, r_1}(s) &\leq \mathbb{E} \left[\exp \left(-s \sum_{i \in \Phi_U \cap b(r_0, d_F) + i \in \Phi_U \cap b(r_1, d_F)} g_i R_i^{-\eta} \right) \right] \\
&= \mathbb{E}_{\Phi_U} \left[\prod_{i \in \Phi_U \cap b(r_0, d_F) + i \in \Phi_U \cap b(r_1, d_F)} \mathbb{E}_{g_i}[\exp(-s g_i R_i^{-\eta})] \right] \\
&= \mathbb{E}_{\Phi_U} \left[\prod_{i \in \Phi_U \cap b(r_0, d_F) + i \in \Phi_U \cap b(r_1, d_F)} \frac{\mu}{\mu + s R_i^{-\eta}} \right] = (a) \exp \left(-\lambda_U \int_{b(r_0, d_F) + b(r_1, d_F)}^\infty \frac{1}{1 + \frac{\mu x^\eta}{s}} dx \right) \\
&= \exp \left(-\lambda_U \left(\int_{b(r_0, d_F)}^\infty \frac{1}{1 + \frac{\mu x^\eta}{s}} dx + \int_{b(r_1, d_F)}^\infty \frac{1}{1 + \frac{\mu x^\eta}{s}} dx \right) \right)
\end{aligned}$$

Where both terms in (a) follows from the PGFL of PPP of Φ_U .

$$\begin{aligned}
&= (b) \exp \left(-\lambda_U \left(2\pi \int_{r_0-d_F}^{r_0+d_F} \frac{\frac{1}{\pi} \cos^{-1} \left(\frac{x^2 + r_0^2 - d_F^2}{2r_0x} \right)}{1 + \frac{\mu x^\eta}{s}} x dx + 2\pi \int_{r_0-d_F}^{r_0+d_F} \frac{\frac{1}{\pi} \cos^{-1} \left(\frac{x^2 + r_1^2 - d_F^2}{2r_1x} \right)}{1 + \frac{\mu x^\eta}{s}} x dx \right) \right) \\
&= \exp \left(-2\lambda_U (A_1(s, r_0, d_F) + A_1(s, r_1, d_F)) \right)
\end{aligned}$$

Where $A_1(s, r_0, d_F) = \int_{r_0-d_F}^{r_0+d_F} \frac{\cos^{-1} \left(\frac{x^2 + r_0^2 - d_F^2}{2r_0x} \right)}{1 + \frac{\mu x^\eta}{s}} x dx$

Where second term in (b) follows from the cosine law: $x^2 + r_0^2 - 2xr_0 \cos\theta(x) = d_F^2$ in which $\lambda(x) = \frac{\lambda_U}{\pi} \cos^{-1} \left(\frac{x^2 + r_0^2 - d_F^2}{2r_0x} \right)$ [63].

We note that this formula does not account for the overlap between the two holes. So, at big d_F or high density of the points at center (Φ_{BS}), the formula will not give a lower bound because the users in the shared area between the two disks will be accounted two times.

Next, we decondition on the distances $\|r_0\|$ and $\|r_1\|$. This is done by getting the joint PDF of the distance:

$$\begin{aligned}
f_{R_0, R_1}(r_0, r_1) &= f_{R_1}(r_1|r_0) f_{R_0}(r_0, r < d_F) = 2\pi\lambda_{BS}r_1 \frac{\exp(-\pi\lambda_{BS}r_1^2)}{\exp(-\pi\lambda_{BS}r_0^2)} 2\pi\lambda_{BS}r_0 \exp(-\pi\lambda_{BS}r_0^2) = \\
&(2\pi\lambda_{BS})^2 r_0 r_1 \exp(-\pi\lambda_{BS}r_1^2)
\end{aligned}$$

Then, we decondition the result on r_0 and r_1 by using the joint PDF:

$$L_{I_{U_{IBFD}}}(s) \leq \int_0^{d_F} \int_{r_0}^{\infty} (2\pi\lambda_{BS})^2 r_0 r_1 \exp(-\pi\lambda_{BS}r_1^2) \exp(-2\lambda_U (A_1(r_0, d_F) + A_1(r_1, d_F))) dr_1 dr_0 \quad (1)$$

To account for the possible overlap between the two disks, we can follow two ways, either subtract the overlap and this will lead to some complexity in the formula because the overlap will depend on many conditions. Or, we can simply avoid it, so instead of trying to incorporate the exact effect of overlaps, we say that the nearest disk is bounded by:

$$\begin{aligned}
A_2(s, r_1, d_F, r_0) &= \int_{\max(r_1-d_F, r_0+d_F)}^{r_1+d_F} \frac{\cos^{-1} \left(\frac{x^2 + r_1^2 - d_F^2}{2r_1x} \right)}{1 + \frac{\mu x^\eta}{s}} x dx \quad \text{instead of} \quad A_1(s, r_1, d_F) = \\
&\int_{r_1-d_F}^{r_1+d_F} \frac{\cos^{-1} \left(\frac{x^2 + r_1^2 - d_F^2}{2r_1x} \right)}{1 + \frac{\mu x^\eta}{s}} x dx
\end{aligned}$$

Upper bound for the LT of $I_{U_{IBFD}}$ case 1:

Is similar to case 2, but we calculate the interference from one disk $b(r_0, d_F)$. So, r_1 does not exist which leads to less tighter result.

Lower bound for the LT of $I_{U_{IBFD}}$:

$$L_{I_{U_{IBFD}}}(s) = \mathbb{E} \left[\exp \left(-s \sum_{i \in \Phi_{U_{IBFD}}} g_i R_i^{-\eta} \right) \right] = (a) \mathbb{E}_{\Phi_{BS}} \left[\exp \left(-\lambda_U \int_{\mathbb{E}} \frac{1}{1 + \frac{\mu x^\eta}{s}} dx \right) \right]$$

Where (a) comes from the PGFL of PPP ϕ_U given \mathcal{E} which represents all the disks created by ϕ_{BS} with radius d_F and covers the users of ϕ_U operating at IBFD.

The exact integral over \mathcal{E} is not easy to compute due to the possible overlap between the disks. So, we compute the interference from the users in the IBFD disks without accounting for the overlaps which results in overestimate in interference. For that the lower bound is used in our case (inner-city model) which is:

$$\int_{\mathcal{E}} \frac{1}{1+\frac{\mu x^\eta}{s}} dx \leq \sum_{i \in \phi_{BS}} \int_{b(i, d_F)} \frac{1}{1+\frac{\mu x^\eta}{s}} dx \rightarrow - \int_{\mathcal{E}} \frac{1}{1+\frac{\mu x^\eta}{s}} dx \geq - \sum_{i \in \phi_{BS}} \int_{b(i, d_F)} \frac{1}{1+\frac{\mu x^\eta}{s}} dx$$

Where we have an equality when there is no overlap between the disks, i.e. d_F and density λ_{BS} are small. Thus:

$$\begin{aligned} L_{I_{U_{IBFD}}}(s) &\geq \mathbb{E}_{\phi_{BS}} \left[\exp \left(-\lambda_U \sum_{y \in \phi_{BS}} \int_{b(y, d_F)} \frac{1}{1+\frac{\mu x^\eta}{s}} dx \right) \right] = (b) \mathbb{E}_{\phi_{BS}} \left[\prod_{y \in \phi_{BS}} \exp(-2\lambda_U A_1(s, y, d_F)) \right] \\ &= \exp \left[-2\pi\lambda_{BS} \int_0^\infty \left(1 - \exp(-2\lambda_U A_1(s, y, d_F)) \right) y dy \right] \end{aligned}$$

$$\text{With } A_1(s, y, d_F) = \int_{y-d_F}^{y+d_F} \frac{\cos^{-1}\left(\frac{x^2+y^2-d_F^2}{2yx}\right)}{1+\frac{\mu x^\eta}{s}} x dx$$

Upper bound for the LT of $I_{U_{e,IBFD}}$ 'case 2:

At first, following the same approach we get the interference upper bound for $L_{I_{U_{e,IBFD}}}\left(\mu \frac{P_{s_2} L_{p_2} r^{\eta T}}{P_{s_1} L_{p_1}}\right)$ which is the interference from edge users operating at IBFD without applying the FFR scheme.

Then we apply the FFR scheme which will get $L_{I_{U_{e,IBFD}}}'\left(\mu \frac{P_{s_2} L_{p_2} r^{\eta T}}{P_{s_1} L_{p_1}}\right)$

These users are in the region of disk d_F and outside the region of $SINR_1 > T_{edge}$, to keep ourselves dealing with inner city models (areas of disks) and to simply things we approximate this region ($SINR > T_{edge}$) with a disk of radius $a_1 = p_{c_2}' d_F = d_F \frac{\mathbb{P}[SINR_1 > T_{edge}, r < d_F]}{\mathbb{P}[r < d_F]} =$

$$d_F \frac{2\pi\lambda_{BS} r}{1 - \exp(-\pi\lambda_{BS} d_F^2)} \int_0^{d_F} e^{-\mu \frac{r^\eta T_{edge} (P_n + \beta P_{s_2})}{P_{s_1} L_{p_1}} - \pi\lambda_{BS} r^2} \left(1 + (T_{edge})^{\frac{2}{\eta}} \int_{T_{edge}}^\infty \frac{dy}{\eta(1+y)^{\eta/2}} \right) - \pi\lambda_{U_{IBFD}} r^2 \left(\frac{P_{s_2} L_{p_2} T_{edge}}{P_{s_1} L_{p_1}} \right)^{\frac{2}{\eta}} \int_0^\infty \frac{dy}{(1+y)^{\eta/2}} dr$$

Where p_{c_2}' is obtained from the probability of having $SINR_1$ greater than T_{edge} inside the IBFD disk, and we assume this by using one of the definitions of the probability of coverage. Which is the average fraction of the network area that has $SINR$ greater than T_{edge} at any time. We understand that such approximation may not be very accurate because the coverage region is not circular due to the fading and different interferers, but we see it as a necessary approximation to keep the tractability of the model. Furthermore, such definition will work with any network configuration, and it will fit as a statistical approximation. In Figure 4.17, we compare this approximation to the real edge and core users existing in the network, the same accuracy holds for a lot of different network inputs.

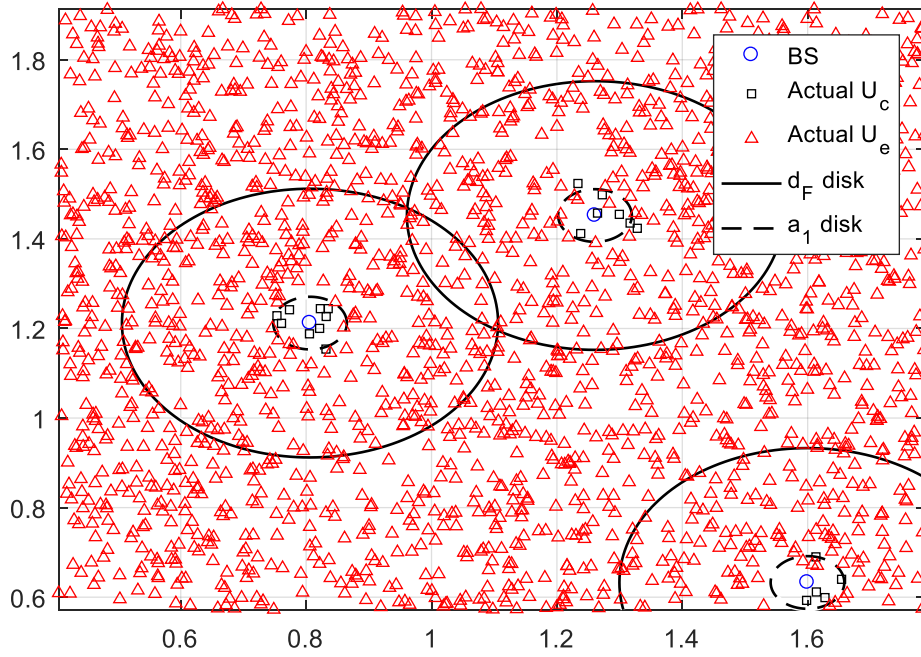


Figure 4.17: Approximating the region separating the core-edge users as circular for the network configuration $d_F = 0.3$ km and $T_{\text{edge}} = -1$ dB.

So, we approximate the edge users operating at IBFD in the same disk by $b_0 = b(r_0, d_F) - b(r_0, a_1)$ and the other nearest disk by $b_1 = b(r_1, d_F) - b(r_1, a_1)$. This can be clarified by checking Figure 4.3.

$$\begin{aligned}
L_{I_{U_e, \text{IBFD}} | r_0, r_1} \left(\mu \frac{P_{s_2} L_{p_2} r^\eta T}{P_{s_1} L_{p_1}} \right) &\leq \mathbb{E} \left[\exp \left(-s_2 \sum_{i \in \Phi_U \cap b_0 + i \in \Phi_U \cap b_1} g_i R_i^{-\eta} \right) \right] \\
&= \mathbb{E}_{\Phi_U} \left[\prod_{i \in \Phi_U \cap b_0 + i \in \Phi_U \cap b_1} \mathbb{E}_{g_i} [\exp(-s_2 g_i R_i^{-\eta})] \right] = (a) \mathbb{E}_{\Phi_U} \left[\prod_{i \in \Phi_U \cap b_0 + i \in \Phi_U \cap b_1} \frac{1}{1 + \frac{s_2 R_i^{-\eta}}{\mu}} \right] \\
&= \exp \left(-\lambda_U \left(\int_{b_0 \cup b_1} \frac{1}{1 + \frac{\mu x^\eta}{S_2}} dx \right) \right) = \exp \left(-\lambda_U \left(\int_{b_0} \frac{1}{1 + \frac{\mu x^\eta}{S_2}} dx + \int_{b_1} \frac{1}{1 + \frac{\mu x^\eta}{S_2}} dx \right) \right) \\
&= (b) \exp \left(-\lambda_U \left(\int_{b(r_0, d_F)} \frac{1}{1 + \frac{\mu x^\eta}{S_2}} dx - \int_{b(r_0, a_1)} \frac{1}{1 + \frac{\mu x^\eta}{S_2}} dx + \int_{b(r_1, d_F)} \frac{1}{1 + \frac{\mu x^\eta}{S_2}} dx - \int_{b(r_1, a_1)} \frac{1}{1 + \frac{\mu x^\eta}{S_2}} dx \right) \right)
\end{aligned}$$

Where (a) follows from Rayleigh fading and (b) follows from the definition of the regions b_0 and b_1 .

$$\begin{aligned}
L_{I_{U_e, \text{IBFD}} | r_0, r_1} \left(\mu \frac{P_{s_2} L_{p_2} r^\eta T}{P_{s_1} L_{p_1}} \right) \\
\leq \exp \left(-2\lambda_U (A_1(s_3, r_0, d_F) - A_1(s_3, r_0, a_1)) \right) \exp \left(-2\lambda_U (A_2(s_3, r_1, d_F, r_0) - A_3(s_3, r_1, a_1, r_0, d_F)) \right)
\end{aligned}$$

$$A_1(s_3, r_0, d_F) = \int_{r_0-d_F}^{r_0+d_F} \frac{\cos^{-1}\left(\frac{x^2+r_0^2-d_F^2}{2r_0x}\right)}{1+\frac{\mu}{s_3}x^\eta} x dx \text{ and } A_2(s_3, r_1, d_F, r_0) =$$

$$\int_{\max(r_1-d_F, r_0+d_F)}^{r_1+d_F} \frac{\cos^{-1}\left(\frac{x^2+r_1^2-d_F^2}{2r_1x}\right)}{1+\frac{\mu}{s_3}x^\eta} x dx$$

$$\text{Where } A_3(s_3, r_1, a_1, r_0, d_F) = \int_{\max(r_1-a_1, r_0+d_F)}^{\max(r_1+a_1, r_0+d_F)} \frac{\cos^{-1}\left(\frac{x^2+r_1^2-a_1^2}{2r_1x}\right)}{1+\frac{\mu}{s_3}x^\eta} x dx$$

We similarly decondition on r_0 and r_1 to get the final results for the two cases.

Lower bound for the LT of $I_{U_{e,IBFD}}$:

Lower bound can be derived similarly as that in $I_{U_{IBFD}}$ case.

Define the difference between the inner-city model of radius d_F and the disks which consists another inner-city model with radius $a_1 = p_{c2}d_F$ as $\mathcal{E}_{c1} = \mathcal{E}_{dF} - \mathcal{E}_{a1}$

$$L_{I_{U_{e,IBFD}}}\left(\mu \frac{P_{s_2} L_{p_2} r^\eta T}{P_{s_1} L_{p_1}}\right) = L_{I_{U_{e,IBFD}}}(s_3) = \mathbb{E}\left[\exp\left(-s_3 \sum_{i \in \mathcal{E}_{c1}} g_i R_i^{-\eta}\right)\right]$$

$$= \mathbb{E}_{\phi_{BS}}\left[\exp\left(-\lambda_U \int_{\mathcal{E}_{c1}} \frac{1}{1+\frac{\mu x^\eta}{s_3}} dx\right)\right]$$

$$= \mathbb{E}_{\phi_{BS}}\left[\exp\left(-\lambda_U \left(\int_{\mathcal{E}_{dF}} \frac{1}{1+\frac{\mu x^\eta}{s_3}} dx - \int_{\mathcal{E}_{a1}} \frac{1}{1+\frac{\mu x^\eta}{s_3}} dx\right)\right)\right]$$

$$\geq (a) \mathbb{E}_{\phi_{BS}}\left[\prod_{y \in \phi_{BS}} \exp\left(-2\lambda_U (A_1(s_3, y, d_F) - A_1(s_3, y, a_1))\right)\right]$$

$$= \exp\left[-2\pi \lambda_{BS} \int_0^\infty \left(1 - \exp\left(-2\lambda_U (A_1(s_3, y, d_F) - A_1(s_3, y, a_1))\right)\right) y dy\right]$$

And we get $I_{U_{e,IBFD}}'$ from $I_{U_{e,IBFD}}$ by substituting λ_{BS} by $\frac{\lambda_{BS}}{N}$

$$L_{I_{U_{e,IBFD}}}'\left(\mu \frac{P_{s_2} L_{p_2} r^\eta T}{P_{s_1} L_{p_1}}\right) \geq \mathbb{E}_{\phi_{BS}}\left[\prod_{y \in \phi_{BS}} \exp\left(-2\lambda_U (A_1(s_3, y, d_F) - A_1(s_3, y, a_1))\right)\right]$$

$$= \exp\left[-2\pi \frac{\lambda_{BS}}{N} \int_0^\infty \left(1 - \exp\left(-2\lambda_U (A_1(s_3, y, d_F) - A_1(s_3, y, a_1))\right)\right) y dy\right]$$

Where (a) is the same as before, it is greater than because we are not accounting for the overlap between the disks. And (b) from the PGFL of PPP Φ_{BS} .

Upper and Lower bounds for the LT of $I_{U_{IBFD}}$

The joint LT of $I_{U_{e,IBFD}}', I_{U_{IBFD}}$ is derived in a similar fashion.

Upper bound for the LT of $I_{U_{e,IBFD}}', I_{U_{IBFD}}$ case 2 and 1:

$$\begin{aligned}
& L_{I_{U_e,IBFD}, I_{U_{IBFD}|r_0,r_1}} \left(\mu \frac{P_{s_2} L_{p_2} r^\eta}{P_{s_1} L_{p_1}} T, \mu \frac{P_{s_2} L_{p_2} r^\eta}{P_{s_1} L_{p_1}} T_{edge} \right) \\
& \leq \mathbb{E} \left[\exp \left(s_3 \sum_{y \in \Phi_U \cap (b_0+b_1)} g_i' R_i^{-\eta} \mathbf{1}(\text{Un}_0) + s_4 \sum_{y \in \Phi_U \cap (b(r_0,dF)+b(r_1,dF))} g_i R_i^{-\eta} \right) \right] \\
& = (a) \exp \left(-\lambda_U \left(\int_{b(r_0,dF)} \frac{1}{1 + \frac{\mu x^\eta}{s_4}} dx + \int_{b(r_1,dF)} \frac{1}{1 + \frac{\mu x^\eta}{s_4}} dx \right) \right) \left[1 - \mathbb{E}[\mathbf{1}(\text{Un}_0)] \left(1 - \exp \left(-\lambda_U \left(\int_{b_0} \frac{1}{1 + \frac{\mu x^\eta}{s_3}} dx + \int_{b_1} \frac{1}{1 + \frac{\mu x^\eta}{s_3}} dx \right) \right) \right) \right] \\
& = (b) \exp \left(-\lambda_U \left(\int_{b(r_0,dF)} \frac{1}{1 + \frac{\mu x^\eta}{s_4}} dx + \int_{b(r_1,dF)} \frac{1}{1 + \frac{\mu x^\eta}{s_4}} dx \right) \right) \left[1 \right. \\
& \quad \left. - \frac{1}{N} \left(1 - \exp \left(-\lambda_U \left(\int_{b(r_0,dF)} \frac{1}{1 + \frac{\mu x^\eta}{s_3}} dx - \int_{b(r_0,a_1)} \frac{1}{1 + \frac{\mu x^\eta}{s_3}} dx + \int_{b(r_1,dF)} \frac{1}{1 + \frac{\mu x^\eta}{s_3}} dx - \int_{b(r_1,a_1)} \frac{1}{1 + \frac{\mu x^\eta}{s_3}} dx \right) \right) \right) \right] \\
& = (c) \exp \left(-2\lambda_U (A_1(s_4, r_0, d_F) + A_2(s_4, r_1, d_F, r_0)) \right) \left[1 \right. \\
& \quad \left. - \frac{1}{N} \left(1 - \exp \left(-2\lambda_U (A_1(s_3, r_0, d_F) - A_1(s_3, r_0, a_1) + A_2(s_3, r_1, d_F, r_0) - A_3(s_3, r_1, a_1, r_0, d_F)) \right) \right) \right]
\end{aligned}$$

With

$$\begin{aligned}
A_1(s_4, r_0, d_F) &= \int_{r_0-d_F}^{r_0+d_F} \frac{\cos^{-1}\left(\frac{x^2+r_0^2-d_F^2}{2r_0x}\right)}{1+\frac{\mu}{s_4}x^\eta} x dx \text{ and} \\
A_2(s_4, r_1, d_F, r_0) &= \int_{\max(r_1-d_F, r_0+d_F)}^{r_1+d_F} \frac{\cos^{-1}\left(\frac{x^2+r_1^2-d_F^2}{2r_1x}\right)}{1+\frac{\mu}{s_4}x^\eta} x dx \\
A_3(s_3, r_1, a_1, r_0, d_F) &= \int_{\max(r_1-a_1, r_0+d_F)}^{\max(r_1+a_1, r_0+d_F)} \frac{\cos^{-1}\left(\frac{x^2+r_1^2-a_1^2}{2r_1x}\right)}{1+\frac{\mu}{s_3}x^\eta} x dx
\end{aligned}$$

the same applies for other A1 and A2 with different parameters

Where in (a) we have used the same approach to account for the FFR scheme, and in (b) the expectation of indicator function is equivalent to making thinning N on the density of the disks (i.e. the disk center i.e. λ_{BS}). In (c) we have used again A3 which is needed because sometimes r_0+dF may be bigger than r_1+a_1 or r_1-a_1 , so the disk $b(r_1, a_1)$ may not exist or we may need to not account all of it (see previous figure second drawing which shows that r_0+dF is bigger than r_1+a_1 so in second disk we only account for the area from r_0+dF to r_1+dF and we don't need to subtract any area from disk $b(r_1, a_1)$).

We note that in (a) we can use a different approach to account for nearest interfering disk with applying the FFR with reuse N. This approach is to don't use the indicator function $\mathbf{1}(\cdot)$, but rather use the nearest 'N' disk rather than the first nearest disk with the indicator function. But, such an approach will require to use a joint pdf for the distance of the centers of the disks r_0, r_1 and r_N (when we de-condition the Laplace formula on r), which will result in a complex equation, and I don't know if such PDF exists. Thus, we see that using the indicator function will be better because it will make thinning on the density λ_{BS} by N. Which will account for the FFR scheme.

Then, we de-condition on r_0 and r_1 to get the final result.

Lower bound for the LT of $I_{U_e,IBFD}, I_{U,IBFD}$:

We take all the disks of the inner-city model $\mathcal{E}_{c1} = \mathcal{E}_{dF} - \mathcal{E}_{a1}$ where from the definition $dF > a1$, else they do not exist. And we apply $\frac{\lambda_{BS}}{N}$ on $I\{-Ue-IBFD\}$, which will account for the st-FFR.

$$\begin{aligned} L_{I_{U_e,IBFD}, I_{U,IBFD}} & \left(\mu \frac{P_{s_2} L_{p_2} r^\eta}{P_{s_1} L_{p_1}} T, \mu \frac{P_{s_2} L_{p_2} r^\eta}{P_{s_1} L_{p_1}} T_{edge} \right) \\ & = (a) \mathbb{E} \left[\exp \left(-s_3 \sum_{y \in \mathcal{E}_{c1}} g_y' R_y^{-\eta} \mathbf{1}(n_y = n_0) - s_4 \sum_{y \in \mathcal{E}_{dF}} g_y R_y^{-\eta} \right) \right] \\ & = \mathbb{E}_{\phi_{BS}} \left[\exp \left(-\lambda_U \left(\mathbf{1}(Un_0) \int_{\mathcal{E}_{c1}} \frac{1}{1 + \frac{\mu x^\eta}{s_3}} dx + \int_{\mathcal{E}_{dF}} \frac{1}{1 + \frac{\mu x^\eta}{s_4}} dx \right) \right) \right] \end{aligned}$$

Where the indicator function in (a) indicates that only the edge users that uses the same FFR bands are causing interference.

$$\begin{aligned} & \geq (b) \mathbb{E}_{\phi_{BS}} \left[\prod_{y \in \phi_{BS}} \exp(-2\lambda_U A_1(s_4, y, d_F)) \left[1 - \mathbb{E}[\mathbf{1}(Un_0)] \left(1 - \exp(-2\lambda_U (A_1(s_3, y, d_F) - A_1(s_3, y, a_1))) \right) \right] \right] \\ & = \mathbb{E}_{\phi_{BS}} \left[\prod_{y \in \phi_{BS}} \exp(-2\lambda_U A_1(s_4, y, d_F)) \left[1 - \frac{1}{N} \left(1 - \exp(-2\lambda_U (A_1(s_3, y, d_F) - A_1(s_3, y, a_1))) \right) \right] \right] \end{aligned}$$

$$L_{I_{U_e,IBFD}, I_{U,IBFD}} \left(\mu \frac{P_{s_2} L_{p_2} r^\eta}{P_{s_1} L_{p_1}} T, \mu \frac{P_{s_2} L_{p_2} r^\eta}{P_{s_1} L_{p_1}} T_{edge} \right) \geq \exp \left[-2\pi \lambda_{BS} \int_0^\infty (1 - \xi(y)) y dy \right]$$

Where $\xi(y) = \exp(-2\lambda_U A_1(s_4, y, d_F)) \left[1 - \frac{1}{N} \left(1 - \exp(-2\lambda_U (A_1(s_3, y, d_F) - A_1(s_3, y, a_1))) \right) \right]$

Appendix IV.H

Upper bound for the LT of $I_{UC,IBFD}, I_{U,IBFD}$ case 2 and 1:

The interference $I_{U,IBFD}$ and $I_{UC,IBFD}$ are shown in Figure 4.3 (a) and (b) respectively. Its joint LT is obtained in a similar manner, where for case 2, $I_{UC,IBFD}$ is evaluated at $b(r_0, a_1)$ and $b(r_1, a_1)$, while $I_{U,IBFD}$ is evaluated at $b(r_0, d_F)$ and $b(r_1, d_F)$. For case 1, we only evaluate at r_0 .

Lower bound for the LT of $I_{UC,IBFD}, I_{U,IBFD}$:

We have the inner-city model for the core users operating at IBFD \mathcal{E}_{a_1} of radius a_1 , and the inner city model for the IBFD users \mathcal{E}_{d_F} of radius d_F .

$$\begin{aligned}
L_{U_c, IBFD, U_{IBFD}} \left(\mu \frac{P_{s_2} L_{p_2} r^\eta}{P_{s_1} L_{p_1}} \max\{T, T_{edge}\}, \mu \frac{P_{s_2} L_{p_2} r^\eta}{P_{s_1} L_{p_1}} T_{edge} \right) &= \mathbb{E} \left[\exp \left(-s_5 \sum_{i \in \mathcal{E}_{a_1}} g_i' R_i^{-\eta} - s_4 \sum_{i \in \mathcal{E}_{d_F}} g_i R_i^{-\eta} \right) \right] \\
&= (a) \mathbb{E}_{\phi_{BS}} \left[\exp \left(-\lambda_U \left(\int_{\mathcal{E}_{a_1}} \frac{1}{1 + \frac{\mu x^\eta}{s_5}} dx + \int_{\mathcal{E}_{d_F}} \frac{1}{1 + \frac{\mu x^\eta}{s_4}} dx \right) \right) \right] \\
&\geq \mathbb{E}_{\phi_{BS}} \left[\exp \left(\prod_{y \in \phi_{BS}} \exp \left(-2\lambda_U (A_1(s_5, y, a_1) + A_1(s_4, y, d_F)) \right) \right) \right] \\
&= \exp \left[-2\pi\lambda_{BS} \int_0^\infty \left(1 - \exp \left(-2\lambda_U (A_1(s_5, y, a_1) + A_1(s_4, y, d_F)) \right) \right) y dy \right]
\end{aligned}$$

With $A_1(s, y, d_F) = \int_{y-d_F}^{y+d_F} \frac{\cos^{-1}\left(\frac{x^2+y^2-d_F^2}{2yx}\right)}{1+\frac{\mu x^\eta}{s}} x dx$ and $A_1(s, y, a_1) = \int_{y-a_1}^{y+a_1} \frac{\cos^{-1}\left(\frac{x^2+y^2-a_1^2}{2yx}\right)}{1+\frac{\mu x^\eta}{s}} x dx$

BIBLIOGRAPHY

- [1] S. N. Chiu, D. Stoyan, W. Kendall, and J. Mecke, *Stochastic geometry and its applications*, 3rd edition, John Wiley & Sons, 2013.
- [2] M. Haenggi, *Stochastic geometry for wireless networks*, Cambridge University Press, 2012.
- [3] Th. S. Rappaport, *Wireless communications: principles and practice*, Vol. 2. New Jersey: Prentice Hall PTR, 1996.
- [4] B. Hagerman, "Downlink relative co-channel interference powers in cellular radio systems," *1995 IEEE 45th Vehicular Technology Conference. Countdown to the Wireless Twenty-First Century*, Chicago, IL, 1995, pp. 366-370 vol.1.
- [5] A. M. Ibrahim, T. ElBatt and A. El-Keyi, "Coverage probability analysis for wireless networks using repulsive point processes," *2013 IEEE 24th Annual International Symposium on Personal, Indoor, and Mobile Radio Communications (PIMRC)*, London, 2013, pp. 1002-1007.
- [6] H. S. Dhillon, R. K. Ganti, F. Baccelli and J. G. Andrews, "Modeling and Analysis of K-Tier Downlink Heterogeneous Cellular Networks," in *IEEE Journal on Selected Areas in Communications*, vol. 30, no. 3, pp. 550-560, April 2012.
- [7] Chun Chung Chan and S. V. Hanly, "Calculating the outage probability in a CDMA network with spatial Poisson traffic," in *IEEE Transactions on Vehicular Technology*, vol. 50, no. 1, pp. 183-204, Jan 2001.
- [8] P. C. Pinto, A. Giorgetti, M. Z. Win and M. Chiani, "A stochastic geometry approach to coexistence in heterogeneous wireless networks," in *IEEE Journal on Selected Areas in Communications*, vol. 27, no. 7, pp. 1268-1282, September 2009.
- [9] C. h. Lee and M. Haenggi, "Interference and Outage in Poisson Cognitive Networks," in *IEEE Transactions on Wireless Communications*, vol. 11, no. 4, pp. 1392-1401, April 2012.
- [10] A. Ghasemi and E. S. Sousa, "Interference Aggregation in Spectrum-Sensing Cognitive Wireless Networks," in *IEEE Journal of Selected Topics in Signal Processing*, vol. 2, no. 1, pp. 41-56, Feb. 2008.
- [11] V. Chandrasekhar and J. G. Andrews, "Uplink capacity and interference avoidance for two-tier femtocell networks," in *IEEE Transactions on Wireless Communications*, vol. 8, no. 7, pp. 3498-3509, July 2009.
- [12] W. C. Cheung, T. Q. S. Quek and M. Kountouris, "Throughput Optimization, Spectrum Allocation, and Access Control in Two-Tier Femtocell Networks," in *IEEE Journal on Selected Areas in Communications*, vol. 30, no. 3, pp. 561-574, April 2012.
- [13] O. Dousse, M. Franceschetti and P. Thiran, "On the throughput scaling of wireless relay networks," in *IEEE Transactions on Information Theory*, vol. 52, no. 6, pp. 2756-2761, June 2006.
- [14] N. Deng, S. Zhang, W. Zhou and J. Zhu, "A stochastic geometry approach to energy efficiency in relay-assisted cellular networks," *2012 IEEE Global Communications Conference (GLOBECOM)*, Anaheim, CA, 2012, pp. 3484-3489.
- [15] M. Haenggi, J. G. Andrews, F. Baccelli, O. Dousse and M. Franceschetti, "Stochastic geometry and random graphs for the analysis and design of wireless networks," in *IEEE Journal on Selected Areas in Communications*, vol. 27, no. 7, pp. 1029-1046, September 2009.
- [16] H. ElSawy, E. Hossain and M. Haenggi, "Stochastic Geometry for Modeling, Analysis, and Design of Multi-Tier and Cognitive Cellular Wireless Networks: A Survey," in *IEEE Communications Surveys & Tutorials*, vol. 15, no. 3, pp. 996-1019, Third Quarter 2013.
- [17] M. Haenggi, and R. K. Ganti, "Interference in large wireless networks", *Foundations and Trends® in Networking* 3, no. 2, pp. 127-248, 2009.
- [18] A. Guo and M. Haenggi, "Spatial Stochastic Models and Metrics for the Structure of Base Stations in Cellular Networks," in *IEEE Transactions on Wireless Communications*, vol. 12, no. 11, pp. 5800-5812, November 2013.
- [19] J. G. Andrews, F. Baccelli and R. K. Ganti, "A Tractable Approach to Coverage and Rate in Cellular Networks," in *IEEE Transactions on Communications*, vol. 59, no. 11, pp. 3122-3134, November 2011.
- [20] T. D. Novlan, H. S. Dhillon and J. G. Andrews, "Analytical Modeling of Uplink Cellular Networks," in *IEEE Transactions on Wireless Communications*, vol. 12, no. 6, pp. 2669-2679, June 2013.
- [21] F. J. Martin-Vega, M. Di Renzo, M. C. Aguayo-Torres, G. Gomez and T. Q. Duong, "Stochastic geometry modeling and analysis of backhaul-constrained Hyper-Dense Heterogeneous cellular

- networks," *2015 17th International Conference on Transparent Optical Networks (ICTON)*, Budapest, 2015, pp. 1-4.
- [22] R. K. Ganti and M. Haenggi, "Interference and Outage in Clustered Wireless Ad Hoc Networks," in *IEEE Transactions on Information Theory*, vol. 55, no. 9, pp. 4067-4086, Sept. 2009.
- [23] P. D. Mankar, G. Das and S. S. Pathak, "Modeling and Coverage Analysis of BS-Centric Clustered Users in a Random Wireless Network," in *IEEE Wireless Communications Letters*, vol. 5, no. 2, pp. 208-211, April 2016.
- [24] Y. Wang and Q. Zhu, "Modeling and Analysis of Small Cells Based on Clustered Stochastic Geometry," in *IEEE Communications Letters*, vol. 21, no. 3, pp. 576-579, March 2017.
- [25] H. S. Jo, Y. J. Sang, P. Xia and J. G. Andrews, "Heterogeneous Cellular Networks with Flexible Cell Association: A Comprehensive Downlink SINR Analysis," in *IEEE Transactions on Wireless Communications*, vol. 11, no. 10, pp. 3484-3495, October 2012.
- [26] H. Wei, N. Deng, W. Zhou and M. Haenggi, "Approximate SIR Analysis in General Heterogeneous Cellular Networks," in *IEEE Transactions on Communications*, vol. 64, no. 3, pp. 1259-1273, March 2016.
- [27] CH Lee, CY Shih, and YS Chen, "Stochastic geometry based models for modeling cellular networks in urban areas", *Wireless networks*, pp. 1-10, 2013.
- [28] OpenCellID. Available. [Online]. <http://opencellid.org/>.
- [29] Y. Zhou, R. Li, Z. Zhao, X. Zhou and H. Zhang, "On the α -Stable Distribution of Base Stations in Cellular Networks," in *IEEE Communications Letters*, vol. 19, no. 10, pp. 1750-1753, Oct. 2015.
- [30] Alpha-Stable Distribution and its Applications in Cellular Networks. Available. [Online]. <http://www.rongpeng.info/stable/>
- [31] L. Chiaraviglio *et al.*, "What is the Best Spatial Distribution to Model Base Station Density? A Deep Dive into Two European Mobile Networks," in *IEEE Access*, vol. 4, no. , pp. 1434-1443, 2016.
- [32] L. Chiaraviglio *et al.*, "A reality check of Base Station Spatial Distribution in mobile networks," *2016 IEEE Conference on Computer Communications Workshops (INFOCOM WKSHPS)*, San Francisco, CA, 2016, pp. 1065-1066.
- [33] 3GPP TR 38.913 V14.2.0. Study on scenarios and requirements for next generation access technologies. 2017.
- [34] H. ElSawy, E. Hossain and M. Haenggi, "Stochastic Geometry for Modeling, Analysis, and Design of Multi-Tier and Cognitive Cellular Wireless Networks: A Survey," in *IEEE Communications Surveys & Tutorials*, vol. 15, no. 3, pp. 996-1019, Third Quarter 2013.
- [35] Anderssen, Robert S., Saiful A. Husain, and R. J. Loy. "The Kohlrausch function: properties and applications." *Anziam journal* 45 (2004): 800-816.
- [36] Kohlrausch, Rudolph. "Theorie des elektrischen Rückstandes in der Leidener Flasche." *Annalen der Physik* 167, no. 2 (1854): 179-214.
- [37] K. Górska, and K. A. Penson. "Lévy stable distributions via associated integral transform" *Journal of Mathematical Physics* 53, no. 5 (2012): 053302.
- [38] J. Abate and PP Valkó. Multi-precision Laplace transform inversion. *International Journal for Numerical Methods in Engineering*, 60(5), 979-993, 2004.
- [39] P. Ribereau, E. Masiello and P. Naveau. Skew generalized extreme value distribution: Probability-weighted moments estimation and application to block maxima procedure. *Communications in Statistics-Theory and Methods*, 45(17), 5037-5052, 2016.
- [40] K. M. K. H. Leong, Yuanxun Wang and T. Itoh, "A radar target transceiver using a full duplex capable retrodirective array system," *IEEE MTT-S International Microwave Symposium Digest, 2003*, Philadelphia, PA, USA, 2003, pp. 1447-1450 vol.2.
- [41] M. Duarte and A. Sabharwal, "Full-duplex wireless communications using off-the-shelf radios: Feasibility and first results," *2010 Conference Record of the Forty Fourth Asilomar Conference on Signals, Systems and Computers*, Pacific Grove, CA, 2010, pp. 1558-1562.
- [42] Knox, Michael E. "Single antenna full duplex communications using a common carrier." *Wireless and microwave technology conference (WAMICON), 2012 IEEE 13th annual*. IEEE, 2012.
- [43] E. Everett, A. Sahai and A. Sabharwal, "Passive Self-Interference Suppression for Full-Duplex Infrastructure Nodes," in *IEEE Transactions on Wireless Communications*, vol. 13, no. 2, pp. 680-694, February 2014.

- [44] D. Kim, H. Lee and D. Hong, "A Survey of In-Band Full-Duplex Transmission: From the Perspective of PHY and MAC Layers," in *IEEE Communications Surveys & Tutorials*, vol. 17, no. 4, pp. 2017-2046, Fourthquarter 2015.
- [45] Sabharwal, P. Schniter, D. Guo, D. W. Bliss, S. Rangarajan and R. Wichman, "In-Band Full-Duplex Wireless: Challenges and Opportunities," in *IEEE Journal on Selected Areas in Communications*, vol. 32, no. 9, pp. 1637-1652, Sept. 2014.
- [46] Choi, Jung Il, et al. "Achieving single channel, full duplex wireless communication." *Proceedings of the sixteenth annual international conference on Mobile computing and networking*. ACM, 2010.
- [47] J. Kim, M. S. Sim, M. Chung, D. K. Kim, and C. B. Chae, "Full-duplex Radios in 5G: Fundamentals, Design and Prototyping," in *Signal Processing for 5G: Algorithms and Implementations*, pp. 539-560.
- [48] Z. Tong and M. Haenggi, "Throughput Analysis for Full-Duplex Wireless Networks With Imperfect Self-Interference Cancellation," in *IEEE Transactions on Communications*, vol. 63, no. 11, pp. 4490-4500, Nov. 2015.
- [49] A. AlAmmouri, H. ElSawy, O. Amin and M. S. Alouini, "In-Band alpha-Duplex Scheme for Cellular Networks: A Stochastic Geometry Approach," in *IEEE Transactions on Wireless Communications*, vol. 15, no. 10, pp. 6797-6812, Oct. 2016.
- [50] S. Goyal, et al. "Analyzing a full-duplex cellular system." *Information Sciences and Systems (CISS), 2013 47th Annual Conference on*. IEEE, 2013.
- [51] S. Goyal, P. Liu and S. S. Panwar, "User Selection and Power Allocation in Full-Duplex Multicell Networks," in *IEEE Transactions on Vehicular Technology*, vol. 66, no. 3, pp. 2408-2422, March 2017.
- [52] A. H. Sakr; E. Hossain, "On User Association in Multi-Tier Full-Duplex Cellular Networks," in *IEEE Transactions on Communications*, vol. PP, no.99, pp.1-1
- [53] K. S. Ali, H. ElSawy and M. S. Alouini, "Modeling Cellular Networks With Full-Duplex D2D Communication: A Stochastic Geometry Approach," in *IEEE Transactions on Communications*, vol. 64, no. 10, pp. 4409-4424, Oct. 2016.
- [54] S. Wang, V. Venkateswaran and X. Zhang, "Fundamental Analysis of Full-Duplex Gains in Wireless Networks," in *IEEE/ACM Transactions on Networking*, vol. 25, no. 3, pp. 1401-1416, June 2017.
- [55] I. Atzeni and M. Kountouris, "Full-Duplex MIMO Small-Cell Networks: Performance Analysis," *2015 IEEE Global Communications Conference (GLOBECOM)*, San Diego, CA, 2015, pp. 1-6.
- [56] A. Sharma, R. K. Ganti and J. K. Milleth, "Joint Backhaul-Access Analysis of Full Duplex Self-Backhauling Heterogeneous Networks," in *IEEE Transactions on Wireless Communications*, vol. 16, no. 3, pp. 1727-1740, March 2017.
- [57] T. D. Novlan, R. K. Ganti, A. Ghosh and J. G. Andrews, "Analytical Evaluation of Fractional Frequency Reuse for OFDMA Cellular Networks," in *IEEE Transactions on Wireless Communications*, vol. 10, no. 12, pp. 4294-4305, December 2011.
- [58] T. D. Novlan, R. K. Ganti, A. Ghosh and J. G. Andrews, "Analytical Evaluation of Fractional Frequency Reuse for Heterogeneous Cellular Networks," in *IEEE Transactions on Communications*, vol. 60, no. 7, pp. 2029-2039, July 2012.
- [59] H. Zhuang and T. Ohtsuki, "Analytical evaluation of fractional frequency reuse for MIMO heterogeneous cellular networks," *2014 IEEE Global Communications Conference*, Austin, TX, 2014, pp. 4275-4280.
- [60] U. Sawant and R. Akl, "A novel metric to study the performance of sectorized fractional frequency reuse techniques in LTE," *2017 Wireless Telecommunications Symposium (WTS)*, Chicago, IL, 2017, pp. 1-7.
- [61] U. Sawant and R. Akl, "Evaluation of adaptive and non adaptive LTE Fractional Frequency Reuse mechanisms," *2017 26th Wireless and Optical Communication Conference (WOCC)*, Newark, NJ, 2017, pp. 1-6.
- [62] M. Haenggi, *Stochastic geometry for wireless networks*, Cambridge University Press, 2012.
- [63] Z. Yazdanshenasan, H. S. Dhillon, M. Afshang and P. H. J. Chong, "Poisson Hole Process: Theory and Applications to Wireless Networks," in *IEEE Transactions on Wireless Communications*, vol. 15, no. 11, pp. 7531-7546, Nov. 2016.
- [64] Y. J. Chun and M. O. Hasna. Analysis of heterogeneous cellular networks interference with biased cell association using poisson cluster processes. In *2014 Int. Conf. on Inf. and Comm. Tech. Convergence (ICTC)*, pages 319–324, Oct 2014.